UNIVERSITY OF TARTU
Faculty of Science and Technology
Institute of Technology

Philip Arthur Morehead

Deploying *Pseudomonas putida* for the conversion of aromatic compounds from fractionated industrial hydrolysis lignin

Master's Thesis (30 ECTS)

Curriculum Bioengineering

Supervisors:
Senior Specialist, MSc Scott Bottoms
Associate Professor, PhD Siim Salmar
Professor, PhD Mart Loog

Tartu 2023

Deploying *Pseudomonas putida* for the conversion of aromatic compounds from fractionated industrial hydrolysis lignin

Abstract:

The world's most abundant natural aromatic polymer is paradoxically one of its most underutilized feedstocks. Lignin is the pulp and paper industry's primary by-product, and it shows great potential as a renewable and carbon-neutral source of industrially relevant chemicals. The utilization of *Pseudomonas putida*, a robust bacterium known to catabolize aromatic compounds natively, was explored in this study as a promising approach for lignin valorization. To this end, dry hydrolysis lignin (HL) was used as the feedstock, and various HL fractionation techniques were applied, including alkaline extraction, to obtain lignin monomers, dimers, and trimers in solution for use as a growth medium. The composition of the fractionated HL media was ascertained using a range of analytical techniques. Changes in composition during flask cultivations helped inform the selection of target genes for deletion to direct compounds in the benzoate degradation pathway towards the production of *cis,cis*-muconic acid, an intermediate of nylon 6,6, which finds applications in industrial components, textiles, automotive parts, and electronics.

Keywords:

Lignin valorization, *Pseudomonas putida*, lignin fractionation, aerobic fermentation

CERCS:

Pseudomonas putida kasutamine fraktsioneeritud tööstusliku toore ligniini aroomsete ühendite muundamiseks

Lühikokkuvõte:

Maailma kõige rohkearvulisem looduslik aromaatne polümeer lignin on paradoksaalsel kombel üks kõige alakasutatumaid tooraineid. Ligniin on tselluloosi ja paberi tööstuse peamine kõrvalsaadus ning omab suurt potentsiaali taastuva ja süsinikuneutraalse allikana tööstuslikult oluliste kemikaalide saamiseks. Selles töös uuriti ligniini väärindamiseks paljutõotava lähenemisviisina *Pseudomonas putida* kasutamit, kuna teadaolevalt see vastupidav bakter kataboliseerib aromaatseid ühendeid. Toorainaena kasutati kuivatatud tööstuslikku hüdrolüüsi ligniini (HL) ning HL-i fraktsioneeriti vesilahusesse, sealhulgas leeliselise ekstraktsiooniga, et saada ligniini monomeerid, dimeerid ja trimere lahustes kasutamiseks kasvukeskkonnana. Fraktsioneeritud HL-i lahuste koostist määrati erinevate

analüütiliste meetodite abil. Koostise muutused kultiveerimisel aitasid valida sihtgeene, mille kustutamisel suunata ühendid bensoaadi lagundamisrada pidi *cis,cis*-mukoonhappe tootmisele, mis on vaheühend nailon 6,6 tootmiseks.

Võtmesõnad:

Ligniini väärindamine, *Pseudomonas putida*, ligniini fraktsioneerimine, aeroobne käärimine

CERCS:

TABLE OF CONTENTS

TERMS, ABBREVIATIONS AND NOTATIONS 7

1 INTRODUCTION 9

2 LITERATURE REVIEW 10

2.1 Climate change and mitigation efforts 10

2.1.1 Impact of greenhouse gas emissions on climate change 10

2.1.2 Plastic emissions 10

2.1.3 Importance of sustainable and low-carbon strategies 11

2.2 An overview of lignin 12

2.2.1 Definition, structure, and properties of lignin 12

2.2.2 Sources and availability of industrial crude HL 13

2.2.3 Challenges and limitations of lignin valorization 14

2.3 Characteristics and applications of *Pseudomonas putida* 19

2.3.1 Overview of *Pseudomonas putida* 19

2.3.2 Industrially relevant genetic and metabolic features 20

2.3.3 Utilization of *Pseudomonas putida* for lignin valorization 21

2.4 Project objectives 22

3 THE AIMS OF THE THESIS 24

4 EXPERIMENTAL PART 25

4.1 MATERIALS AND METHODS 25

4.1.1 Growth conditions, strains, and media 25

4.1.2 Plate reader growth assays 25

4.1.3 Shake flask cultivations 26

4.1.3.1 Batch cultivations 26

4.1.3.2 Simulated fed-batch cultivations 26

4.1.4 Preparation of fractionated lignin 26

4.1.4.1 Wx/M9 fractionation 26

4.1.4.2 Alkaline extractions and steam explosion.....27
4.1.4.3 Fractionation with MMPAM…….....27
4.1.5 Genomic DNA extraction and PCR.....27
4.1.5.1 Genomic DNA and pGNW2 plasmid extraction.....27
4.1.5.2 Muconate cycloisomerase HR amplification.....28
4.1.5.3 pGNW2 plasmid linearization.....29
4.1.5.4 Protocatechuate 3,4-dioxygenase HR amplification.....29
4.1.5.5 DNA gel extraction and nanodrop.....29
4.1.6 Strain screening..... 30
4.1.7 Analytical methods.....30
4.1.7.1 HPLC methods.....30
4.1.7.2 UV-Vis spectroscopy.....30
4.1.7.3 Ion chromatography and spectrophotometry.....31
4.1.7.4 GC-MS.....31
4.2 RESULTS AND DISCUSSION.....31
4.2.1 Strain Characterization 31
4.2.1.1 Glucose osmolarity..... 31
4.2.1.2 Xylose osmolarity.....32
4.2.1.3 pH tolerance.....33
4.2.2 Preliminary fractionated lignin cultivation.....33
4.2.3 Simulated fed-batch cultivation.....34
4.2.4 HL slurry fermentations.....36
4.2.5 Strain screening.....38
4.2.6 Initial molecular biology procedures 40
4.2.7 Additional analyses.....41
4.2.7.1 Ion chromatographic analysis of fractionated HL.....41
4.2.7.2 UV-vis spectrophotometric analysis of fractionated HL.....41

4.2.7.3 Dimereric to monomeric shift in alkaline HL fermentation.....42

SUMMARY 43

Acknowledgments.....44

REFERENCES 45

Supplementary Materials 59

NON-EXCLUSIVE LICENCE TO REPRODUCE THESIS AND MAKE THESIS PUBLIC 87

TERMS, ABBREVIATIONS AND NOTATIONS

$Ca(OH)_2$	Calcium hydroxide
CCMA	*cis*,*cis*-muconic acid
CE	Circular economy
CO_2e	Carbon dioxide equivalent
GC	Guanine-Cytosine
GC-MS	Gas chromatography-mass spectrometry
GHG	Greenhouse gas
HPLC	High performance liquid chromatography
HL	Hydrolysis lignin
HL slurry	Hydrolysis lignin suspension in minimal medium without separation of solid fraction
5-HMF	5-Hydroxymethylfurfural
HR	Homology region
KOH	Potassium hydroxide
KL	Kraft lignin
MCI	Muconate cycloisomerase
μ_{max}	Maximum specific growth rate
MMPAM	Modified minimal medium
NaOH	Sodium hydroxide
NH_4OH	Ammonium hydroxide
OD_{600}	Optical density at 600 nm
3,4-PCD	Protocatechuate 3,4-dioxygenase
P. putida	*Pseudomonas putida*

PAM511-0001	Standardized hydrolysis lignin fractionation with modified minimal medium
PCA	Protocatechuic acid
ppm	Parts per million
tD	Doubling time
UV-Vis	Ultraviolet-Visible
Wx/M9	Minimal medium

1 INTRODUCTION

Lignin, a plentiful natural aromatic polymer, has been underutilized despite its abundance. As a by-product of the pulp and paper industry, lignin holds immense potential as a renewable and carbon-neutral resource for producing relevant chemicals. This study investigates the use of *P. putida*, for hydrolysis lignin (HL) valorization. Various fractionation techniques, including alkaline extraction, were used to obtain lignin monomers, dimers, and trimers in solution, creating an optimal growth medium for *P. putida*. The composition of the fractionated HL media was analyzed, providing a preliminary understanding of its chemical constituents.

Multiple fractionation techniques were evaluated for their effectiveness in solubilizing HL and promoting *P. putida* growth. Chemical characterization of each fractionated HL batch focused on identifying benzoate degradation pathway monomers and other major peaks detected through high-performance liquid chromatography (HPLC). Additionally, changes in the composition of *P. putida* cultures were monitored over time to gain insights into metabolic transformations during bacterial cultivation.

Furthermore, this project sought to identify *P. putida* and other candidate strains capable of breaking down lignin-derived compounds or producing specific compounds, particularly *cis,cis*-muconic acid. This project also aimed to identify the optimal growth conditions for selected strains, considering factors like temperature, pH, and nutrient availability to enhance the production of targeted lignin-derived compounds.

The study also aimed to identify genetic targets for modification to enhance the synthesis of *cis,cis*-muconic acid by redirecting metabolic precursors towards it while minimizing downstream catalysis.

2 LITERATURE REVIEW

2.1 Climate change and mitigation efforts

2.1.1 Impact of greenhouse gas emissions on climate change

Currently, the most critical environmental issue globally is the rising concentration of atmospheric greenhouse gases (GHG), which leads to climate change due to increased global temperatures (Guo *et al.,* 2021). Whereas the phenomenon of climate change typically occurs over several thousand years (Ghiasi *et al.,* 2019), anthropogenic emissions occur beyond the framework of the natural carbon cycle, which circulates carbon between the atmosphere, the oceans, and the terrestrial biosphere over timescales ranging from less than a day to millennia (Archer *et al.,* 2009). Of the several GHGs causing climate change, CO_2 is the most abundant, accounting for 76% of the total anthropogenic GHG emissions in 2010 (IPCC, 2014).

Since *circa* 1750, the atmospheric CO_2 concentration has steadily risen from around 277 ppm to approximately 410 ppm in 2019 (Joos and Spahni, 2008; Dlugokencky and Tans, 2020). Initially, the rise in CO_2 concentration beyond pre-industrial levels was mainly attributed to deforestation and changes in land use practices (Ciais *et al.,* 2013). However, from around 1950 onwards, fossil fuels became the primary source of anthropogenic emissions, and their combustion has progressively increased their relative contribution ever since (Archer *et al.,* 2009; Reis *et al.,* 2008). The pursuit of rapid economic growth reliant on fossil fuels has raised concerns regarding social and environmental development as emissions and pollution levels have reached unprecedented levels not seen in the past 800,000 years (Teixeira *et al.,* 2018). Climate change has therefore emerged as a crucial global issue with far-reaching implications for energy security, economic growth, and environmental stability.

Failure to take adequate measures to reduce global GHG emissions may lead to a temperature increase exceeding 2 °C above pre-industrial levels, resulting in significant socio-economic and environmental consequences worldwide (Xiaosong *et al.,* 2019). The agricultural sector, coastal regions, and vulnerable populations are especially at risk from the impacts of climate change (Afrifa *et al.,* 2020; Abid *et al.,* 2022). Mid-latitude regions, such as Mediterranean Europe, are especially vulnerable to climate change effects such as increased droughts and widespread forest fires (IPCC, 2015).

2.1.2 Plastic emissions

As the impact of climate change continues to raise environmental concerns, it is crucial to address another significant issue closely intertwined with it—plastic emissions. The production of plastics has experienced remarkable growth, becoming an integral part of the global economy. Plastic production has surged from 2 million tons in 1950 to 380 million tons in 2015, cementing its status as the material with the highest global production growth (IEA, 2018; Geyer *et al.*, 2017). Future projections indicate a significant increase in plastic production, with estimates suggesting a doubling by 2050 and a tripling by 2100 compared to 2020 levels (Stegmann *et al.,* 2022).

This surge in plastics demand, which has quadrupled over the past four decades, amplifies the environmental and health impacts associated with their usage (Law & Thompson, 2014; Rochman *et al.,* 2013). While considerable attention has been given to the environmental consequences of microplastic pollution and plastics incineration in research studies (Law & Thompson, 2014; Rochman, 2018; Ryberg *et al.*, 2018; Shen *et al.*, 2020; Hamilton *et al.*, 2019), the environmental impacts of plastics production, particularly greenhouse gas emissions, have received relatively less scrutiny (Posen *et al.*, 2017; Dormer *et al.*, 2013). Notably, Cabernard *et al.* (2022) showed that the carbon footprint of plastics doubled between 1995 and 2015, amounting to 2 gigatons of CO_2e, equivalent to 4.5% of global carbon emissions in 2015. The primary driver behind this bigger carbon footprint has been the increased use of coal for plastics production. Moreover, production accounts for 96% of the carbon footprint associated with plastics, while end-of-life stages, encompassing recycling, incineration, and landfilling, contribute a smaller fraction.

To mitigate the environmental impact of plastics, two promising strategies include utilizing biomass as feedstock and implementing CE measures such as recycling (Zheng and Suh, 2019; Bazzanella and Ausfelder, 2017; Meys *et al.,* 2021). These approaches can potentially reduce the use of fossil feedstock and associated greenhouse gas (GHG) emissions in the plastics sector. Moreover, they can contribute to developing a circular plastics bioeconomy, even reducing harmful CO_2 emissions by sequestering biogenic carbon in plastic products for long-term utilization (de Oliveira *et al.,* 2020; Stegman *et al.,* 2020). Furthermore, incorporating renewable energy sources into plastic production and waste management can further decrease GHG emissions by the plastics industry (Stegmann *et al.,* 2022).

2.1.3 Importance of sustainable and low-carbon strategies

The urgency to avoid a "Hothouse Earth" scenario, characterized by irreversible and catastrophic climate impacts, has been highlighted in various scientific studies (Drijfhout *et al.*,

2015; Stocker *et al.*, 2013). A temperature increase of 2 °C is suggested as a critical threshold due to the potential activation of tipping elements and the subsequent cascade effect (Schellnhuber *et al.*, 2016; Lenton *et al.*, 2008). Even if the Tokyo Protocol target of limiting temperature rise to 1.5 °C to 2.0 °C is met, the risk of a feedback cascade pushing the planet irreversibly towards a Hothouse Earth trajectory cannot be excluded. Consequently, deliberate decisions must be made to maintain the Earth System within Holocene-like conditions (Steffen *et al.*, 2018). Achieving a "Stabilized Earth" necessitates deep cuts in greenhouse gas emissions, protection of biosphere carbon sinks, CO_2 removal from the atmosphere, solar radiation management, and adaptation to unavoidable warming impacts (Rockström *et al.*, 2017).

Furthermore, the cumulative CO_2 emissions released by the end of this century will strongly influence future warming (Allen *et al.*, 2013; IPCC, 2013). To stabilize climate below a 2 °C increase with a 66% likelihood, a *finite quota* of cumulative CO_2 emissions, not exceeding 1,200 gigatons from 2015 onwards, is necessary (Friedlingstein *et al.*, 2014). Deliberate strategies to remove CO_2 from the atmosphere, particularly sustainable bioenergy with carbon capture and storage (BECCS), are proposed as essential mitigation options (Fuss *et al.*, 2014; Clarke *et al.*, 2014). However, large-scale bioenergy and carbon capture deployment presents challenges and requires significant upscaling efforts (Creutzig *et al.*, 2014; Le Quéré *et al.*, 2014; Ciais *et al.*, 2013).

Parallel to climate change mitigation, the circular economy is recognized as a promising approach to address global sustainability pressures (Ellen MacArthur Foundation, 2014; European Commission, 2014). Circular economy strategies involve boosting recycling, preventing material loss, creating jobs, and reducing greenhouse emissions and environmental impacts (European Commission, 2014). The concept of a circular economy, rooted in ecological economics, emphasizes the complete or nearly complete internal cycling of materials and the recognition of the limits to resource and energy use (Ayres, 1994; Commoner, 1971). Transitioning from a linear business model to a circular economy paradigm requires a shift in focus from generating profits from selling artifacts to generating profits from material and product flows over time (Bakker *et al.*, 2014).

2.2 An overview of lignin

2.2.1 Definition, structure, and properties of lignin

Lignin, the second most abundant natural biopolymer after cellulose, plays essential roles in plant adaptation, providing structural integrity, stiffness, and strength to the cell wall (Chabannes *et al.,* 2001; Jones *et al.,* 2001). It also waterproofs the cell wall, facilitating water and solute transport, and contributes to plant defense against pathogens (Sarkanen and Ludwig, 1971). Lignin is a complex aromatic heteropolymer derived from a few monomers; p-coumaryl alcohol, coniferyl alcohol, and sinapyl alcohol (Freudenberg and Neish, 1968). Incorporation of these monolignols results in p-hydroxyphenyl, guaiacyl, and syringyl phenylpropanoid units within the lignin polymer (Campbell and Sederoff, 1996). Although dicotyledonous angiosperm (hardwood) lignins predominantly consist of guaiacyl and syringyl units with traces of p-hydroxyphenyl units, and gymnosperm (softwood) lignins mainly comprise guaiacyl units with low levels of p-hydroxyphenyl units, grass lignins incorporate comparable levels of guaiacyl and syringyl units and more p-hydroxyphenyl units (Baucher *et al.,* 1998).

It has been observed that lignins can incorporate other monomers derived from truncated monolignol biosynthesis, resulting in the formation of novel cyclic structures, such as benzodioxanes (Ralph *et al.,* 2001a; Boerjan *et al.,* 2003). These findings challenge previous assumptions about the limited number of lignin structures and provide valuable insights into the complexity and diversity of lignin composition.

2.2.2 Sources and availability of industrial lignin

Lignocellulosic biomass is a widely utilized resource on a global scale, contributing to the production of bioenergy and various value-added products. (Cao *et al.,* 2018; Sagues *et al.,* 2018). Traditionally, lignin, a component of this biomass, was considered a low-value waste product. However, recent advancements have revealed the potential to convert it into value-added products (Ragauskas *et al.,* 2014; Luo and Abu-Omar, 2017). The pulp and paper industry stands out as a considerable source of lignin, generating an annual output of 50–70 million tons, with an estimated increase to 225 million tons per year by 2030 (Luo and Abu-Omar, 2017; Mandlekar *et al.,* 2018). Unfortunately, the production of paper results in the discharge of large volumes of wastewater, averaging around 695.7 million cubic meters globally (Elango *et al.,* 2017). This effluent contains lignin and its derivatives and threatens aquatic life due to its toxicity (Raj *et al.,* 2014; Haq and Raj, 2020). Various physical and chemical techniques have been developed to address this environmental concern by removing lignin from paper mill wastewater (Kamali and Khodaparast, 2015).

One of the primary sources of industrial lignin is the kraft pulping process, which yields KL as a by-product. Annually, this process generates 50–90 million tons of KL, primarily used for energy production, while only around 2% is employed producing value-added products (Bajpai, 2018; Christopher, 2012). Another standard method for lignin production is the sulfite process, which produces approximately 7 million tons of sulfite lignin annually. However, the dominance of kraft pulping has led to the displacement of sulfite lignin production in Japan, North America, and Europe, although it remains prevalent in China and India (Lora, 2008). Soda lignin, generated as a co-product from various non-wood fibers through the soda anthraquinone process, finds applications in South American and Asian developing countries, particularly in producing paper, packaging materials, and cardboard (Lora, 2008). Another type of lignin is organosolv lignin. Organosolv is extracted from pulp using delignifying organic solvents (Haq *et al.,* 2020). This process breaks the α-aryl ether bonds, and cleaves, to a lesser extent, the β-aryl ether bonds (Lancefield *et al.,* 2017). Organosolv lignin exhibits desirable properties such as relative hydrophobicity, low molecular weight, low ash and carbohydrate content, and the absence of sulfur, making it attractive for various applications (Bauer *et al.,* 2012; Zijlstra *et al.,* 2019).

2.2.3 Challenges and limitations of lignin valorization

Lignin valorization has emerged as a significant challenge in pursuing sustainable and profitable lignocellulosic biorefineries (Xie *et al.,* 2014). By utilizing lignin-containing biorefinery waste to make valuable products, it is possible to enhance CO_2 mitigation, achieve net energy gain, improve waste management, and enhance the cost-effectiveness of biofuels (Ragauskas *et al.,* 2014). However, lignin depolymerization faces fundamental challenges due to its complex nature as a racemic, cross-linked, and highly heterogeneous aromatic macromolecule (Xie *et al.,* 2015). Moreover, the significant variations in lignin content and composition among different plants further complicate the design of efficient lignin depolymerization processes (Xie *et al.,* 2016).

While various chemical and thermochemical processes for lignin depolymerization have been developed, most involve high temperature, high pressure, and high energy costs while also generating inhibitors for microbial growth (Upton and Kasko, 2016; Panday and Kim, 2011; Wang *et al.,* 2013). Enzymatic lignin depolymerization, on the other hand, offers the advantage of mild conditions and potentially fewer inhibitors for microbes (Xie *et al.,* 2016). However, this approach currently yields a low amount of fragmented and soluble lignin, primarily due to inefficient electron transfer during the redox reaction (Zhao *et al.,* 2016).

The recalcitrant nature of lignin poses a significant challenge for biotechnologies aiming to produce commodity chemicals from lignocellulose sustainably (Robinson, 1990; Janusz *et al.*, 2017; Floudas *et al.*, 2012). Biological depolymerization and modification of lignin have mainly focused on aerobic systems, as lignin-degrading organisms, such as white rots, thrive in oxygen (Beckham *et al.*, 2016). Most characterized lignin-modifying enzymes are limited in diversity and rely on oxygen-dependent mechanisms, making lignin deconstruction in anaerobic environments unlikely (Janusz *et al.*, 2017; Pollegioni *et al.*, 2015). While aerobic bacteria produce some lignin-active enzymes, no known lignin-active enzyme has been identified in anaerobic organisms (Pollegioni *et al.*, 2015; Silva *et al.*, 2021).

The research and development of translational biorefineries have become a global effort driven by energy security, rural development, and environmental concerns (Ragauskas *et al.*, 2014). In the United States alone, it has been suggested that over 1.3 billion tons of biomass can be sustainably produced from agricultural and forestry sources, which, when coupled with advanced biomass-conversion technologies and land-use changes, can meet the nation's liquid transportation fuel needs without impacting food, feed, or fiber production (Perlack and Stokes, 2011; Nonhebel, 2005). Lignin is the only abundant renewable feedstock comprised of polymerized aromatic compounds (Tuck *et al.*, 2012). Despite considerable research efforts focused on converting lignin into chemicals, materials, and fuels, the translation of fundamental research into commercial practice has been limited (Ragauskas *et al.*, 2014).

To facilitate lignin modification, researchers have extensively investigated reducing lignin levels or altering its structure in plants, aiming to enhance processes such as pulping, forage digestibility, and bioenergy feedstock development (Reddy *et al.*, 2005; Dien *et al.*, 2009). Various approaches have been explored to reduce lignin levels. For example, the conversion of L-phenylalanine to primary monolignols involves eleven enzymes, many of which have been targeted for down-regulation to develop plants with reduced lignin levels (Vanholme *et al.*, 2012; Van Acker *et al.*, 2013; Li *et al.*, 2003). Another approach to effectively decrease lignin levels is to target pathways that lead to monolignol biosynthesis precursors, such as C1 metabolism for methyl group supply, manipulation of transcription factors, or the introduction of engineered enzymes that generate non-polymerizable monolignol analogs (Zhang *et al.*, 2012; Shen *et al.*, 2002). While these strategies have improved biomass digestibility, they sometimes compromise plant growth (Gallego-Giraldo *et al.*, 2011). Nevertheless, even

a 50% or less reduction of lignin from wild-type levels has been shown to eliminate the need for pre-treatment in efficient saccharification processes (Chapple *et al.,* 2007).

Two critical factors must be addressed to exploit lignin's potential in biorefineries: the ease of extracting lignin from other cell wall polymers and the lignin structure's suitability for downstream processing (Ragauskas *et al.,* 2014). Current lignocellulosic biorefineries generate lignin-rich streams by either extracting plant carbohydrates, leaving lignin in the solid residue, or pretreating biomass to extract lignin before carbohydrate conversion (Poursorkhabi *et al.,* 2013; Laskar *et al.,* 2013). Pre-treatments may involve the use of dilute acids, hot water, or high pH conditions to break down hemicellulose and increase cellulose accessibility while leaving lignin in the solid residue (Humbird *et al.,* 2012; Ragauskas *et al.,* 2014).

Lignin's diverse industrial applications include synthesizing plant-derived plastics, composites, engineering plastics, thermoplastic elastomers, polymeric foams, and membranes that exhibit comparable properties to petroleum-derived products (Chung and Washburn, 2013). Moreover, lignin is an additive for cement, dust suppression, drilling fluids for oil recovery, and expanders for lead batteries (Lora, 2008; Hirai *et al.,* 2009; DeAngelis and Reale, 2006). However, lignin depolymerization presents significant challenges due to the diverse bond strengths found in C-O and C-C linkages, as well as the propensity of low-molecular-weight species to undergo recondensation, leading to the formation of more recalcitrant compounds (Ragauskas *et al.,* 2014). These complexities hinder efficient lignin breakdown into smaller, usable components. Furthermore, regarding chemical production using lignin, ensuring compliance with stringent product purity specifications remains uncertain (Ragauskas *et al.,* 2014). Achieving the required purity level for lignin-derived chemicals poses a significant hurdle in valorization.

One of the major obstacles in using lignin lies in determining if there are economically viable pathways for converting lignin into value-added fuels and chemicals (Ragauskas *et al.,* 2014). Whether lignin can be efficiently transformed into high-value products while maintaining cost-effectiveness and sustainability remains a critical concern. Despite these challenges, potential routes for lignin conversion to chemicals hold promise for enhancing overall economics and sustainability in integrated biorefineries. For instance, the conversion of lignin into 1,4-butanediol and adipic acid has shown improvements in process economics and the potential to reduce greenhouse gas emissions significantly compared to lignin-based electricity production (Davis *et al.,* 2013). These developments demonstrate the potential for

lignin to contribute to a more sustainable and economically viable bio-based industry. Achieving commercial vanillin production from lignin sets a powerful precedent for future advances in lignin valorization (Araujo *et al.,* 2010). It highlights the potential for lignin to serve as a valuable source for synthesizing high-demand compounds, thereby expanding its applications and economic value.

Hydrothermal depolymerization and catalytic liquefaction of lignocellulosic biomass have shown promise in replacing petroleum-derived chemicals with more sustainable alternatives (Huber *et al.,* 2006). However, most current depolymerization and liquefaction processes are conducted heterogeneously, necessitating strict conditions regarding solvent, temperature, and pressure (Long *et al.,* 2012). To efficiently transform lignocellulosic biomass into fuels and chemicals, shifting from using lignin primarily for combustion to producing valuable chemicals and biomaterials is essential (Matsakas *et al.,* 2018). The recovery of high-purity lignin plays a vital role in this process, as the obtained lignin should ideally be free from extensive modifications that often hinder its utilization (Parsell *et al.,* 2013). However, current pre-treatment technologies often fail to yield high-purity lignin and, due to their harsh conditions, result in modifications of the lignin molecule (Parsell *et al.,* 2013). Despite KL's potential for industrial applications, its heterogeneous structural features severely limit its utilization in specific applications (Ponnuchamy *et al.,* 2020).

Hydrolysis lignin (HL) is a by-product obtained from processes in cellulosic ethanol plants, consisting primarily of lignin (up to 90%) alongside unreacted cellulose, as well as mono- and oligosaccharides (Yuan *et al.,* 2011).

Alkaline conditions have been used for a long time in the paper industry to fractionate lignocellulosic biomass (Dixon, 1948; Dahl, 1884). Two main processes, the Kraft and soda processes, rely on alkaline chemicals to dissolve lignin, low molecular weight hemicelluloses, and other extractives from wood (Christensen, 1982). NaOH is the preferred alkali due to its high extraction yields for lignin (60-80%) and hemicelluloses (50%) (Kim *et al.,* 2016; Peng *et al.,* 2012). Adequate alkali concentration is vital as insufficiently high alkalinity is ineffective for catalyzing cellulose/lignin hydrolysis and may also affect the reaction pathways (Karagöz *et al.,* 2006; Knill and Kennedy, 2003). However, increasing the loading of NaOH to 10% (w/w) of the HL substrate can lead to efficient depolymerization of HL and a 55.6% yield by weight of depolymerized HL with low molecular weight (Knill and Kennedy, 2003). Lignin is normally insoluble under neutral or acidic conditions but can be solubilized and depolymerized in alkaline conditions. Acidic moieties such as carboxylic or phenolic

groups that are ionized in alkaline media contribute to solubilization, while hydrolysis occurs from the cleavage of β-O-4 ether bonds in polyphenolic units (Sun *et al.,* 1995; Lora and Glasser, 2002). Phenolic monomers, such as ferulic and p-coumaric acid, formed under alkaline conditions, can be solubilized and used as food additives in cosmetic and pharmaceutical products (Oriez *et al.,* 2020). Alkaline solutions are also suitable for valorizing lignin for synthesizing phenolic resins, as the lignin produced by alkaline fractionation is sulfur-free, unlike the lignin produced by Kraft and sulfite pulping processes. This feature is beneficial for further chemical activation and offers valorization pathways such as fuel additives or bio-based polymers (adhesives and asphalt extenders) (Kim *et al.,* 2016). While $Ca(OH)_2$ is commonly employed for fractionation under alkaline conditions, its fractionation effect is not as strong as NaOH or ammonia (Peng *et al.,* 2012; Chaturvedi and Verma, 2013).

Acid fractionation, specifically using sulfuric acid at loading rates of 2-4% by weight, is a well-known technique for the hydrolysis of lignocellulosic biomasses. This approach offers several advantages, including high catalytic activity, lower corrosion rates compared to other acids, and a favorable balance between efficient liquefaction and effective retardation of recondensation reactions (Hu *et al.,* 2014). However, it has been observed that the yield of depolymerized HL obtained under acidic conditions is significantly lower than using water as a solvent under neutral conditions. Moreover, the depolymerized HL produced through acid-catalyzed cleavage of alkyl-aryl ether linkages in lignin and breakage of 1,4'-β-glycosidic bonds in cellulose has a much lower molecular weight than lignin obtained via depolymerization in neutral media (Mahmood *et al.,* 2015; Xu *et al.,* 2012). Despite these challenges, acid fractionation remains the preferred method for lignocellulosic biomasses in various ethanol production processes (Cardona *et al.,* 2010; Oriez *et al.,* 2019).

Organosolv pre-treatment/fractionation, which involves the use of mixtures of organic solvents, water, and optionally a catalyst at temperatures ranging from 100 to 250 °C, is considered an auspicious method for biomass delignification and fractionation (Matsakas *et al.,* 2018b; Sun *et al.,* 2018). This process yields three distinct streams: a cellulose-rich solid stream, a liquid stream containing solubilized hemicellulose, and a solid stream of high-purity lignin (Raghavendran *et al.,* 2018). The resulting lignin demonstrates favorable characteristics, such as low ash content, absence of sulfur, and a preserved structure resembling natural lignin, including the retention of β-ether bonds (Azadi *et al.,* 2013; Matsakas *et al.,* 2018b; Sun *et al.,* 2018). Various organic solvents, including alcohols, ketones, esters, ethers, chlorinated solvents, and alkenes, have been examined for this purpose (Park *et al.,*

2018; Duval *et al.,* 2016). The solubilization yield of lignin in organic solvents depends on the solvent's chemical properties as well as the characteristics of the lignin source, such as molecular mass, monomeric composition, and chemical functionality (Dodd *et al.,* 2015).

Steam explosion treatment (SE) is an efficient and eco-friendly method for biomass pretreatment, developed commercially for bioethanol production (Alvira *et al.,* 2010). During SE treatment, the lignocellulosic biomass undergoes high-pressure and high-temperature steam treatment, followed by a release of explosive pressure (Hendricks and Zeeman, 2009). This process causes hydrolysis and redistribution of biomass components, improving the enzymatic digestibility of cellulose and polysaccharides for biofuel production through fermentation (Sharma *et al.,* 2015).

2.3 Characteristics and applications of *Pseudomonas putida*

2.3.1 Overview of *Pseudomonas putida*

The *Pseudomonas* genus is known for its versatility and adaptability, which have allowed its members to thrive in hostile and fluctuating environments (Silby *et al.,* 2011). *P. putida*, one of the more than 255 described species in this genus (Parte, 2018), is commonly found in polluted soil and aquatic environments and has been extensively studied for its biodegradation abilities and stress-tolerance mechanisms (Udaondo *et al.,* 2012; Ramos *et al.,* 2001; Timmis *et al.,* 1994). Its adaptability is attributed to various features, such as high genetic plasticity and broad metabolic, transport, signaling, and regulatory capabilities (dos Santos *et al.,* 2004). This biochemical versatility has made *P. putida* an excellent candidate for industrial biocatalysis (Nikel and de Lorenzo, 2018).

Within the taxonomic group of *Pseudomonas*, more than 255 species have been described (Parte, 2018). The genus was initially classified into five rRNA subgroups using genetic techniques, with *Pseudomonas sensu stricto* remaining in the RNA group I within the Gammaproteobacteria (Palleroni *et al.,* 1973; Kersters *et al.,* 1996; Palleroni, 2003). Further analysis through multi-locus sequence analyses (MLSA) identified ten distinct groups within the genus *Pseudomonas sensu stricto,* including *P. fluorescens, P. syringae, P. lutea, P. putida, P. anguilliseptica, P. straminea, P. aeruginosa, P. oleavorans, P. stutzeri, and P. oryzihabitans.* Each group encompasses various species (Mulet *et al.,* 2010).

P. putida, previously known as *Bacillus putidus*, was isolated in 1889 (Palleroni, 2005; Migula, 1984). It exhibits optimal growth between temperatures of 25-30°C and can be dis-

tinguished from *P. aeruginosa* by its inability to liquefy gelatin, produce phenazine pigments, denitrify, egg-yolk reactions, or grow at 41°C (Palleroni, 2005). *P. putida* strains are not known to be animal or plant pathogens and are considered environmentally benign saprophytes (Timmis, 2002).

The first fully sequenced *Pseudomonas* strain was *P. putida* strain KT2440 (Nelson, 2002). This strain, derived from the highly studied toluene-degrading bacterium *P. arvilla* strain mt-2, has been extensively characterized (Bagdasarian *et al.*, 1981; Nakazawa, 2002; Williams and Murray, 1974). KT2440 has significantly contributed to various areas of research, including biodegradation, stress-tolerance mechanisms, rhizosphere colonization, global and specific transcription regulation, and biotechnological applications (Nikel and de Lorenzo, 2018; Martínez-García *et al.*, 2014; Nikel *et al.*, 2014).

2.3.2 Industrially relevant genetic and metabolic features

Pseudomonas putida has become a valuable "virtually domesticated" laboratory workhorse due to its distinct characteristics obtained through synthetic biology (Nikel *et al.*, 2014). Setting itself apart from other microorganisms, *P. putida* naturally possesses a remarkable array of biochemical functions and adaptable metabolisms (Poblete-Castro *et al.*, 2017). Its relatively high GC content makes *P. putida* suitable for expressing genes from GC-rich bacterial clades, such as actinobacteria or myxobacteria, which are known for their abundance of secondary metabolite biosynthesis gene clusters (Loeschcke and Thies, 2015).

In addition, *P. putida* offers an extensive range of cofactors, particularly beneficial for biosynthesis processes, as well as a versatile metabolism with diverse enzymatic capabilities for production purposes (Blank *et al.*, 2010; Tiso *et al.*, 2014; Nelson *et al.*, 2002). The bacterium also demonstrates a high tolerance to xenobiotics, including antibiotics and organic solvents, owing to complex adaptations such as efficient efflux systems that are activated in the presence of xenobiotics (Fernández *et al.*, 2009; Simon *et al.*, 2014), making it an ideal producer of such compounds.

Analysis of the genome sequence of *P. putida* KT2440, revised in 2016, confirmed the absence of conspicuous virulence factors among the 5592 coding sequences present (Belda *et al.*, 2016). The updated genome annotation of strain KT2440 revealed novel biochemical functions not previously identified in *P. putida*. These included catabolic pathways for various carbon, nitrogen, and phosphorus sources, and rich secondary metabolism intricately connected to a robust core biochemistry (Nikel and de Lorenzo, 2018).

P. putida KT2440 possesses a cyclic metabolic architecture known as the EDEMP cycle, formed by the combined activity of enzymes from the Entner-Doudoroff pathway, the pentose phosphate pathway, and the incomplete Embden-Meyerhof-Parnas route (Nikel and de Lorenzo, 2018). This metabolic architecture allows *P. putida* to achieve high rates of NADPH regeneration through partially recycling triose-phosphates, particularly when growing on hexose sugars. The regulation of this metabolic property is influenced by the presence and extent of oxidative stress conditions (Nikel *et al.*, 2015a).

Chakrabarty obtained the first US patent for a genetically modified organism by conducting directed bacterial conjugation experiments with *P. putida* in 1981. These experiments resulted in strains capable of breaking down a significant portion of hydrocarbons found in crude oil spills at remarkably accelerated rates compared to previous descriptions (Chakrabarty *et al.*, 1975).

2.3.3 Utilization of *Pseudomonas putida* for lignin valorization

Lignin valorization, which involves the depolymerization and upgrading of lignin subunits into value-added products, is a crucial process in achieving environmental sustainability and economic viability for various industrial applications (Anthony *et al.*, 2019; Wu *et al.*, 2018). Compared to traditional fossil routes and second-generation biorefineries, the biological conversion of lignin and lignin-model compounds offers a more sustainable alternative (Corona *et al.*, 2018).

In the pursuit of lignin valorization, cascaded processes have shown promise. These processes involve the initial depolymerization of lignin into mixtures of small aromatics, followed by the biological conversion of these aromatics into valuable chemicals (Linger *et al.*, 2014). One particularly appealing application is the conversion of aromatics into *cis,cis*-muconic acid (Xie *et al.*, 2014b). The bacterial production of muconic acid using lignin-based carbon sources is gaining attention as muconic acid can be used as a precursor for the synthesis of adipic acid and terephthalic acid, which are raw materials for plastics production (Becker and Wittmann, 2019; Becker *et al.*, 2018; Vardon *et al.*, 2016).

P. putida is a highly versatile bacterium with the ability to process aromatic compounds through biochemical routes, as recognized by several studies (Salvachúa *et al.*, 2020; Lee *et al.*, 2019; Corona *et al.*, 2018; Nikel and de Lorenzo, 2018). One of the notable capabilities of *Pseudomonas* is the secretion of oxidative enzymes that induce the degradation of lignin

and generate lignin oligomers (Wang *et al.,* 2018). These generated oligomers are then catabolized through aromatic pathways (Salvachúa *et al.,* 2020; de Gonzalo *et al.,* 2016; Rahmanpour and Bugg, 2015).

P. putida KT2440, in particular, has demonstrated remarkable potential in utilizing lignin and lignin compounds as carbon sources to synthesize and store polyhydroxyalkanoates (PHAs) (Linger *et al.,* 2014). It possesses a specific β-ketoadipate route that enables using monomeric lignin derivatives as the sole carbon and energy source for producing value-added products (Wang *et al.,* 2018). The metabolic pathway involving this route leads to the production of protocatechuate and catechol as end products, which can be further transformed into β-carboxymuconate and muconate, respectively, by enzymes protocatechuate 3,4-dioxygenase and catechol 1,2-dioxygenase (Dikshit *et al.,* 2020). Catechol, in particular, plays a central role in the production of *cis,cis*-muconic acid, which is a target product and can be directly converted by catechol-1,2-dioxygenase (Nikel and de Lorenzo, 2018).

While *P. putida* KT2440 has demonstrated the utilization of lignin for PHA production, further research and technological development are needed to improve the yield and quality of PHAs (Kumar *et al.,* 2021). Deploying biotechnological tools in bacterial PHAs production offers opportunities for modifying the PHA biosynthesis pathway through gene insertion or deletion (Kumar *et al.,* 2020). The inactivation of muconate cycloisomerase in *P. putida* enables the accumulation of muconic acid from benzoate and toluene via the catechol branch of the β-ketoadipate pathway (van Duuren *et al.,* 2011; Chua and Hsieh, 1990).

Engineered *P. putida* strains capable of producing *cis,cis*-muconic acid were the first successful case of lignin-to-Nylon-6,6 production through a cascaded biochemical and chemical integrated process. However, the dependence on sugars compromises the industrial value of lignin-derived substrates. Therefore, novel metabolic engineering strategies are being explored to overcome this limitation and shift towards utilizing lignin hydrolysates as the sole carbon source for the process (Nikel and de Lorenzo, 2018).

2.4 Project objectives

This research project encompassed a preliminary investigation into HL fractionation, bacterial culture growth, chemical characterization, strain selection, growth optimization, and genetic modification. The primary objective was to determine the most effective fractionation method to maximize the amount of HL in solution, while concurrently promoting bacterial culture growth of *P. putida*. Various fractionation techniques were employed and evaluated

for their efficiency in solubilizing HL while creating an optimal environment for *P. putida* growth.

Additionally, a tentative characterization was conducted on the chemical composition of each fractionated HL batch. The analysis focused on identifying monomers in the benzoate degradation pathway and other major peaks detected through HPLC. Changes in the composition of the *P. putida* cultures were monitored over time. Moreover, this project focused on identifying specific strains of *P. putida* and other candidate strains that could either break down or produce targeted HL-derived compounds, with a particular emphasis on *cis,cis*-muconic acid. Strains are screened based on their ability to catabolize available compounds or synthesize desired compounds.

This project also sought to identify the optimal growth conditions for select strains and optimize their growth and productivity. Factors such as temperature, pH, nutrient availability, and other environmental parameters were carefully optimized to enhance the targeted HL-derived compound production.

Furthermore, the project aimed to pinpoint the most appropriate genetic targets for modification and further optimize the synthesis of *cis,cis*-muconic acid by channeling metabolic precursors towards it and minimizing its downstream catalysis. By studying the underlying genetics and metabolic pathways of *P. putida*, specific genetic elements were identified as potential targets for modification.

By examining the partial chemical makeup of the HL fractions, valuable insights were gained regarding the potential transformations that HL undergoes during the bacterial culture process. The outcomes of this study contribute to the advancement of industrial HL valorization strategies and provide perspective into the potential industrial applications of *P. putida* in HL-derived compound production.

3 THE AIMS OF THE THESIS

- To determine the most effective fractionation method that maximizes the amount of HL-derived target compounds in solution while promoting bacterial culture growth of *P. putida*.
- To quantify the target compounds of interest of each fractionated HL batch and monitor the changes in the composition of the *P. putida* cultures over time.
- To identify *P. putida* and other candidate strains capable of catabolizing or producing specific HL-derived compounds of interest, focusing on CCMA
- To investigate the optimal growth conditions for selected *P. putida* strains.
- Determine the most appropriate genetic targets for modification to optimize CCMA synthesis and employ genetic recombineering techniques to achieve CCMA accumulation.

4 EXPERIMENTAL PART

4.1 MATERIALS AND METHODS

4.1.1 Growth conditions, strains, and media

All *P. putida* cultures were incubated at 30 °C, and liquid cultures were shaken at 230 rpm. *Escherichia coli* carrying the pGNW2 plasmid (Table S1) was grown at 37 °C using Luria Broth (LB) medium supplemented with 50 μg·mL^{-1} kanamycin. Rich complex undefined medium (LB) was prepared using 10 g·L^{-1} tryptone, 10 g·L^{-1} NaCl, and 5 g·L^{-1} yeast extract. Wx/M9 minimal medium was based on Ariaki *et al.* (2020) containing 5.7156 g·L^{-1} KH_2PO_4, 3.407 g·L^{-1} Na_2HPO_4, 1.0163 g·L^{-1} NH_4Cl, 0.526 g·L^{-1} NaCl, and 1x trace elements solution containing 26.875 mg·L^{-1} MgO, 0.128 ml·L^{-1} HCl, 5 mg·L^{-1} $CaCO_3$, 1.125 mg·L^{-1} $FeSO_4{\cdot}7H_2O$, 3.6 mg·L^{-1} $ZnSO_4{\cdot}7H_2O$, 2.8 mg·L^{-1} $MnSO_4{\cdot}H_2O$, 0.625 mg·L^{-1} $CuSO_4{\cdot}5H_2O$, 0.7 mg·L^{-1} $CoSO_4{\cdot}7H_2O$, and 0.15 mg·L^{-1} H_3BO_3. Modified defined minimal medium (MMPAM) formulation was based on Borrero-de Acuña *et al.* (2021) containing 6 g·L^{-1} KH_2PO_4, 7.09 g·L^{-1} Na_2HPO_4, 5 g·L^{-1} $(NH_4)_2SO_4$, and 0.5 g·L^{-1} NaCl (Table S2). The trace element composition remained the same. Minimal media containing fractionated crude HL were named in batches (Table S3).

4.1.2 Plate reader growth assays

Precultures were made by inoculating 5 mL LB medium with a single colony from an LB agarose plate. The tubes were incubated and shaken at 30 °C and 230 rpm overnight in an orbital shaker. Half the culture volume was discarded and replaced with fresh LB medium. The cultures were then incubated and shaken for 90 minutes (approximately two doubling times) under the same parameters to ensure the cultures were in log phase. Osmotic stress tolerance assays were carried out using Wx/M9 medium supplemented with glucose or xylose at 2%, 4%, 6%, 8%, 10%, 12%, 15%, and 20% in 96-well microtiter plates with optically clear lids. pH tolerance assays were also performed using Wx/M9 medium supplemented with glucose at 6% concentration. The pH of the samples was adjusted to 7.1, 7.3, 7.5, 7.7, 7.9, 8.1, 8.3, 8.7, 9.1, and 9.5 with NaOH. The OD_{600} values of the precultures were measured for each strain to ensure the starting inoculates were the same and adjusted with sterile milliQ water. 2 µL of inoculum was combined with 198 µL medium in each well. All microtiter assays were incubated at 30 °C in a BioTek Synergy MX plate reader, and OD_{600} readings were taken every 15 minutes for 25 hours. Growth rates and curves were calculated from triplicate samples from each plate reader experiment.

4.1.3 Shake flask cultivations

4.1.3.1 Batch cultivations

Precultures were prepared under the same parameters as the plate reader growth assay except that Wx/M9 minimal medium at 2% glucose concentration was used. Precultures were inoculated into media with a starting OD_{600} of 0.1. The medium-to-flask volume ratio was 1:5 in all experiments. The cultures were incubated and shaken at 30 °C and 230 rpm. Media composition varied depending on the experiment being run and the cultures were periodically sampled to measure OD_{600} and pH, total sugars, organic acids, and selected HL monomer composition by HPLC. All cultures were grown in duplicate or triplicate.

4.1.3.2 Simulated fed-batch cultivations

The simulated fed-batch media were prepared with components from EnPresso GmbH (Berlin, Germany). These components consisted of a powder-based polysaccharide added to the medium and an enzyme to release glucose from the polysaccharide over time. This allowed for simulated carbon-limited fermentation. Precultures were prepared as described for the plate reader assays. A 200 $g \cdot L^{-1}$ stock EnPresso Pump 200 substrate solution was made using Wx/M9 medium and sterilized through a 0.2-micron bottlecap filter. Fractionated HL medium was supplemented with the stock solution to 20 $g \cdot L^{-1}$ in sterile flasks. The volume varied between 50 mL and 100 mL depending on the length of the cultivation and the number of samples to be collected. Enzyme reagent 0.6% was added at hour 4 or 6 post-inoculation depending on the initial glucose concentration in the media and the doubling time under the culture environment. The OD_{600} of the precultures was measured, and the flasks were inoculated to a working OD_{600} of 0.1. Samples were taken periodically to measure the OD_{600}, pH, and for composition analysis by HPLC.

4.1.4 Preparation of fractionated HL

The reactive extrusion crude HL used in this study is obtained from Fibenol OÜ. The dried crude HL powder was used for further fractionation upon arrival from the biorefinery.

4.1.4.1 Wx/M9 fractionation

One liter of Wx/M9 medium was alkalized to pH 11.03 with 3 g of NaOH flakes. The alkaline medium was slowly added to dry crude HL while vigorously stirring at a proportion of 600 g medium to 100 g dry crude HL. The mixture was continuously stirred for 30 minutes with a magnetic stir bar, and the resulting 680 mL mixture was divided into conical tubes and centrifuged at 110K rpm for 5 minutes. The supernatant from each conical tube was

filtered through a 0.2 µm bottlecap filter into a sterile glass jar. Samples were taken for pH and HPLC analysis. The remaining volume was used for flask cultivations.

4.1.4.2 Alkaline extractions and steam explosion

Three HL fractionations were performed using Wx/M9 media alkalized with NaOH, KOH, and NH_4OH, and one using a non-alkalized Wx/M9 medium. To make the alkalized media, 240 g of Wx/M9 were adjusted to pH 11 with 10 M NaOH and KOH, and to pH 10.5 with 10 M NH_4OH. Each was then slowly combined with 40 g dry crude HL and vigorously agitated for 45 minutes with a magnetic stir bar. The non-alkalized fractionation was conversely performed by combining 60 g Wx/M9 with 10 g dry crude HL. 120 mL of each resultant alkaline slurry and 20 mL of the resultant non-alkaline slurry were added to flasks and autoclaved at 121 °C for 20 minutes. The autoclaved slurries were used in simulated fed-batch duplicate cultivations. EnPresso Pump 200 substrate solution was added at hour 4 at a final concentration of 20 $g \cdot L^{-1}$. Samples were taken before and after autoclaving and periodically during cultivation for analytics, and the pHs were recorded (Table S4).

4.1.4.3 Fractionation with MMPAM

A 1 L lab scale crude HL fractionation was performed using the modified minimal media formulation MMPAM, described in section 2.1. The fractionation was performed by combining 443 g of MMPAM medium with 74 g dry crude HL in one 1 L bioreactor and agitating at 1000 rpm for 3 hours at 25 °C. The resultant slurry was centrifuged for 30 minutes at 4200 rpm, and the supernatant was filtered through a 0.2 µm bottlecap filter. The pH was subsequently normalized to 7.4 with 2.81 g of 10 M NH_4OH, and a 50 mL sample was taken for GC-MS analysis. The remaining volume was autoclaved at 121 °C for 20 minutes and subsequently used for analytics, simulated fed-batch cultivation, and *Pseudomonas* strain screening experiments. This batch of fractionated HL medium is recorded as PAM511-0001.

4.1.5 Genomic DNA extraction and PCR

4.1.5.1 Genomic DNA and pGNW2 plasmid extraction

Four colonies of KT2440 were picked and grown overnight in 5 mL of LB media. The saturated cultures were centrifuged at 3250 RPM for 10 minutes at room temperature (RT), and the supernatant was discarded. The resulting cell pellets were stored at -20 °C overnight. The frozen pellets were thawed at RT for 10 minutes and then washed with cold phosphate-buffered saline (PBS). The cell suspension was centrifuged at 2000 RPM for 8 minutes.

Next, the cell pellet was added to 1 mL of lysis buffer (10 mM Tris-HCl, 400 mM NaCl, and 2 mM Na_2EDTA, pH 8.2). The cells were washed once with PBS by resuspending them and centrifuging at 2000 RPM for 8 minutes at RT. The cell pellet was subsequently resuspended in 600 µL of lysis buffer.

For lysis and enzyme treatment, 40 µL of 10% SDS, 100 µL of protease K solution (0.2 mg protease K in 1% SDS and 2 mM Na_2EDTA), and 7.5 µL of RNAse A stock-solution (10 $mg \cdot mL^{-1}$) were added to the cell suspension. The tube was vigorously inverted 10 times to mix the components thoroughly. The mixture was then incubated at +50 °C and 700 RPM for 1 hour.

After the incubation, 200 µL of saturated NaCl (approximately 5-6 M) was added to the tube. The contents were vigorously shaken for 15 seconds and then centrifuged at 8600 RPM at RT for 15 minutes. The resulting protein pellet settled at the bottom of the tube. 470 µL was carefully transferred to a new Eppendorf tube to collect the DNA-containing supernatant. Two volumes of room-temperature absolute ethanol (or 95% ethanol) were added to precipitate the DNA, and the tube was vigorously inverted several times. The precipitated DNA was collected by centrifugation at 10,400 RPM at RT for 15 minutes.

The supernatant was removed, and the DNA pellet was washed with 1 mL of 70% ethanol by centrifuging at 10,400 RPM at RT for 15 minutes. The supernatant was decanted, and the DNA pellet was air-dried for 5-10 minutes. The DNA pellet was then resuspended in an appropriate amount of TE buffer.

Finally, the washed DNA was placed in a 50 °C oven for 15 minutes to remove residual ethanol. The DNA was solubilized in 100 µL of autoclaved water, and its concentration was determined using a Nanodrop spectrophotometer. The recorded results for the four samples (A, B, C, and D) were as follows: A: 822.5 $ng \cdot \mu L^{-1}$, B: 481.5 $ng \cdot \mu L^{-1}$, C: 602.2 $ng \cdot \mu L^{-1}$, and D: 828.8 $ng \cdot \mu L^{-1}$ (Table S5). Samples were stored at -20 °C until use.

pGNW2 plasmid was extracted from *E. coli* with the Monarch® Plasmid DNA Miniprep Kit. The plasmid concentration was measured by nanodrop to be 60.3 $ng \cdot \mu L^{-1}$.

4.1.5.2 Muconate cycloisomerase HR amplification

The complete P. putida genome was obtained from the NCBI database and visualized using SnapGene. The annotated MCI gene (*catB*) was also obtained from the NCBI database (https://www.ncbi.nlm.nih.gov/nuccore/NC_021505.1?from=2405938&to=2407059&report=fasta). The DNA sequence is in Table S6. The primers were designed using SnapGene

for HRs between 400 and 700 bp on either side of the *catB* gene (Table S7). The upstream and downstream HRs of the *P. putida catB* gene were amplified by polymerase chain reaction (PCR) from genomic DNA extracts, prepared as described in section 3.1.5.1. The PCR was based on the New England Biolabs Protocol for Phusion® Hot Start Flex DNA Polymerase. Each 50 µL reaction contained 1x GC buffer, 200 µM dNTPs, 0.5 µM of each primer, 100 ng gDNA, and 1.0 units Phusion DNA polymerase. Amplification occurred in a SimpliAmp™ Thermal Cycler and the program was based on the Phusion High Fidelity DNA Polymerase 3-Step template, consisting of denaturing for 30 seconds at 98 °C; 40 cycles of 10 seconds at 98 °C, 15 seconds at 68 °C (annealing), 90 seconds at 72 °C (extension); one cycle of 10 minutes at 72 °C; and cooling at 10 °C.

4.1.5.3 pGNW2 plasmid linearization

The pGNW2 suicide vector was linearized using the pGNW_Gib_Lin_FW and pGNW_Gib_Lin_RV primers. The master mix composition was the same as described in section 3.1.5.2. Linearization and amplification occurred in a SimpliAmp™ Thermal Cycler and the program was based on the Phusion High Fidelity DNA Polymerase 2-Step template, consisting of denaturing for 30 seconds at 98 °C; 35 cycles of 10 seconds at 98 °C, 3 minutes at 72 °C (annealing/extension); one cycle of 10 minutes at 72 °C; and cooling at 10 °C.

4.1.5.4 Protocatechuate 3,4-dioxygenase HR amplification

The annotated sequence of the alpha (*pcaG*) and beta (*pcaH*) subunits were obtained from https://www.ncbi.nlm.nih.gov/nuccore/NC_021505.1?from=826906&to=827511&report=fasta and https://www.ncbi.nlm.nih.gov/nuccore/NC_021505.1 ?from=826176&to=826895&report=fasta respectively. The primers were designed using SnapGene. The upstream HR for *pcaH* was 640 bp and the downstream HR for *pcaG* was 636 bp. Upstream HR amplification of the protocatechuate 3,4-dioxygenase gene (*pcaH*) occurred using the same instrument and PCR template described in section 3.1.5.2. The annealing temperature used was 68 °C.

4.1.5.5 DNA gel extraction and nanodrop

The DNA gel extraction was done with the FavorPrep™ Gel/PCR Purification Kit. The 1% agarose gels were excised and transferred into a microcentrifuge tube. 500 µL of FADF buffer was added to the sample. The sample was incubated at 55 °C for 10 minutes and vortexed every 2 minutes until the gel was completely dissolved. The sample was then cooled to room temperature, transferred to a FADF column and centrifuged at 11,000G for

30 seconds. The process was repeated with 750 µL of wash buffer, centrifuging at 11,000G for 30 seconds. The column matrix was dried by centrifuging at 18,000G for 3 minutes. 40 µL of warm nuclease-free water was added to the center of the FADF column membrane for 5 minutes. The DNA was eluted by centrifuging at 18,000G for 1 minute. The concentrations of the eluted DNA were determined by nanodrop.

4.1.6 Strain screening

Thirty bacterial strains (Table S37) were picked using a 1 µL sterile loop from R2A agar plates and cultivated in a 120-hour batch cultivation at 30 °C and 150 RPM, using 5 mL of the fractionated HL medium PAM511-0001. The growth media were not supplemented with glucose. Two uninoculated media blanks served as controls. Samples were collected and centrifuged for 1 minute at 13,000 RPM at 24 hours for 21 strains and 120 hours for all 30 strains. The supernatant was stored at -20 °C and subsequently thawed and diluted for HPLC analysis to determine the HL monomer composition.

4.1.7 Analytical methods

4.1.7.1 HPLC methods

The HPLC parameters for the monosaccharide and organic acid analyses were adapted from Monteiro de Oliveira *et al*. (2021) and modified slightly. For monosaccharide detection, 20 µL of the sample was injected into a Shimadzu LC-2030C 3D Plus system equipped with a Rezex^{TM} RPM-Monosaccharide Pb+2 (8%), LC column (300 X 7.8 mm) at 85 °C using a mobile phase of MilliQ H_2O at a flow rate of 0.6 mL·min^{-1} and a Shimadzu RID-20A refractive index detector. Organic acid detection analyses were performed by injecting 20 µL of sample through the same system equipped with a Rezex^{TM} ROA-Organic Acid H+ (8%), LC column (300 X 7.8 mm) at 45 °C using a mobile phase of 5 mM H_2SO_4 at a flow rate of 0.6 mL·min^{-1}. HL monomers were identified by HPLC, similar to Reyes-Rivera *et al.*, (2015). Analyses for detection of HL monomers were performed by injecting 8 µL of sample through the same system equipped with a Kinetex® 2.6 µm C18 100 Å, LC column (150 X 4.6 mm) at 45 °C using a mobile phase of 80:20:0.16 MilliQ H_2O, methanol, and formic acid (v/v/v) at a flow rate of 0.6 mL·min^{-1} and wavelength of 265 nm. Retention times for catechol and CCMA are listed in Table S8.

4.1.7.2 UV-Vis spectroscopy

A UV-Vis spectrophotometer (Thermo Scientific Evolution 160 using VisionLite 4.0 software) was used to measure the absorbance of the samples. Samples obtained from

the various HL fractionations and the fermentations with *P. putida* were filtered and stored at -20 °C to prevent degradation or contamination. To measure the absorption spectra appropriate dilutions were prepared using MilliQ water. The instrument was calibrated using a blank solution containing MilliQ water and set to the wavelength range of 200-600 nm. Each sample was measured in triplicate quartz cuvettes with a 10 mm path length.

4.1.7.3 Ion chromatography and spectrophotometry

Analysis of the concentrations of fluoride, chloride, nitrite, nitrate, bromide, phosphate, and sulfate was performed by injecting 20 µL of sample onto a Metrohm 930 Compact IC Flex system using a mobile phase of 0.1 M Na_2CO_3 and 0.1 M $NaHCO_3$. Optical density at 600 nm (OD_{600}) was measured using a Hitachi U-1800 spectrophotometer. Samples used to measure total nitrogen were prepared using the LATON® LCK138 kit, incubated in a Hach Lange LT200 instrument, and measured using a Hach Lange DR 2800 spectrophotometer.

4.1.7.4 GC-MS

The GC-MS was carried out similarly to Zhao *et al.,* 2020. A 10 mL sample of fractionated crude HL was taken at hour 0 and hour 120 during a simulated fed-batch fermentation with *P. putida* KT2240. The sample was extracted with dichloromethane (4×10 mL), washed with saturated NH_4Cl, dried with anhydrous $MgSO_4$, and concentrated. The resulting oil products were acetylated using pyridine (1 mL) and acetic anhydride (1 mL) for 4 hours. The acetylated products were dissolved in 1 mL of dichloromethane and analyzed using the Agilent 7890A GC System with Agilent 5975 Inert XL MSD with Triple-Axis Detector and Agilent DB-5MS 30m x 0.250mm 0.25 micron column.

GC-MS parameters included an inlet temperature of 300 °C, a total flow rate of Helium carrier gas at 21.1 $mL \cdot min^{-1}$, an ion source temperature of 250 °C, an interface temperature of 300 ºC, and an ion range of 45-800 (m/z). The oven program consisted of an initial temperature of 80 °C for 5 minutes, a ramp rate of 8 $°C \cdot min^{-1}$ up to 250 °C, a ramp rate of 5 $°C \cdot min^{-1}$ up to 300 °C, and a 30-minute hold at the final temperature, resulting in a total analysis time of 66.25 minutes (Zhao *et al.*, 2020).

4.2 RESULTS AND DISCUSSION

4.2.1 Strain characterization

4.2.1.1 Glucose osmolarity

Characterizing the two initial bacterial strains was essential before proceeding with other tasks in this project. The objective was to ascertain the optimal growing conditions and to investigate how the strains reacted to different osmotic stress conditions. A physiological assessment was undertaken to achieve this, involving osmolarity experiments to determine the glucose and xylose tolerances of *P. putida* KT2440 and PaW85. The osmolarity microplate experiment results demonstrated higher overall optical densities and a broader OD range (Figures 1 & S9) compared to the xylose osmolarity experiments (Figures S10 & S11). Moreover, the glucose osmolarity experiment revealed similar tD between 20 $g \cdot L^{-1}$ and 6 $g \cdot L^{-1}$ concentrations (Figures S12 & S13) and similar μ_{max} between 20 and 60 $g \cdot L^{-1}$ glucose concentration (Figures S14 and S15). Neither strain could tolerate a 200 $g \cdot L^{-1}$ glucose concentration. These results allow the glucose concentration of the HL fractionation to be adjusted to a more optimal concentration if necessary before cultivation. Exponential growth trendlines and R^2 values can be seen in the supplementary materials (S16 & S17).

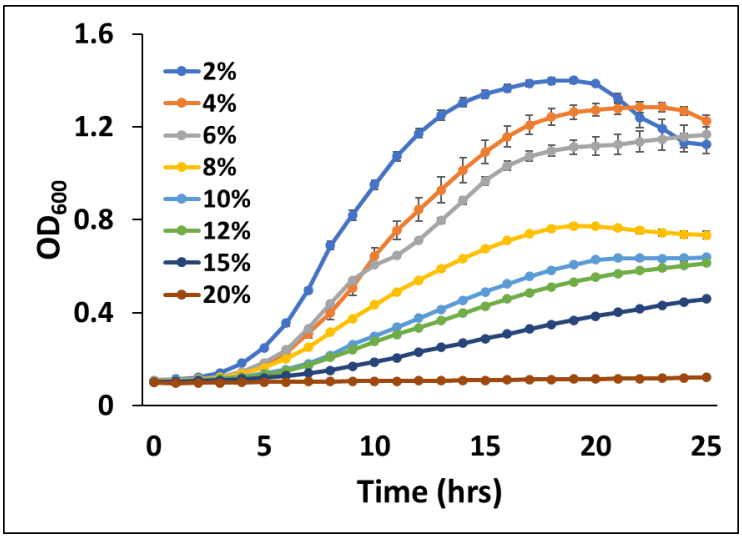

Figure 1. Glucose osmolarity profile of *P. putida* KT2440. Growth curves at varying glucose concentrations in Wx/M9 minimal medium at 30 °C pH 7.2 over 25 hours. Standard error was used for error bars.

4.2.1.2 Xylose osmolarity

The xylose osmolarity experiments exhibited minimal variation in absolute terms, with an OD range of less than 0.05. Irrespective of the xylose concentration used for cultivation, the optical densities remained consistently low for KT2440 and PaW85. However, the experiments did uncover particular distinctions between the KT2440 and PaW85 strains. Notably, the KT2440 strain exhibited the shortest doubling times within the range of 60 and 100 $g \cdot L^{-1}$ xylose concentrations, whereas PaW85 demonstrated the shortest doubling times between 40 and 80 $g \cdot L^{-1}$. It is essential to highlight that even under these conditions, tD for most cases still exceeded 24 hours (Figures S18 & S19). The μ_{max} was below 0.1 at all concentrations

for PaW85 (Figure S20), but KT2440 was approximately 0.25 at 100 $g \cdot L^{-1}$ (Figure S21). Exponential growth trendlines and R^2 values can be seen in the supplementary materials (Figures S22 & S23).

4.2.1.3 pH tolerance

Another physiological evaluation conducted to determine the ideal growth conditions for the KT2440 and PaW85 strains involved a pH tolerance investigation. This assessment employed a plate reader growth assay, wherein both strains were cultivated in Wx/M9 minimal medium containing 60 $g \cdot L^{-1}$ glucose. The selection of this concentration was based on the findings of the glucose osmolarity analysis. The strains were subjected to various pH levels ranging from 7.1 to 10. The results revealed that both strains exhibited a significantly broader pH tolerance range than initially expected (Figures 3 & S24). Notably, robust growth was observed at elevated pH levels, with comparable maximum specific growth rates between pH 7.5 and 9.5 (Figures S25 & S26). The tDs were lowest for KT2440 at pH 8.1 and 8.3 (Figure S27). PaW85 exhibited similar tDs at those pH levels (Figure S28). The strains' high pH tolerance is promising because HL is only water soluble in alkaline conditions (Puss *et al.*, 2023). Given that *P. putida* can thrive in alkaline conditions, using alkali-fractionated HL (containing abundant dissolved HL) as an effective growth medium is possible. Exponential growth trendlines and R^2 values can be seen in the supplementary materials (Figures S29 & S30).

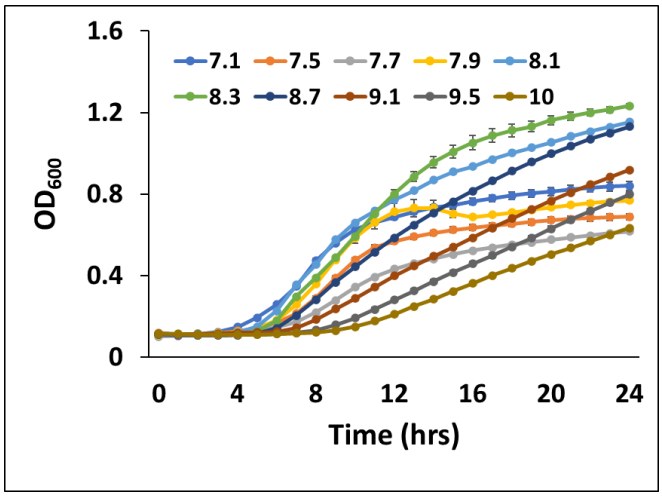

Figure 2. pH tolerance profile of *P. putida* KT2440. Growth curves at varying pH levels in Wx/M9 minimal medium at 30 °C and 60 $g \cdot L^{-1}$ glucose. NaOH was used to adjust pH. Standard error was used for error bars.

4.2.2 Preliminary fractionated HL cultivation

HL fractionation was initially performed using Wx/M9 minimal medium. The resulting solution underwent sterile filtration and was used for initial batch cultivation with *P. putida* KT2440. Samples were collected at regular 24-hour intervals and subjected to HPLC analysis to determine the concentrations of sugars. Additionally, the optical density of the cultures was measured. The outcomes of this cultivation indicated complete consumption of glucose and xylose within the initial 24 hours, with a peak optical density of approximately 4 (Figure 4). The decline in xylose concentration was unexpected since *P. putida* is not known for its ability to metabolize xylose (Bator *et al.*, 2020). These results help demonstrate the viability of fractionated HL as a substrate for *P. putida* cultivation.

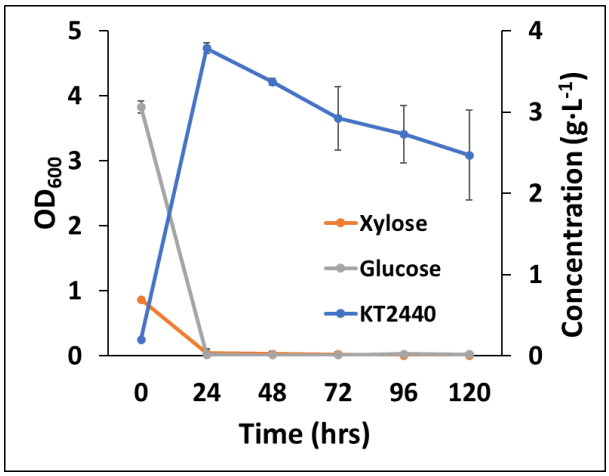

Figure 3. Growth curve and glucose and xylose utilization of *P. putida* KT2440 during 120-hour batch fermentation in Wx/M9-fractionated HL medium. Standard error was used for error bars.

4.2.3 Simulated fed-batch cultivation

The simulated fed-batch cultivation technique involves maintaining carbon-starved conditions for the bacterial culture throughout the fermentation process. Under these conditions, bacteria typically respond to stress by activating alternative metabolic pathways that allow them to scavenge nutrients from their surroundings. In this instance, the available nutrients were HL monomers in solution. The HL was fractioned using Wx/M9 minimal medium alkalized with NaOH. Glucose and xylose were initially measured to be approximately 4 $g \cdot L^{-1}$ and 2 $g \cdot L^{-1}$, respectively. A polysaccharide was added at a concentration of 20 $g \cdot L^{-1}$, and an enzyme reagent was added at 0.6% concentration four hours after the start of the fermentation. Thus, both the KT2440 and PaW85 cultures had a steady supply of glucose during the fermentation due to the enzymatic breakdown of the polysaccharide into glucose. HPLC was used to analyze samples taken every 24 hours. Each strain achieved a maximum optical density of 10 and 12 (Figure 5). The high optical densities of both strains throughout the

fermentations suggest that the nitrogen and phosphate content of the fractionated HL medium was adequate. Over time, the samples lightened in color (Figure 6), and the odor changed from nutty to slightly acidic by hour 96.

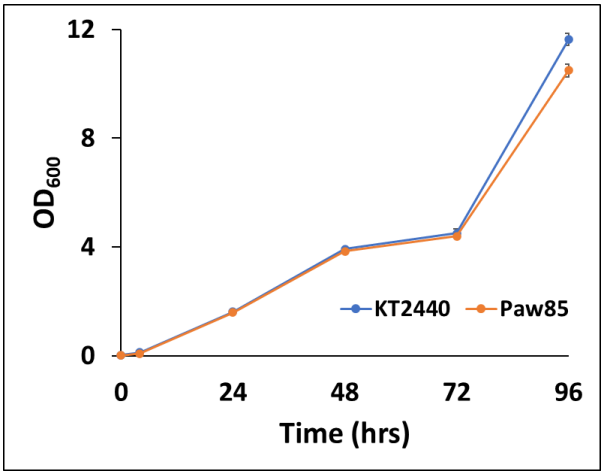

Figure 4. Growth curves of *P. putida* KT2440 and PaW85 during 96-hour simulated fed-batch fermentation in Wx/M9-fractionated HL medium. Standard error was used for error bars.

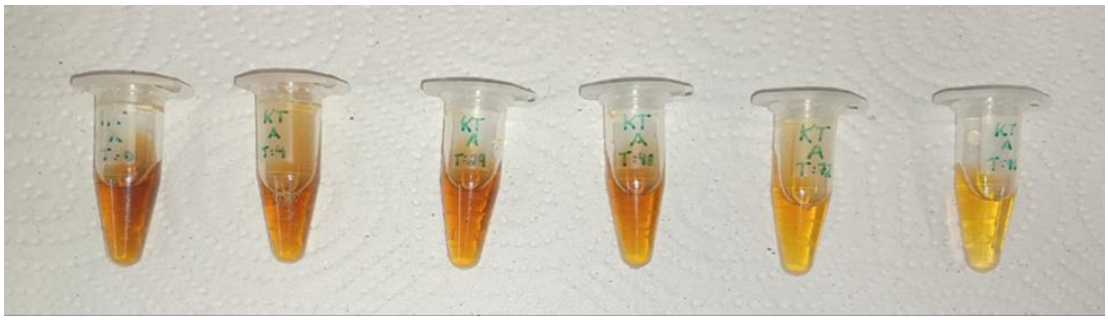

Figure 5. Snapshot of samples taken during 96-hour simulated fed-batch fermentation of *P. putida* KT2440 in Wx/M9-fractionated HL medium.

Changes in the HL monomer concentrations during this simulated fed-batch fermentation were analyzed via HPLC. The results showed that over 0.5 $g \cdot L^{-1}$ of catechol was solubilized from the fractionation. KT2440 and PaW85 completely catabolized the catechol within the first 4 hours, remaining nearly undetectable throughout the experiment. In contrast, the CCMA concentration increased approximately sevenfold within the first 24 hours and then stabilized for the rest of the fermentation (Figure 7). These results indicate that when the catechol concentration is high, CCMA will be produced more quickly than degraded, which is a promising prospect for a fed-batch or continuous cultivation.

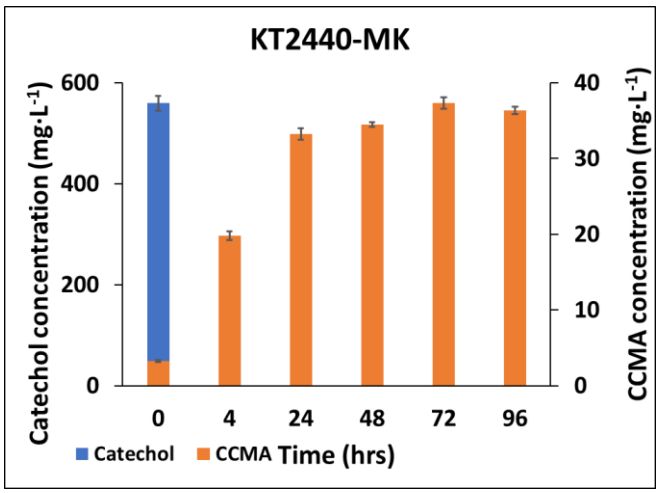

Figure 6. Variation of catechol and *cis,cis*-muconic acid concentrations in Wx/M9-fractionated HL medium during 96-hour simulated fed-batch fermentation with *P. putida* KT2440. Standard error was used for error bars.

4.2.4 HL slurry fermentations

This simulated fed-batch cultivation used an HL slurry as the growth medium. Dry HL was fractionated using three alkaline Wx/M9 media solutions and one non-alkaline medium. The solids were not removed. Prior to inoculation, there was a slight decrease in glucose and xylose concentrations after autoclaving the slurry. This decline can be attributed to the Maillard reaction (Nagai *et al.,* 2014). At time point zero, there was a subsequent decrease in glucose and xylose concentrations due to dilution caused by adding the polysaccharide solution before inoculation. Between 24 and 48 hours, the glucose and xylose concentrations decreased significantly, coinciding with a drop in pH. The glucose concentrations subsequently increased, indicating ongoing hydrolysis of the polysaccharide. However, the culture likely died due to the acidic conditions. The citric acid concentration levels during the fermentation can provide insight into the timing and manner of the cultures' death (Figure S31). There is an increase in citric acid production in all samples until hour 48, after which levels stabilize. Notably, the NH_4OH sample had a significantly higher pH than the others and showed minimal decrease throughout the cultivation. The NH_4OH samples have consistently low levels of citric acid that do not fluctuate throughout the fermentation process. Furthermore, the glucose concentration in the NH_4OH samples remained constant throughout the experiment. This lack of change in glucose concentration can be attributed to the culture dying shortly after inoculation, possibly because the strain could not tolerate the higher level of NH_4OH. The glucose concentration remained low and stable due to the inactivation of the enzyme reagent at such a high pH (Figure 6).

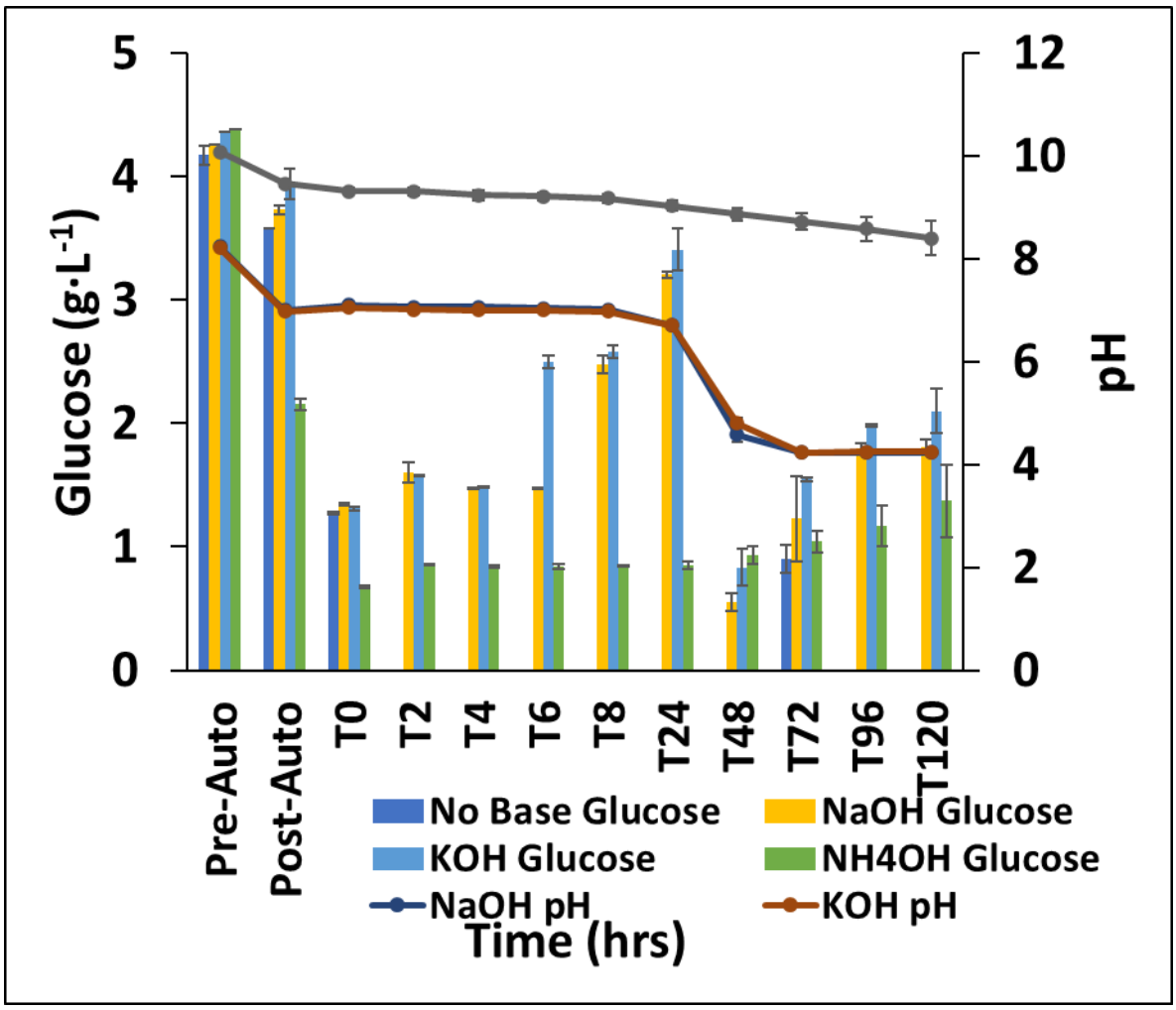

Figure 7. Glucose concentration dynamics and pH level changes during 120-hour simulated fed-batch fermentation with *P. putida* KT2440 in alkalized and non-alkalized HL slurry media. Standard error was used for error bars

HL monomer concentrations of the samples were also assessed using HPLC.In the NaOH, KOH, and non-alkalized samples, catechol increases after the HL slurry is autoclaved. There is also no significant difference in catechol concentration between these three methods (Figures S33-S35) In both the NaOH and KOH-fractionated HL cultivations, catechol was nearly completely catabolized within 4 hours, leading to an initial increase in CCMA concentration, which subsequently stabilizes after 48 hours (Figures 7 & S36). Interestingly, the initial catechol concentration was significantly lower than expected in both cases, even considering the dilution caused by adding the polysaccharide solution. Moreover, the NH_4OH-fractionated HL sample contained less than half as much catechol, indicating that NH_4OH is unsuitable for alkaline fractionation. Furthermore, the concentrations remained constant throughout supporting the conclusion that the culture experienced premature death during fermentation (Figure 8).

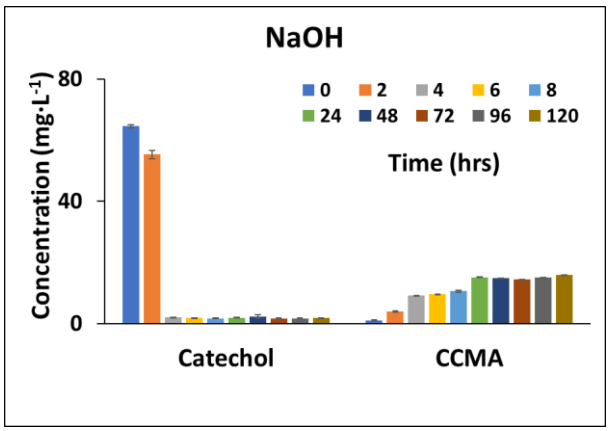

Figure 8. Changes in the concentrations of catechol and *cis,cis*-muconic acid during a 120-hour simulated fed-batch fermentation of an HL slurry made with Wx/M9 minimal medium and alkalized with NaOH. Standard error was used for the error bars.

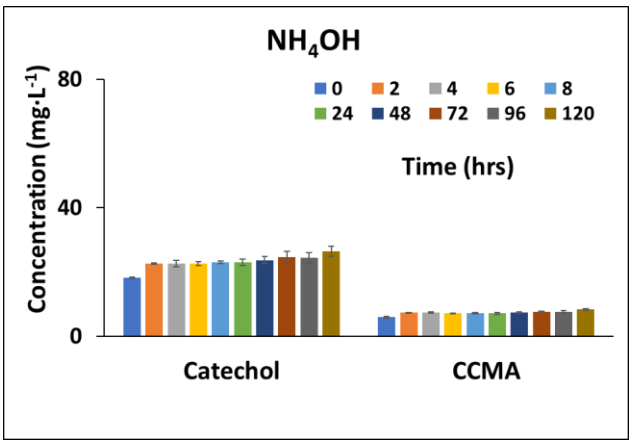

Figure 9. Changes in the concentrations of catechol and *cis,cis*-muconic acid during a 120-hour simulated fed-batch fermentation of an HL slurry made with Wx/M9 minimal medium and alkalized with NH_4OH. Standard error was used for the error bars.

4.2.5 Strain screening

The HPLC data from batch cultivations of each strain was analyzed at different time points. Five compounds were identified that were above the stochastic range. The goal was to identify potential candidates for future research on HL. The strains used in this study can be found in Table S37.

By hour 24, most strains rapidly catabolize catechol. However, most strains' samples exhibit slight increments in catechol concentration by the fifth day. Strains L19, A15, A11B, A4X, and A24 require longer catabolizing catechol entirely. Within the initial 24 hours, their concentrations do not show significant decreases, but by the fifth day, their concentrations resemble those of the other strains. Strain A7, conversely, does not display substantial catechol catabolism, as its concentration remains notably high even by the fifth day. Nevertheless, a

valid comparison cannot be drawn from this experiment due to the unknown relative timing and rate at which the strains consumed the compound. (Figure 9).

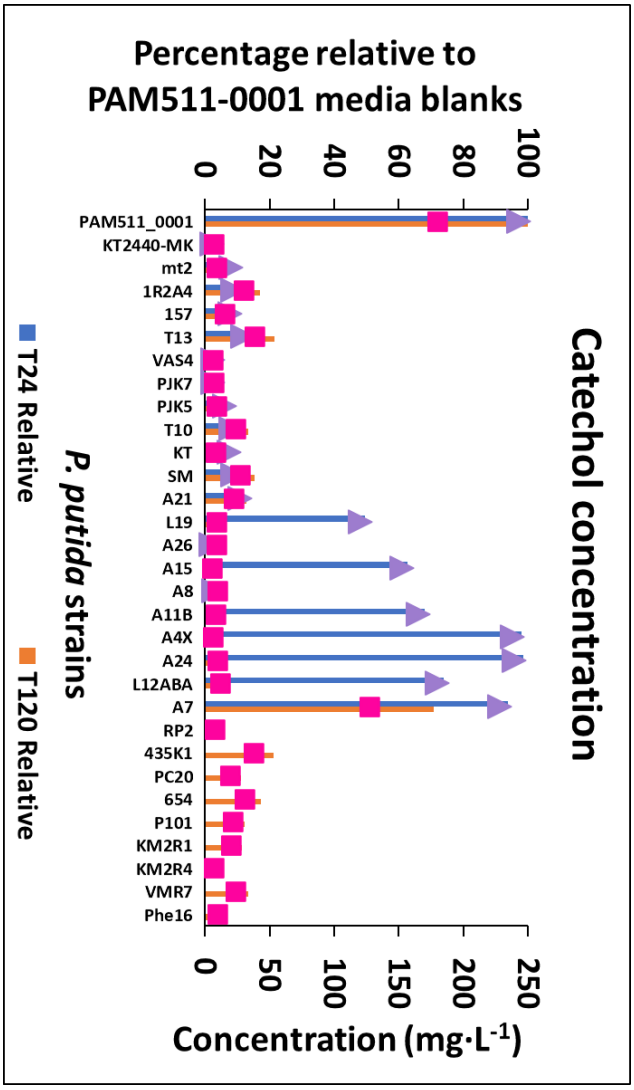

Figure 10. Comparative analysis of catechol concentrations during 120-hour batch fermentation to explore strain variability in *P. putida*. Relative percentages (blue and orange columns) compared to PAM511-0001 media blanks and absolute values (violet triangles and pink squares).

Regarding CCMA, strains KT2440, mt2, 1RSA4, 1S7, VAS4, and PJK7 display the most interesting characteristics. Within five days, the CCMA concentrations in these samples double (Figure 10).

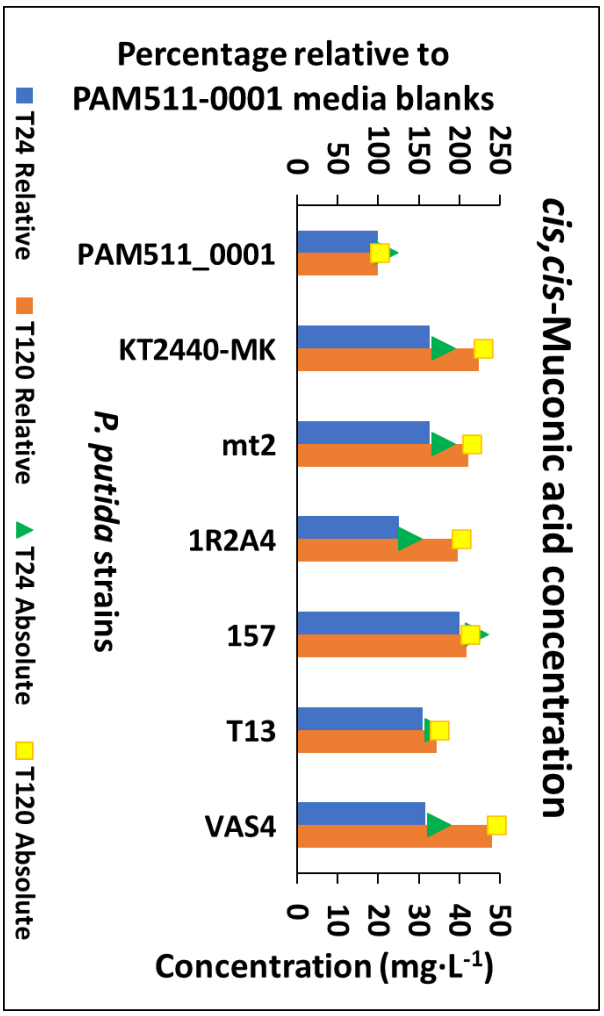

Figure 11. Comparative analysis of *cis,cis*-muconic acid concentrations during 120-hour batch fermentation to explore strain variability in *P. putida*. Relative percentages (blue and orange columns) compared to PAM511-0001 media blanks and absolute values (green triangles and yellow squares).

In most screened strains, 5-HMF concentrations decrease significantly at hour 24 and hour 120. An exception is strain L12ABA, in whose samples 5-HMF remains relatively unchanged. PCA concentrations increase the most in strains T13 and 1R2A4 at hours 24 and 120. Regarding syringic acid, most screened strains show a slight decrease in concentration at 24 hours, except KT2440, mt2, and 1R2A4, which show little change in concentration. Conversely, strains 1S7 and T13 catabolize the most syringic acid at hour 24 and 120. Regarding vanillic acid, the concentrations increase by hour 120 for half the screened strains. Contrarily, strains 1S7 and T13 catabolize nearly all vanillic acid within 24 hours (Figure S38).

4.2.6 Initial molecular biology procedures

The protocatechuate 3,4-dioxygenase (*pcaH* and *pcaG*) and muconate cycloisomerase (*catB*) genes in the benzoate degradation pathway were targeted for deletion (Figure S39) to increase the accumulation of CCMA by preventing ring-opening of PCA and catabolism of CCMA to muconolactone, respectively (Ling *et al.*, 2022).

The inconsistent annealing temperature calculation in different sources posed a challenge in amplifying the HRs of the MCI gene and the 3,4-PCD gene cluster (Table S40). While MCI HR1 was successfully amplified, MCI HR2 faced repeated failures due to a mutation in the catA-1 gene region, preventing the MucCycIso_HR2_RV primer from annealing. To investigate the issue, the HR2_Test primer was specifically designed outside the catA-1 gene, annealed, and amplified, which indicates that the problem did not lie with the MucCycIso_HR2_FW primer. To address this, MCI_HR2a_RV, MCI_HR2b_RV, and MCI_HR2c_RV primers were designed to anneal at three different loci downstream of the original Muc_CycIso_HR2_RV primer. MCI_HR2a_RV annealed, and MCI HR2 was amplified. Simultaneously, the HRs of the 3,4-PCD gene cluster, which includes the pcaH and pcaG genes, were also targeted for amplification, but only the HR1 of the pcaH subunit was amplified. Additionally, the pGNW2 suicide plasmid was linearized by amplification with primers pGNW_Gib_Lin_FW and pGNW_Gib_Lin_RV (Figures S41-S45).

4.2.7 Additional analyses

4.2.7.1 Ion chromatographic analysis of fractionated HL

The ion concentrations in water-fractionated and Wx/M9-fractionated HL were compared to determine the extent of ion dissolution during fractionation and the necessity of fractionation with a defined minimal medium. The findings revealed that approximately 75% of dissolved phosphate originated from the HL in the Wx/M9 fractionation. Nitrate and nitrite levels were similar in both samples, while the Wx/M9 fractionation exhibited higher total nitrogen due to dissolved NH_4OH and components of the medium, promoting sustained bacterial growth. Chloride and sulfate levels were also significantly elevated in the Wx/M9 fractionation. Curiously, fluoride concentration was approximately ten times higher in the water fractionation (Table S46).

4.2.7.2 Uv-vis spectrophotometric analysis of fractionated HL

The absorbance spectra were measured for samples from HL hydrolysate and HL slurry fermentations. The two HL hydrolysate solutions' spectra, taken at 0 and 72 hours, revealed a

significant decrease in absorption between 250 and 300 nm and a slight decrease between 350 and 400 nm (Figures S47 & S48). In the HL slurry samples treated with NaOH, KOH, and without any alkalization, the absorbance of the entire spectrum decreased after the initial time point, and crucially, the absorption peak between 250 and 300 nm disappeared (Figures S49, S50, & S51). This suggests that the aromatic compounds have undergone chemical changes and decreased concentration during fermentations. Notably, no changes were observed in the absorbance spectra of NH_4OH-alkalized HL slurry samples, further indicating that the culture died shortly after the inoculation (Figure S52).

4.2.7.3 Dimeric to monomeric shift in alkaline HL fermentations

Zhao *et al*., (2020) conducted a study wherein common lignin-derived trimers, dimers, and monomers were synthesized and then analyzed using GC-MS. This study used the same Selected Ion Monitoring (SIM) mode parameters to monitor specific mass-to-charge ratios of target compounds in alkalized lignin fractionation samples obtained at hour 0 and hour 120 of a simulated fed-batch fermentation with *P. putida* KT2440. The resulting chromatograms closely aligned with those from Zhao *et al*. (2020) showing a shift to shorter acquisition times in the latter sample, indicating a possible conversion of dimers and trimers into monomers. Notably, no peaks within the 32-to-44-minute range indicate almost complete dissociation of lignin-derived dimers during the fermentation process (Figures S53 & S54) These preliminary results may indicate that P. putida produced extracellular enzymes which depolymerized some of the dimers and trimers in solution.

SUMMARY

This study investigated the impact of crude HL fractionation methods on the media composition and its suitability for *P. putida* growth. Alkaline fractionation methods showed similar sugar profiles between filtered and unfiltered samples, but the filtered fractionation contained over double the amount of dissolved catechol. Among the unfiltered fractionations, the NaOH and KOH samples had approximately eight times more catechol than the NH_4OH sample.

The strains KT2440 and PaW85 exhibited broad pH tolerance and robust growth at elevated pH levels. Simulated fed-batch fermentations using NaOH- and KOH-alkalized HL slurries demonstrated good bacterial growth at pH 8, but acidic pH levels below 5 were not tolerated. Moreover, these strains did not tolerate NH_4OH at pH levels above 9. However, KT2440 showed growth in MMPAM modified minimal medium, which had its pH adjusted closer to the biological pH of 7.4 with NH_4OH.

Of the 27 screened bacterial strains, six showed significant potential: *P. putida* KT2440, *P. putida* mt2, *P. putida* 1S7, *P. putida* PJK7, *Pseudomonas sp./defluvii*, and *Mitsuaria chitosanitabida* 1R2A4. These strains exhibited rapid catechol catabolism and the highest production of CCMA, making them promising candidates for genetic engineering. However, it is important to consider that the screening process may have a cultivation bias towards *Pseudomonas* strains due to the modified MMPAM minimal medium optimized for *P. putida* when creating the PAM511-0001 fractionated HL batch, on which the strains were screened.

Deleting the 3,4-PCD gene aimed to redirect PCA and its metabolic precursors away from β-carboxymuconate, while deleting the *catB* gene aimed to prevent the conversion of CCMA to muconolactone, thereby increasing CCMA accumulation. However, the study did not achieve genetic recombineering of KT2440. The *catB* gene's homology regions and the HR1 of the *pcaH* subunit of the 3,4-PCD gene were amplified, along with the linearized and amplified pGNW2 suicide vector.

Acknowledgments

I want to express profound thanks to Christina Mürk (Tartu University, Chair of Environmental Chemistry, Tartu, Estonia) for their excellent analytical support and training. Victor de Lorenzo (National Centre for Biotechnology, Madrid, Spain) for the generous gift of different plasmids for *P. putida*. Maia Kivisaar, Eeva Heinaru, Signe Viggor, and Merike Jõesaar (Tartu University, Chair of Genetics, Tartu, Estonia) and CELMS (Collection of Environmental and Laboratory Microbial Strains; http://eemb.ut.ee (financed by the Estonian Ministry of Education and Research (RLOMRCELMS)) for strains, media formulation, and experimental support. Henry Vider and Kait Puss (Tartu University, Chair of Organic Chemistry, Tartu, Estonia) for essential support on the GC-MS, HL solution preparation, and writing feedback. Scott Bottoms, Siim Salmar, and Mart Loog (Tartu University, Tartu, Estonia), my supervisors and mentors, for their expertise in experimental design, critical feedback on experiments, analytics, and thesis composition, and unwavering motivation and support throughout my tenure at this institution. This work was financially supported by the Estonian Research Council through the grant ResTA22 (LLTTI19432).

REFERENCES

Anthony, W. E., Carr, R. R., DeLorenzo, D. M., Campbell, T. P., Shang, Z., Foston, M., Moon, T. S., & Dantas, G. (2019). Development of Rhodococcus opacus as a chassis for lignin valorization and bioproduction of high-value compounds. Biotechnology and Biofuels, 12, 192.

Araujo, J. D. P., Grande, C. A., & Rodrigues, A. E. (2010). Vanillin production from lignin oxidation in a batch reactor. Chemical Engineering Research and Design, 88, 1024–1032.

Archer, D., Eby, M., Brovkin, V., Ridgwell, A., Cao, L., Mikolajewicz, U., Caldeira, K., Matsumoto, K., Munhoven, G., Montenegro, A., & Tokos, K. (2009). Atmospheric lifetime of fossil fuel carbon dioxide. Annual Review of Earth and Planetary Sciences, 37, 117–134. https://doi.org/10.1146/annurev.earth.031208.100206

Araki, Y., Hong, I., Gamache, T. R., Ju, S., Jaffe, A. E., Shin, J. H., & Huganir, R. L. (2020). SynGAP isoforms differentially regulate synaptic plasticity and dendritic development. *eLife*, *9*. https://doi.org/10.7554/elife.56273

Bagdasarian, M., Lurz, R., Rückert, B., Franklin, F. C. H., & Bagdasarian, M. M. (1981). Specific-purpose plasmid cloning vectors II. broad host range, high copy number, RSF 1010-derived vectors, and a host-vector system for gene cloning in Pseudomonas. Gene, 16, 237–247.

Bator, I., Wittgens, A., Rosenau, F., Tiso, T., & Blank, L. M. (2020). Comparison of Three Xylose Pathways in *Pseudomonas putida* KT2440 for the Synthesis of Valuable Products. Frontiers in bioengineering and biotechnology, *7*, 480. https://doi.org/10.3389/fbioe.2019.00480

Bayley, S. A., Duggleby, C. J., Worsey, M. J., *et al*. (1977). Two modes of loss of the tol function from *Pseudomonas putida* mt-2. *Molecular Genetics and Genomics, 154, 203-204. https://doi.org/10.1007/BF00330838

Bazzanella, A. M., & Ausfelder, F. (2017). Low carbon energy and feedstock for the European chemical industry. Retrieved from https://cefic.org/app/uploads/2019/01/Low-carbon-energy-and-feedstock-for-the-chemical-industry-DECHEMA_Report-energy_climate.pdf

Becker, J., Kuhl, M., Kohlstedt, M., Starck, S., & Wittmann, C. (2018). Metabolic engineering of Corynebacterium glutamicum for the production of cis, cis-muconic acid from lignin. Microbial Cell Factories, 17, 115.

Becker, J., & Wittmann, C. (2019). A field of dreams: Lignin valorization into chemicals, materials, fuels, and health-care products. Biotechnology Advances, 37, 107360.

Belda, E., van Heck, R. G. A., López-Sánchez, M. J., Cruveiller, S., Barbe, V., Fraser, C., ... Médigue, C. (2016). The re-visited genome of Pseudomonas putida KT2440 enlightens its value as a robust metabolic chassis. Environmental Microbiology, 18, 3403–3424.

Borrero-de Acuña, J. M., Rohde, M., Rohde, M., & Poblete-Castro, I. (2021). Fed-Batch mcl-Polyhydroxyalkanoates Production in Pseudomonas putida KT2440 and ΔphaZ Mutant on Biodiesel-Derived Crude Glycerol. Frontiers in Biotechnology, 9.

Cabernard, L., Pfister, S., Oberschelp, C., & Hellwig, S. (2022). Growing environmental footprint of plastics driven by coal combustion. Nature Sustainability, 5(2), 139-148. https://doi.org/10.1038/s41893-021-00807-2

Cao, L., Yu, I. K. M., Liu, Y., Ruan, X., Tsang, D. C. W., Hunt, A. J., Sik Ok, Y., Song, H., & Zhang, S. (2018). Lignin valorization for the production of renewable chemicals: State-of-the-art review and future prospects. Bioresource Technology. Advance online publication. https://doi.org/10.1016/j.biortech.2018.08.065.

Chua, J. W., & Hsieh, J. H. (1990). Oxidative bioconversion of toluene to 1,3-butadiene-1,4-dicarboxylic acid (cis,cis-muconic acid). World Journal of Microbiology and Biotechnology, 6, 127-143.

Chung, H., & Washburn, N. R. (2013). Chemistry of lignin-based materials. Green Materials, 1, 137-160. doi:10.1680/gmat.12.00009

de Oliveira, C. C. N., Zotin, M. Z., Rochedo, P. R. R., & Szklo, A. (2020). Achieving negative emissions in plastics life cycles through the conversion of biomass feedstock. Biofuels, Bioproducts, and Biorefining. https://doi.org/10.1002/bbb.2165

DeAngelis, F., & Reale, S. (2006). Review – The lignin concept. Chim'Ind-Mila88, 58-65.

Dikshit, P. K., Jun, H. B., & Kim, B. S. (2020). Biological conversion of lignin and its derivatives to fuels and chemicals. Korean Journal of Chemical Engineering, 37, 387-401.

Dlugokencky, E., & Tans, P. (n.d.). Trends in atmospheric carbon dioxide. National Oceanic and Atmospheric Administration, Earth System Research Laboratory (NOAA/ESRL). Retrieved from http://www.esrl.noaa.gov/gmd/ccgg/trends/global.html

Dormer, A., Finn, D. P., Ward, P., & Cullen, J. (2013). Carbon footprint analysis in plastics manufacturing. Journal of Cleaner Production, 51, 133-141.

dos Santos, V. A. P. M., Heim, S., Moore, E. R. B., Stratz, M., & Timmis, K. N. (2004). Insights into the genomic basis of niche specificity of Pseudomonas putida KT2440. Environmental Microbiology, 6, 1264-1286.

Geyer, R., Jambeck, J., & Law, K. (2017). Production, use, and fate of all plastics ever made. Science Advances, 3, 25-29.

Guo, L., She, C., Kong, D., Yan, S., Xu, Y., Khayatnezhad, M., Gholinia, F. (2021). Prediction of the effects of climate change on hydroelectric generation, electricity demand, and emissions of greenhouse gases under climatic scenarios and optimized ANN model. Energy Reports, 7, 5431-5445.

Hendriks, A. T. W. M., & Zeeman, G. (2009). Pretreatments to enhance the digestibility of lignocellulosic biomass. Bioresource Technology, 100(1), 10-18.

Heinaru, E., Truu, J., Stottmeister, U., & Heinaru, A. (2000). Three types of phenol and p-cresol catabolism in phenol- and p-cresol-degrading bacteria isolated from river water continuously polluted with phenolic compounds. FEMS Microbiology Ecology, 31, 195-205.

Hirai, N., Kubo, S., & Magara, K. (2009). Combined cyclic voltammetry and in situ electrochemical atomic force microscopy on lead electrode in sulfuric acid solution with or without lignosulfonate. Journal of Power Sources, 191, 97-102. doi:10.1016/j.jp

Humbird, D., et al. (2012). Process design and economics for biochemical conversion of lignocellulosic biomass to ethanol: Dilute-acid pretreatment and enzymatic hydrolysis of corn stover. Technical Report NREL/TP-5100-47764. National Renewable Energy Laboratory, Golden, CO.

IEA. (2018). The future of petrochemicals. Retrieved from https://www.iea.org/reports/the-future-of-petrochemicals

Jones, L., Ennos, A. R., & Turner, S. R. (2001). Cloning and characterization of irregular xylem4 (irx4): a severely lignin-deficient mutant of Arabidopsis. The Plant Journal, 26, 205-216.

Joos, F., & Spahni, R. (2008). Rates of change in natural and anthropogenic radiative forcing over the past 20,000 years. Proceedings of the National Academy of Sciences, 105, 1425-1430.

Laskar, D. D., Zeng, J., Yan, L., Chen, S., & Yang, B. (2013). Characterization of lignin derived from water-only flow-through pretreatment of Miscanthus. Industrial Crops and Products, 50, 391-399.

Ling, C., Peabody, G. L., Salvachúa, D., Kim, Y. M., Kneucker, C. M., Calvey, C. H., Monninger, M. A., Munoz, N. M., Poirier, B. C., Ramirez, K. J., St John, P. C., Woodworth, S. P., Magnuson, J. K., Burnum-Johnson, K. E., Guss, A. M., Johnson, C. W., & Beckham, G. T. (2022). Muconic acid production from glucose and xylose in Pseudomonas putida via evolution and metabolic engineering. *Nature communications*, *13*(1), 4925. https://doi.org/10.1038/s41467-022-32296-y

Linger, J. G., et al. (2014). Lignin valorization through integrated biological funneling and chemical catalysis. Proceedings of the National Academy of Sciences, 111, 12013-12018.

Loeschcke, A., & Thies, S. (2015). Pseudomonas putida - a versatile host for the production of natural products. Applied Microbiology and Biotechnology, 99, 6197-6214.

Lora, J. (2008). Industrial commercial lignins: Sources, properties, and applications. In M.N. Belgacem & A. Gandini (Eds.), Monomers, Polymers and Composites from Renewable Resources (pp. 225-241). Elsevier.

Luo, H., & Abu-Omar, M.M. (2017). Chemicals from lignin. In Encyclopedia of Sustainable Technologies (pp. 573-585). Elsevier.

Martínez-García, E., Nikel, P. I., Aparicio, T., & de Lorenzo, V. (2014). Pseudomonas 2.0: Genetic upgrading of P. putida KT2440 as an enhanced host for heterologous gene expression. Microbial Cell Factories, 13, 159.

Meys, R., et al. (2021). Achieving net-zero greenhouse gas emission plastics by a circular carbon economy. Science, 374, 71-76.

Monteiro de Oliveira, P., Aborneva, D., Bonturi, N., Lahtvee, P.J. (2021). Screening and growth characterization of non-conventional yeasts in a hemicellulosic hydrolysate. Frontiers in Bioengineering and Biotechnology. DOI: 10.3389/fbioe.2021.659472.

Nagai, R., Shirakawa, J., Fujiwara, Y., Ohno, R., Moroishi, N., Sakata, N., & Nagai, M. (2014). Detection of AGEs as markers for carbohydrate metabolism and protein denaturation. Journal of clinical biochemistry and nutrition. 55. 1-6. 10.3164/jcbn.13-112.

Nakazawa, T. (2002). Travels of a Pseudomonas, from Japan around the world. Environmental Microbiology, 4, 782-786.

Nelson, K. E., et al. (2002). Complete genome sequence and comparative analysis of the metabolically versatile Pseudomonas putida KT2440. Environmental Microbiology, 4, 799-808.

Nikel, P. I., & de Lorenzo, V. (2018). Pseudomonas putida as a functional chassis for industrial biocatalysis: From native biochemistry to trans-metabolism. Metabolic Engineering, 50, 142-.

Nikel, P. I., Martínez-García, E., & de Lorenzo, V. (2014). Biotechnological domestication of pseudomonads using synthetic biology. Nature Reviews Microbiology, 12, 368-379.

Palleroni, N. J. (2005). Genus I. Pseudomonas Migula 1984. In Brenner, D. J., Krieg, N. R., & Staley, J. T. (Eds.), Bergey's Manual of Systematic Bacteriology, 2nd ed. (pp. 323-379). New York, USA: Springer.

Pandey, M. P., & Kim, C. S. (2011). Lignin depolymerization and conversion: A review of thermochemical methods. Chemical Engineering and Technology, 34(1), 29-41.

Parsell, T. H., Owen, B. C., Klein, I., Jarrell, T. M., Marcum, C. L., Haupert, L. J., Amundson, L. M., Kenttämaa, H. I., Ribeiro, F., Miller, J. T., & Abu-Omar, M. M. (2013). Cleavage and hydrodeoxygenation (HDO) of C-O bonds relevant to lignin conversion using Pd/Zn synergistic catalysis. Chemical Science, 4, 806-813.

Parte, A. C. (2018). LPSN – List of prokaryotic names with standing in Nomenclature (bacterio.net), 20 years on. International Journal of Systematic and Evolutionary Microbiology, 68, 1825-1829.

Poblete-Castro, I., Borrero de Acuña, J. M., Nikel, P. I., Kohlstedt, M., & Wittmann, C. (2017). Host organism: Pseudomonas putida. In Industrial Biotechnology: Microorganisms (pp.). Weinheim: Wiley-VCH Verlag GmbH & Co. KGaA.

Ponnuchamy, V., Gordobil, O., Diaz, R., Sandak, A., Sandak, J. (2021). Fractionation of lignin using organic solvents: A combined experimental and theoretical study. International Journal of Biological Macromolecules, 168, 792-805.

Posen, I. D., Jaramillo, P., Landis, A. E., & Griffin, W. M. (2017). Greenhouse gas mitigation for US plastics production: Energy first, feedstocks later. Environmental Research Letters, 12, 034024.

Poursorkhabi, V., Misra, M., & Mohanty, A. K. (2013). Extraction of lignin from a co-product of the cellulosic ethanol industry and its thermal characterization. BioResources, 8, 5083-5101.

Puss, K.K., Loog, M., Salmar, S. (2023). Ultrasound enhanced solubilization of forest biorefinery hydrolysis lignin in mild alkaline conditions. Ultrasonics Sonochemistry, 93, 106288. https://doi.org/10.1016/j.ultsonch.2022.106288.

Ragauskas, A. J., Beckham, G. T., Biddy, M. J., Chandra, R., Chen, F., Davis, M. F., Davison, B. H., Dixon, R. A., Gilna, P., Keller, M., et al. (2014). Lignin valorization: Improving lignin processing in the biorefinery. Science, 344, 1246843.

Ramos, J. L., Gallegos, M. T., Marqués, S., Ramos-González, M. I., Espinosa-Urgel, M., et al. (2001). Responses of gram-negative bacteria to certain environmental stressors. Current Opinion in Microbiology, 4(2), 166-171.

Reyes-Rivera J, Canché-Escamilla G, Soto-Hernández M, Terrazas T (2015) Correction: Wood Chemical Composition in Species of Cactaceae: The Relationship between Lignification and Stem Morphology. PLOS ONE 10(6): e0130240. https://doi.org/10.1371/journal.pone.0130240

Sagues, W. J., Bao, H., Nemenyi, J. L., & Tong, Z. (2018). Lignin-first approach to biorefining: Utilizing Fenton's reagent and supercritical ethanol for the production of phenolics and sugars. ACS Sustainable Chemistry & Engineering, 6(4), 4958-4965.

Sharma, S., Kumar, R., Gaur, R., Agrawal, R., Gupta, R. P., Tuli, D. K., & Das, B. (2015). Pilot scale study on steam explosion and mass balance for higher sugar recovery from rice straw. Bioresource Technology, 175, 350-357.

Silby, M. W., Winstanley, C., Godfrey, S. A. C., Levy, S. B., & Jackson, R. W. (2011). Pseudomonas genomes: diverse and adaptable. FEMS Microbiology Reviews, 35(4), 652-680.

Stegmann, P., Daioglou, V., Londo, M., & Junginger, M. (2022). The plastics integrated assessment model (PLAIA): assessing emission mitigation pathways and circular economy strategies for the plastics sector. MethodsX, 9, 101666.

Timmis, K. N. (2002). Pseudomonas putida: a cosmopolitan opportunist par excellence. Environmental Microbiology, 4(12), 779-781.

Timmis, K. N., Steffan, R. J., & Unterman, R. (1994). Designing microorganisms for the treatment of toxic wastes. Annual Review of Microbiology, 48, 525-557.

Tuck, C. O., Pérez, E., Horváth, I. T., Sheldon, R. A., & Poliakoff, M. (2012). Valorization of biomass: Deriving more value from waste. Science, 337(6095), 695-699. doi:10.1126/science.1218930; pmid:22879509.

Udaondo, Z., Duque, E., Fernández, M., Molina, L., de la Torre, J., et al. (2012). Analysis of solvent tolerance in Pseudomonas putida DOT-T1E based on its genome sequence and a collection of mutants. FEBS Letters, 586(18), 2932-2938.

Upton, B. M., & Kasko, A. M. (2016). Strategies for the conversion of lignin into high-value polymeric materials: review and perspective. Chemical Reviews, 116(4), 2275-2306.

van Duuren, J. B., Wijte, D., Leprince, A., Karge, B., Puchalka, J., Wery, J., Dos Santos, V. A., Eggink, G., & Mars, A. E. (2011). Generation of a catR deficient mutant of P. putida KT2440 that produces cis, cis-muconate from benzoate at high rate and yield. Journal of Biotechnology, 156, 163-172.

Vardon, D. R., Rorrer, N. A., Salvachua, D., Settle, A. E., Johnson, C. W., Menart, M. J., Cleveland, N. S., Ciesielski, P. N., Steirer, K. X., Dorgan, J. R., & Beckham, G. T. (2016).

cis, cis-Muconic acid: separation and catalysis to bio-adipic acid for nylon-6,6 polymerization. Green Chemistry, 18, 3397-3413.

Viggor, S., Jõesaar, M., Soares-Castro, P., Ilmjärv, T., Santos, P. M., Kapley, A., & Kivisaar, M. (2020). Microbial Metabolic Potential of Phenol Degradation in Wastewater Treatment Plant of Crude Oil Refinery: Analysis of Metagenomes and Characterization of Isolates. *Microorganisms*, *8*(5), 652. https://doi.org/10.3390/microorganisms8050652

Wang, H., Tucker, M., & Ji, Y. (2013). Recent development in chemical depolymerization of lignin: a review. Journal of Applied Chemistry, 2013, 1-9.

Williams, P. A., & Murray, K. (1974). Metabolism of benzoate and the methylbenzoates by Pseudomonas putida (arvilla) mt-2: evidence for the existence of a TOL plasmid. Journal of Bacteriology, 120, 416-423.

Wu, X., Fan, X., Xie, S., Lin, J., Cheng, J., Zhang, Q., Chen, L., & Wang, Y. (2018). Solar energy-driven lignin-first approach to full utilization of lignocellulosic biomass under mild conditions. Nature Catalysis, 1, 772-780.

Xie, N. Z., Wang, Q. Y., Zhu, Q. X., Qin, Y., Tao, F., Huang, R. B., & Xu, P. (2014b). Optimization of medium composition for cis, cis-muconic acid production by a Pseudomonas sp. mutant using statistical methods. Prep. Biochem. Biotech., 44(4), 342-354.

Xie, S., Syrenne, R., Sun, S., & Yuan, J. S. (2014a). Exploration of Natural Biomass Utilization Systems (NBUS) for advanced biofuel-from systems biology to synthetic design. Current Opinion in Biotechnology, 27, 195-203.

Yuan, Z., Browne, C. T., & Zhang, X. (2011). Biomass fractionation process for bioproducts [World patent WO2011057413A1].

Zhao, C., Hu, Z., Shi, L., Wang, C., Yue, F., Li, S., Zhang, H., & Lu, F. (2020). Supplementary Materials for "Profiling of the Formation of Lignin-derived Monomers and Dimers from Eucalyptus Alkali Lignin." The Royal Society of Chemistry.

Zheng, J., & Suh, S. (2019). Strategies to reduce the global carbon footprint of plastics. Nature Climate Change, 9, 374-378.

Supplementary Materials

Table S1. Plasmids used in this study

Plasmid Name	Relevant Genotype	Source
pGNW2	N/A (See source link)	https://www.addgene.org/122086/

Table S2. Comparison of Wx/M9 based medium composition and new MMPAM formulation: Original, modified, and reference formulations

Maia Kivisaar	g·L^{-1}	mM	Borrero de Acuña et al., (2021)	g·L^{-1}	mM	New Formulation (MMPAM)	g·L^{-1}	mM
KH_2PO_4	5.7	42	KH_2PO_4	3.0	22.0	KH_2PO_4	6.0	44.1
Na_2HPO_4	3.4	24	$Na_2HPO_4{\cdot}7H_2O$	12.8	47.8	Na_2HPO_4	7.1	50
NH_4Cl	1.0	19	$(NH_4)_2SO_4$	4.7	35.6	$(NH_4)_2SO_4$	5.0	37.8
NaCl	0.5	9	NaCl	0.5	8.6	NaCl	0.5	8.6

Table S3. Standardized MMPAM-fractionated HL solution

Batch	Date
PAM511-0001	21.03.2023

Table S4. pH of media during alkaline extraction experiment

Hour	NaOH_A	NaOH_B	KOH_A	KOH_B	NH_4OH_A	NH_4OH_B	No-Alk_A	No-Alk_B
Pre-Autoclave	8.24	8.24	8.21	8.21	10.08	10.08	7.80	7.80
Post-Autoclave	7.00	7.00	6.98	6.96	9.46	9.46	6.68	6.68
0	7.10	7.11	7.04	7.06	9.36	9.27	6.82	6.78
2	7.05	7.07	7.01	7.03	9.36	9.26	-	-
4	7.06	7.06	7.01	7.00	9.30	9.17	-	-
6	7.04	7.04	7.00	7.00	9.27	9.15	-	-
8	7.01	7.03	6.98	6.98	9.24	8.12	-	-
24	6.73	6.67	6.67	6.75	9.11	8.96	-	-
48	4.68	4.49	4.73	4.87	8.96	8.78	-	-
72	4.24	4.23	4.24	4.24	8.83	8.61	4.20	4.21
96	4.25	4.23	4.23	4.26	8.75	8.41	-	-
120	4.25	4.21	4.25	4.24	8.64	8.16	-	-

Table S5. Amplified MCI HR1, MCI HR2, and pcaH HR1, and linearized pGNW2 vector nanodrop concentrations

	Concentration (ng·µL^{-1})
pGNW2	63.6
MCI HR1	22.5
MCI HR2a	83.2
pcaH HR1	31.2

Table S6. DNA sequences and sources of genes used in this study

Gene name / EC number / Locus tag	**DNA Sequence**	**Source**
catB / 5.5.1.1 / PP4_RS10750	ATGACAAGCGCGCTGATTGAACGTATTGATGC AATTATCGTCGACCTGCCGACCATTCGCCCGC ACAAGCTGGCAATGCACACCATGCAGCAGCA GACCCTGGTGGTATTGCGTGTGCGTTGCAGCG ATGGCGTGGAAGGTATCGGTGAGGCCACCAC CATCGGTGGCCTGGCCTATGGCTACGAAAGCC CCGAGGGCATCAAGGCCAACATCGACGCCCA CCTGGCCCCGGCGCTGATCGGCCTGGCGGCGG ACAACATCAACGCCGCTATGCTCAAGCTTGAC AAGCTGGCCAAGGGCAACACTTTTGCCAAGTC GGGTATCGAAAGCGCCTTGCTCGACGCCCAG GGCAAACGCCTGGGCCTGCCGGTCAGCGAAC TGCTGGGCGGCCGCGTGCGCGACAGCCTGGA AGTGGCCTGGACCCTGGCCAGTGGCGACACG GCCCGTGATATCGCCGAAGCCCGACACATGCT GGAAATTCGCCGTCACCGGGTGTTCAAGCTGA AGATTGGCGCCAACCCGGTGGAGCAGGACCT CAAACACGTGGTGACGATAAAACGCGAACTG GGCGACAGCGCCAGTGTGCGAGTGGACGTGA ATCAGTACTGGGACGAATCCCAGGCCATCCGC GCTTGCCAGGTGCTTGGCGACAACGGCATCGA CCTGATCGAGCAACCGATTTCGCGTATCAACC GCGGTGGCCAGGTGCGCCTGAACCAGCGCAG CCCTGCACCGATCATGGCCGATGAGTCCATCG AAAGCGTCGAGGATGCCTTCAGCCTGGCCGCC GACGGCGCCGCCAGCATCTTTGCCCTGAAAAT CGCCAAGAACGGCGGCCCGCGTGCTGTGCTG CGCACTGCGCAAATCGCCGAGGCCGCCGGTA TCGGCCTGTATGGCGGCACCATGCTCGAGGGC TCGATCGGCACCCTGGCCTCGGCCCACGCCTT CCTTACCTTGCGCCAACTGACCTGGGGCACCG AGCTGTTCGGCCCGCTGCTGCTGACCGAAGAA ATCGTCAACGAGCCGCCGCAATATCGCGACTT CCAGCTGCACATTCCCCGTACCCCAGGCCTGG GCCTGACCCTGGACGAACAGCGCCTGGCGCG CTTCGCCCGTCGCTGA	*https://www.ncbi.nlm.nih.gov/nuccore/NC_021505.1?from=2405938&to=2407059&report=fasta*
pcaG / 1.13.11.3 / PP4_RS03585	ATGCCAATCGAACTGCTGCCGGAAACCCCTTC GCAGACCGCCGGCCCCTACGTGCACATCGGCC TGGCCCTGGAAGCGGCCGGCAACCCGACCCG	*https://www.ncbi.nlm.nih.gov/nuccore/*

	CGATCAGGAAATCTGGAACCGCCTGGCCAAG CCAGACGCGCCAGGCGAGCACATCCTGCTGCT CGGCCAGGTCTATGACGGTAACGGCCACCTG GTGCGCGACTCGTTCCTGGAAGTGTGGCAGGC CGACGCCAATGGCGAGTACCAGGATGCCTAC AACCTGGAAAACGCCTTCAACAGCTTTGGCCG CACCGCTACCACCTTCGATGCCGGTGAATGGA CCCTGCACACGGTCAAGCCGGGTGTGGTGAAT AACGCGGCTGGTGTACCGATGGCGCCGCACA TCAACATCAGCCTGTTTGCCCGTGGTATCAAC ATCCACCTGCACACGCGCCTGTATTTCGATGA CGAAGCCCAGGCCAACGCCAAGTGCCCGGTG CTCAACCTGATCGAGCAGCCACAGCGGCGTG AAACCTTGATTGCCAAGCGTTGCGAAGTGGAC GGGAAGACGGCGTATCGCTTTGATATCCGTAT CCAGGGGGAAGGCGAGACGGTGTTCTTCGAC TTCTGA	*NC_021505.1?from=826906&to=827511&report=fasta*
pcaH / 1.13.11.3 / PP4_RS03580	ATGCCCGCACAGGACAACAGCCGCTTCGTGAT CCGTGATCGCAACTGGCACCCCAAAGCCCTTA CGCCTGACTACAAAACGTCCATTGCCCGCTCG CCGCGTCAGGCACTGGTCAGCATTCCACAGTC GATCAGCGAAACCACTGGTCCGAACTTCTCCC ACCTGGGCTTTGGCGCCCACGACCATGACCTG TTGCTGAACTTCAACAACGGTGGCCTGCCAAT CGGCGAGCGCATCATCGTTGCCGGCCGCGTGG TCGACCAGTACGGCAAGCCTGTGCCGAACAC CCTGGTGGAGATGTGGCAAGCCAACGCCGGT GGCCGCTATCGGCACAAGAACGACCGTTACCT GGCACCGCTGGACCCGAACTTTGGTGGTGTCG GCCGTTGCCTGACCGACAGTGACGGCTATTAC AGCTTCCGCACCATCAAGCCGGGCCCGTACCC ATGGCGCAACGGCCCGAACGACTGGCGCCCG GCGCACATTCACTTCGGCATCAGCGGCCCGTC GATTGCCACCAAGCTGATCACCCAGCTGTATT TCGAGGGTGACCCGCTGATCCCGATGTGCCCG ATCGTCAAGTCGATCGCCAATCCTGAAGCTGT ACAGCAGTTGATCGCCAAGCTCGACATGAGC AACGCCAACCCGATGGACTGCCTGGCCTACCG CTTTGACATCGTGCTGCGCGGCCAGCGCAAGA CCCACTTCGAAAACTGCTGA	*https://www.ncbi.nlm.nih.gov/nuccore/NC_021505.1?from=826176&to=826895&report=fasta*

Table S7. Primers used in this study

Oligo Name	**Sequence (5'-3')**	**Purpose**
MucCycIso_HR1_FW	TCCTGGCGCAGCTCGC	Clone Homology Ends from *P. putida* MCI
MucCycIso_HR1_RV	CATTGTT-GCCAGGTCCCGTCAG	Clone Homology Ends from *P. putida* MCI
MucCycIso_HR2_FW	TGATCAG-CAAACAAGGAGA-TAATCATGCTGTTC	Clone Homology Ends from *P. putida* MCI
MucCycIso_HR2_RV	TCTTCGGTGAT-TTCCAGGTCTTCGAC	Clone Homology Ends from *P. putida* MCI

HR2_Test	CATCGGGCGTAC-CTCATATTGTTCTTGTC	Troubleshoot HR2 Cloning from *P. putida* MCI
MCI_HR2a_RV	GGTCGGTGCCGTCGTCC	Clone Homology Ends from *P. putida* MCI
MCI_HR2b_RV	GGCGACATA-CAGCGGGCC	Clone Homology Ends from *P. putida* MCI
MCI_HR2c_RV	CGGCCACCCAGGCGG	Clone Homology Ends from *P. putida* MCI
pcaH_HR1_FW	GGGTCGCGG-TATTGCTTGCC	Clone Homology Ends from *P. putida* Proto-catechuate 3,4-dioxygenease
pcaH_HR1_RV	CATGCCGGTTTCCTCTCTTGG	Clone Homology Ends from *P. putida* Proto-catechuate 3,4-dioxygenease
pcaG_HR2_FW	TGATGGAAACCCGGGGCC	Clone Homology Ends from *P. putida* Proto-catechuate 3,4-dioxygenease
pcaG_HR2_RV	GCACCGAGACCCG-TATTTGTGC	Clone Homology Ends from *P. putida* Proto-catechuate 3,4-dioxygenease
pGNW_Gib_Lin_FW	AGTCGACCtGCAGGCATGCAAGCTTCT	Linearize pGNW2 for MCI HR1 and 2 insertion
pGNW_Gib_Lin_RV	CGACTCtAGAGGATCCCCGGGTACCG	Linearize pGNW2 for MCI HR1 and 2 insertion

Table S8. Retention times for HPLC standards of catechol and *cis,cis*-muconic acid

Compound	**RID retention time (min)**	**UV retention time (min)**	**Standard curve**
Catechol	5.49	5.18	Y
CCMA	5.83	5.53	Y

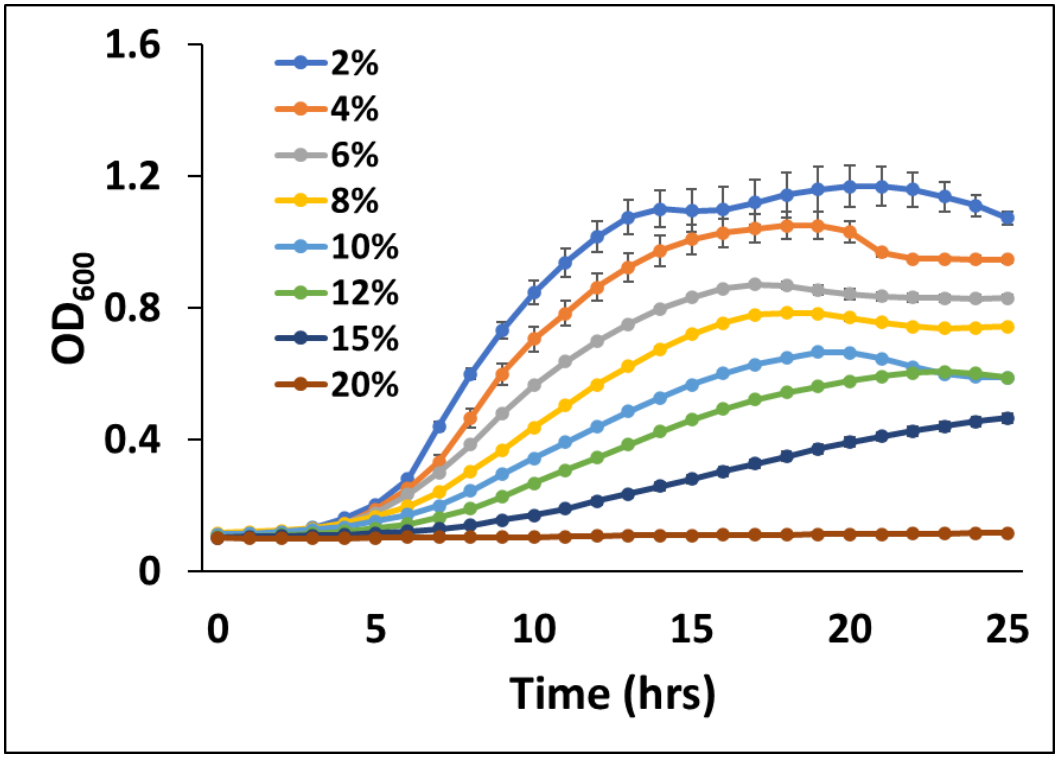

Figure S9. Glucose osmolarity profile of *P. putida* PaW85. Growth curves at varying glucose concentrations of in Wx/M9 minimal medium at 30 °C pH 7.2 over 25 hours. Standard error was used for error bars.

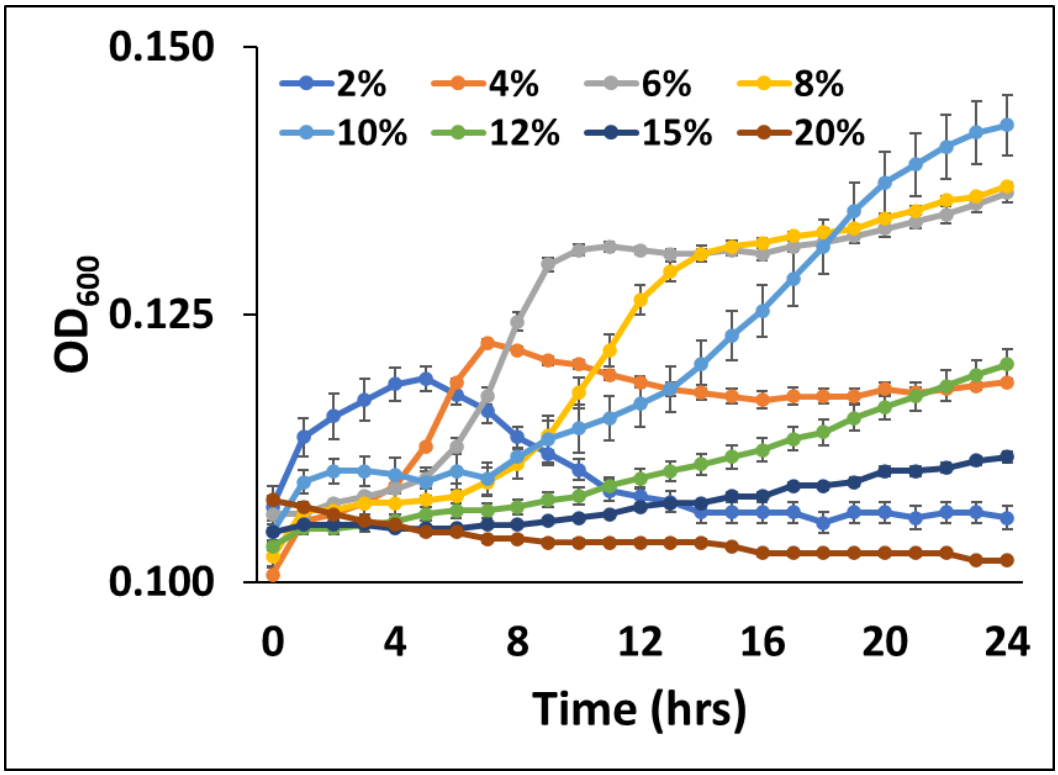

Figure S10. Xylose osmolarity profile of *P. putida* KT2440. Growth curves at varying xylose concentrations of in Wx/M9 minimal medium at 30 °C pH 7.2 over 24 hours. Standard error was used for error bars

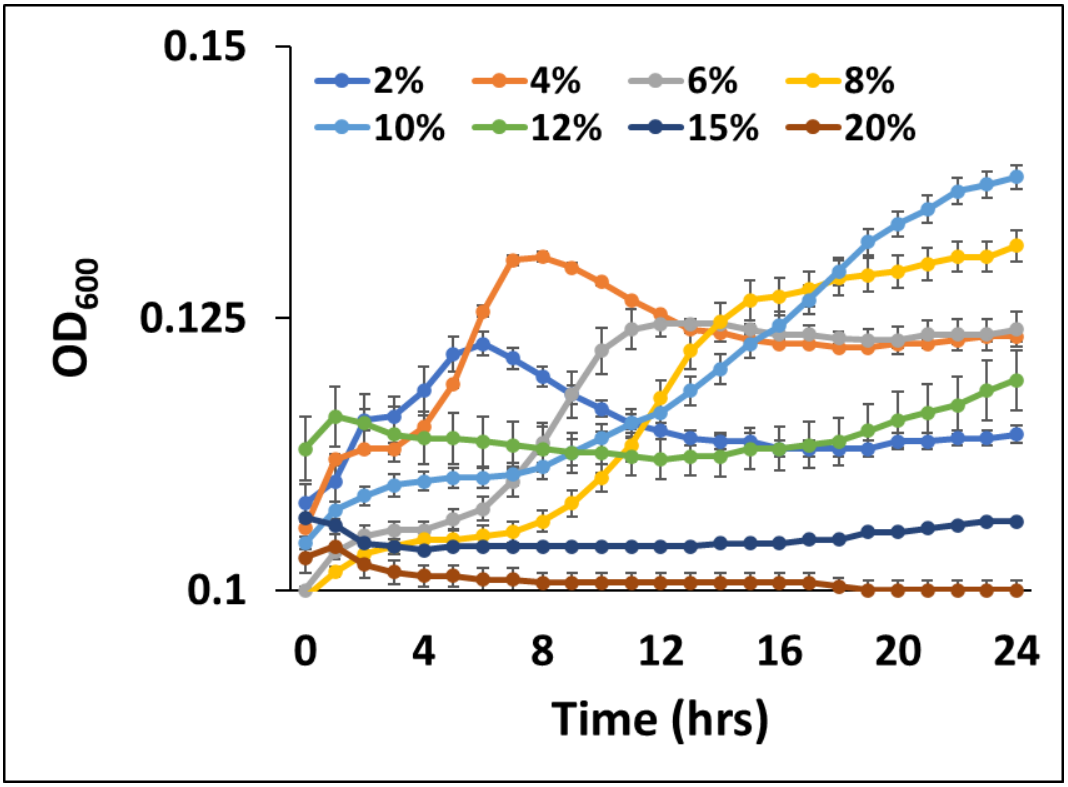

Figure S11. Xylose osmolarity profile of *P. putida* PaW85. Growth curves at varying xylose concentrations of in Wx/M9 minimal medium at 30 °C pH 7.2 over 24 hours. Standard error was used for error bars.

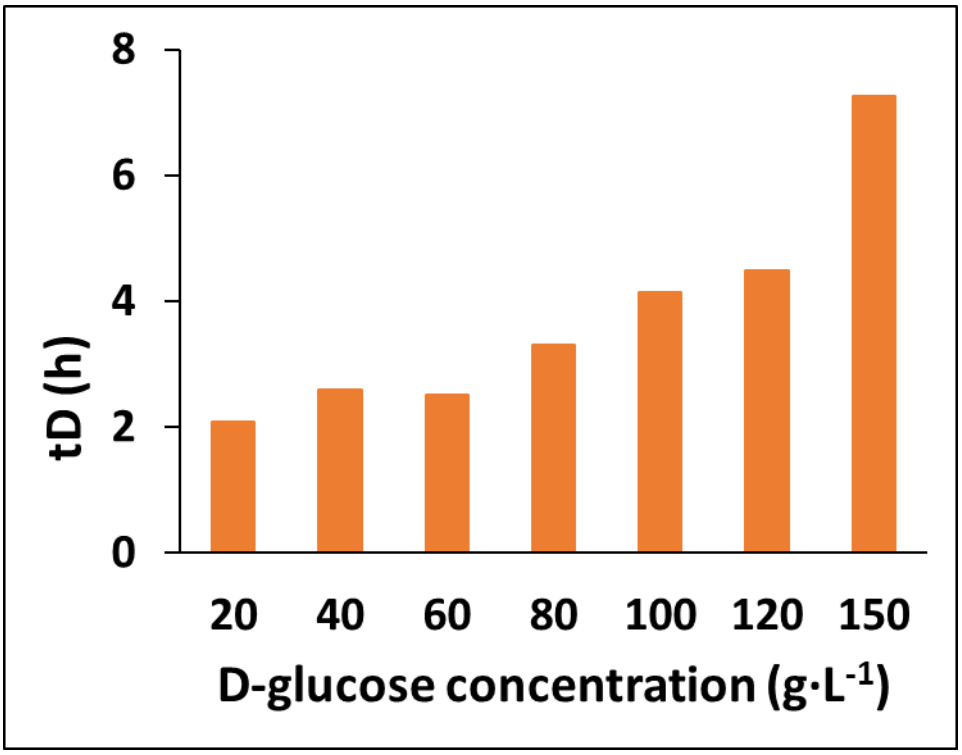

Figure S12: Glucose osmolarity doubling time in hours of *P. putida* KT2440 in Wx/M9 minimal medium with various glucose concentrations at 30 °C and pH 7.2

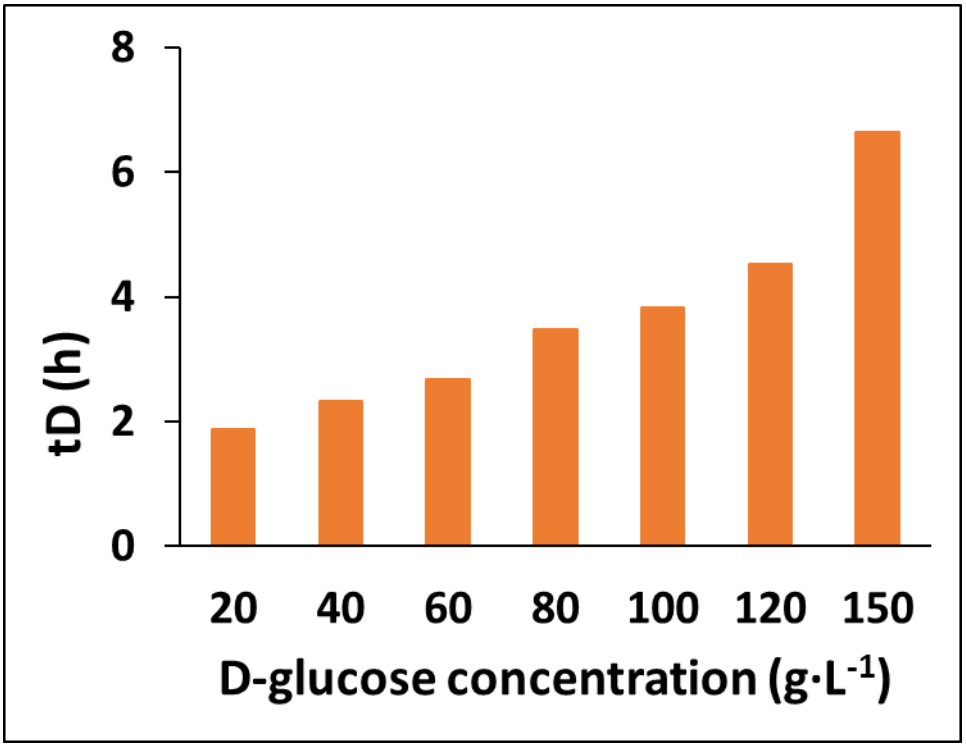

Figure S13: Glucose osmolarity doubling time in hours of *P. putida* PaW85 in Wx/M9 minimal medium with various glucose concentrations at 30 °C and pH 7.2

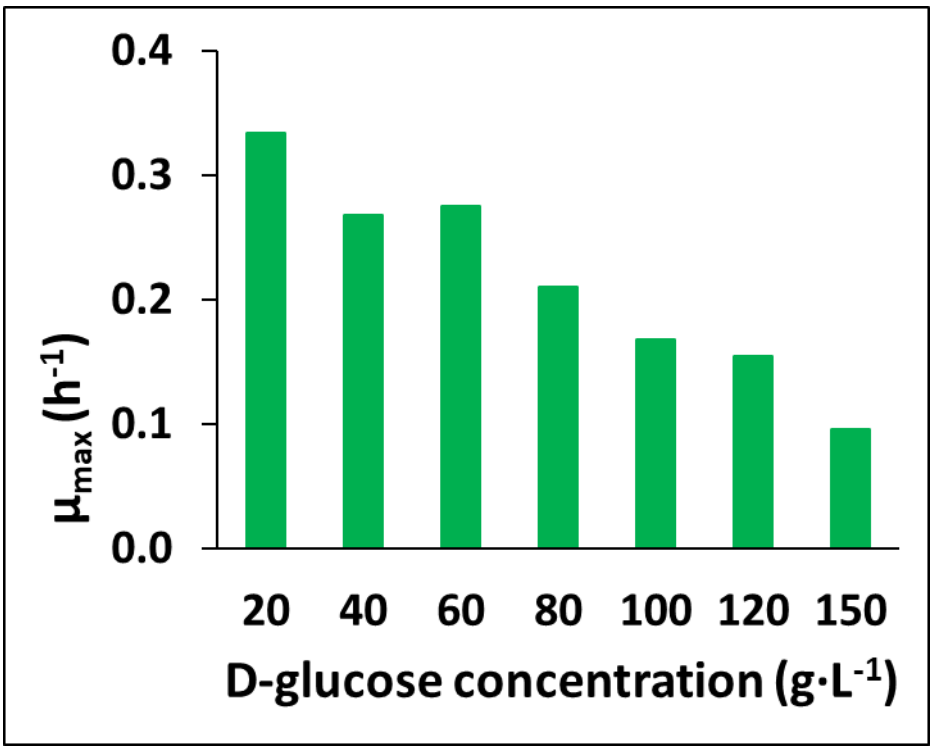

Figure S14. Maximum specific growth rate of *P. putida* KT2440 in Wx/M9 minimal medium with varying glucose concentrations ($g \cdot L^{-1}$) at 30 °C and pH 7.2 during glucose osmolarity experiment.

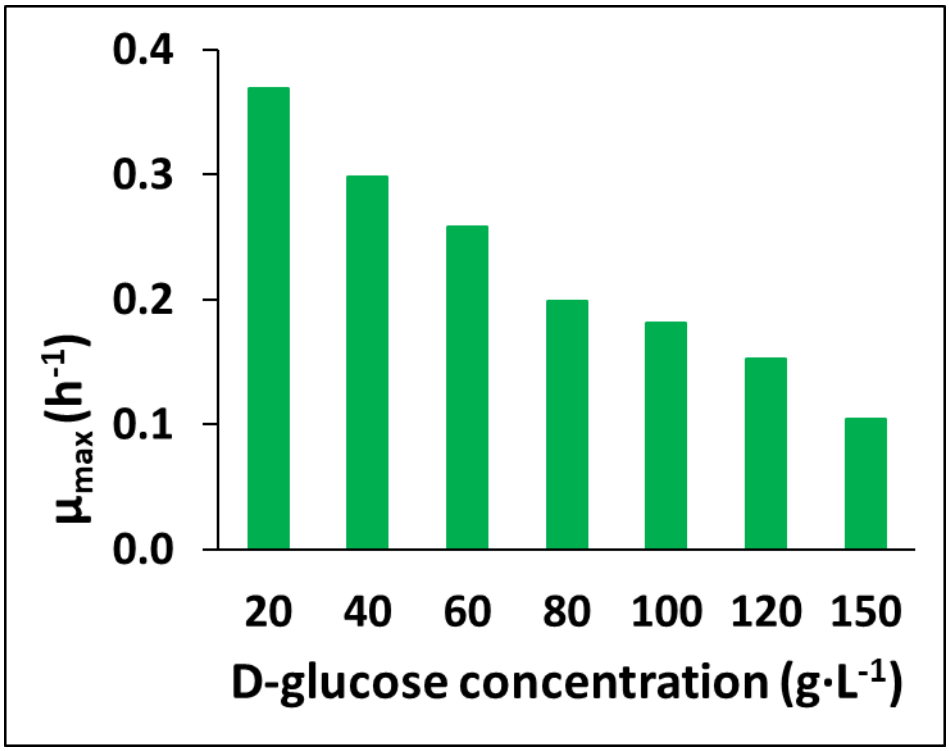

Figure S15. Maximum specific growth rate of *P. putida* PaW85 in Wx/M9 minimal medium with varying glucose concentrations ($g \cdot L^{-1}$) at 30 °C and pH 7.2 during glucose osmolarity experiment.

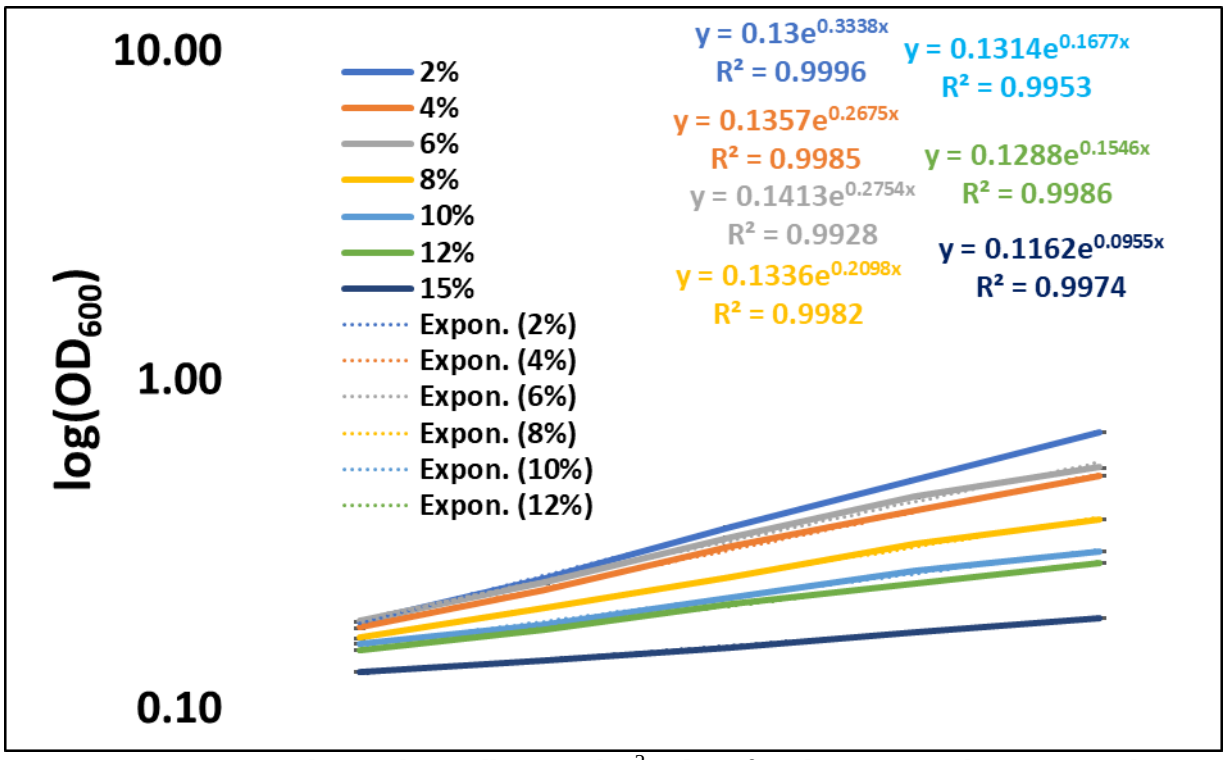

Figure S16: Exponential growth trendlines and R^2 values for glucose osmolarity microplate experiment with *P. putida* KT2440

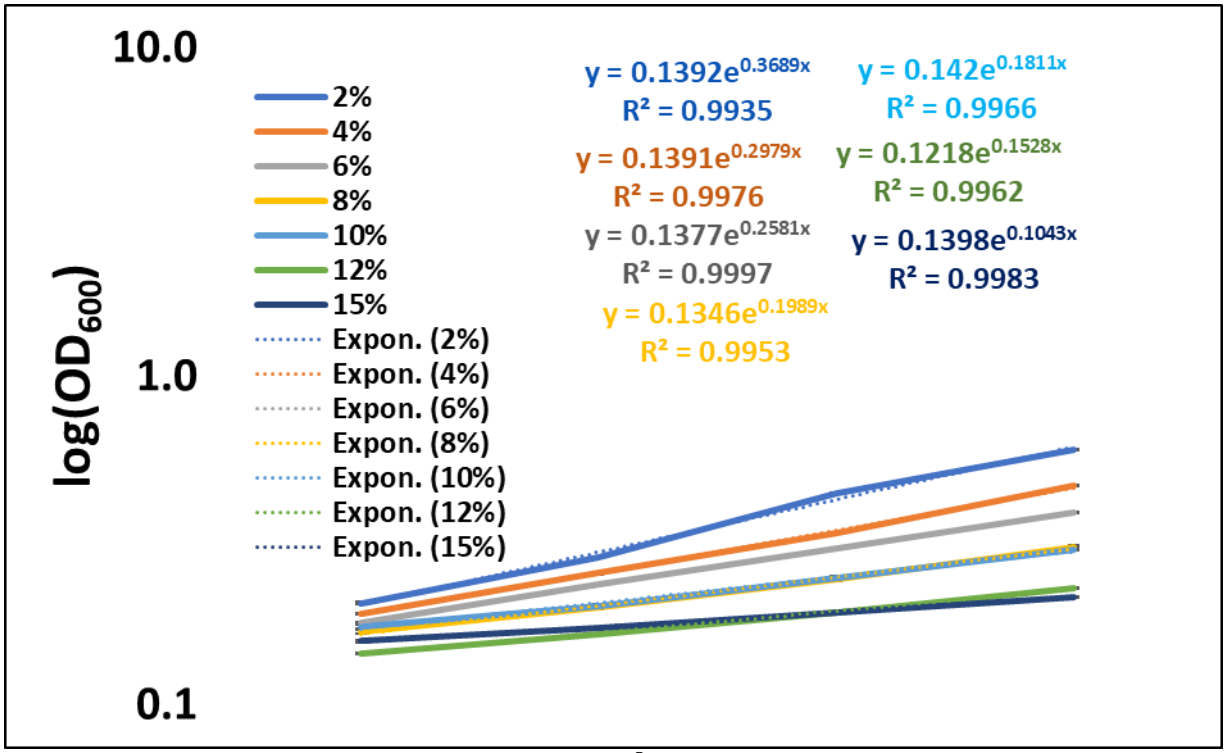

Figure S17: Exponential growth trendlines and R^2 values for glucose osmolarity microplate experiment with *P. putida* PaW85.

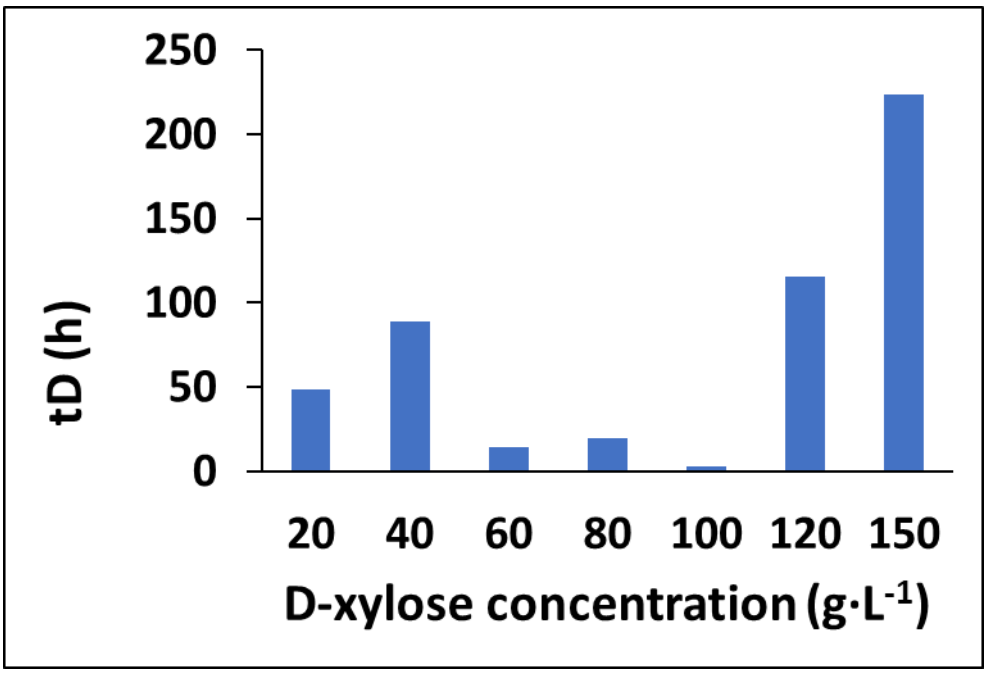

Figure S18. Xylose osmolarity doubling time in hours of *P. putida* KT2440 in Wx/M9 minimal medium with various xylose concentrations at 30 °C and pH 7.2

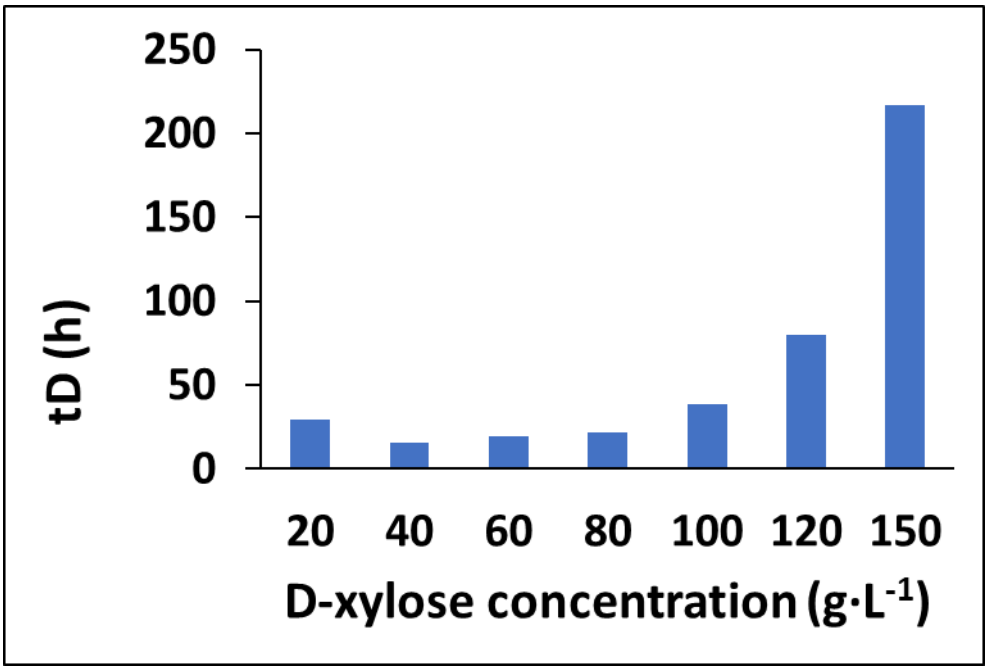

Figure S19. Xylose osmolarity doubling time in hours of *P. putida* PaW85 in Wx/M9 minimal medium with various xylose concentrations at 30 °C and pH 7.2

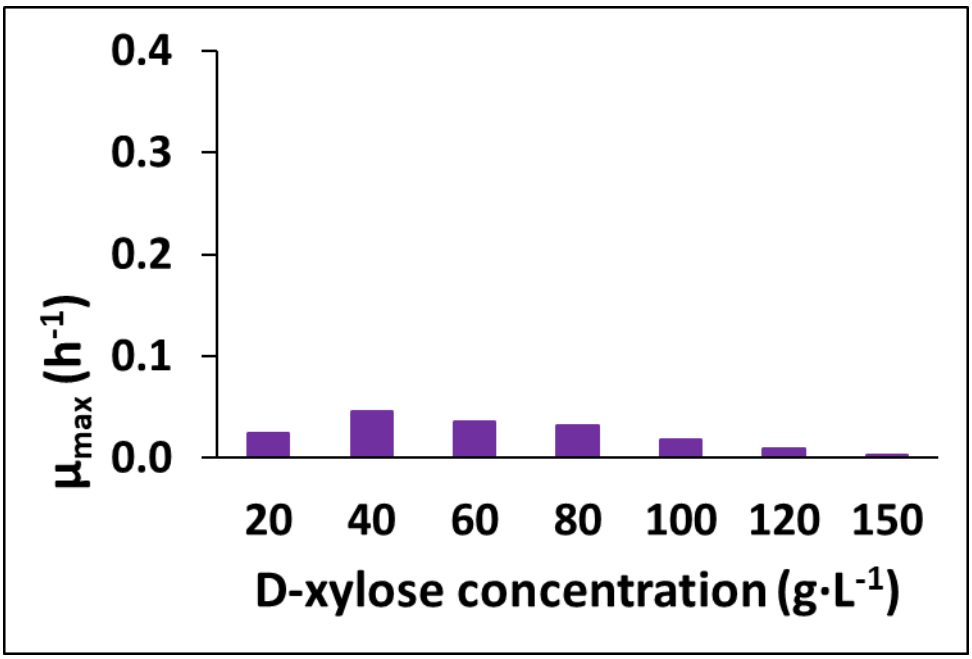

Figure S20. Maximum specific growth rate of *P. putida* PaW85 in Wx/M9 minimal medium with varying xylose concentrations ($g \cdot L^{-1}$) at 30 °C and pH 7.2 during xylose osmolarity experiment.

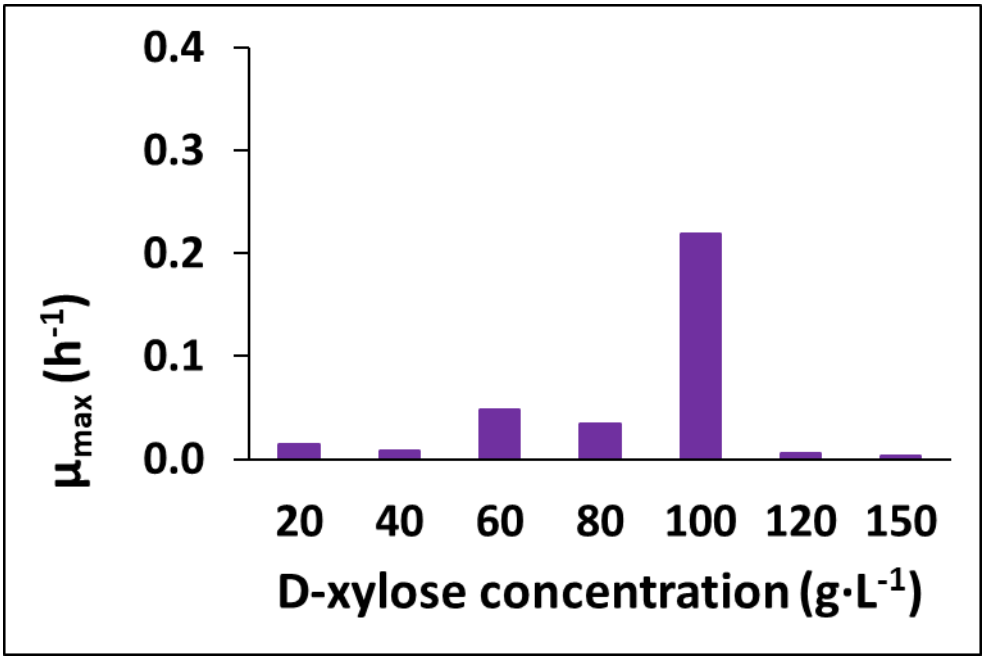

Figure S21. Maximum specific growth rate of *P. putida* KT2440 in Wx/M9 minimal medium with varying xylose concentrations ($g \cdot L^{-1}$) at 30 °C and pH 7.2 during xylose osmolarity experiment.

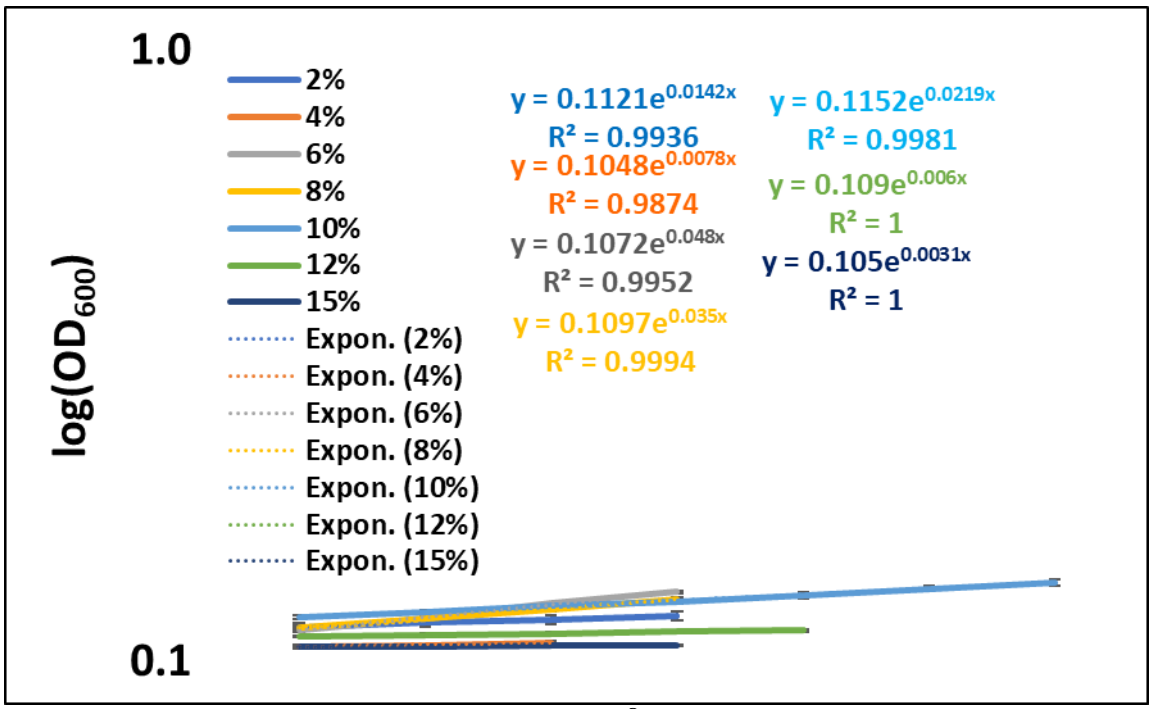

Figure S22: Exponential growth trendlines and R^2 values for xylose osmolarity microplate experiment with *P. putida* KT2440.

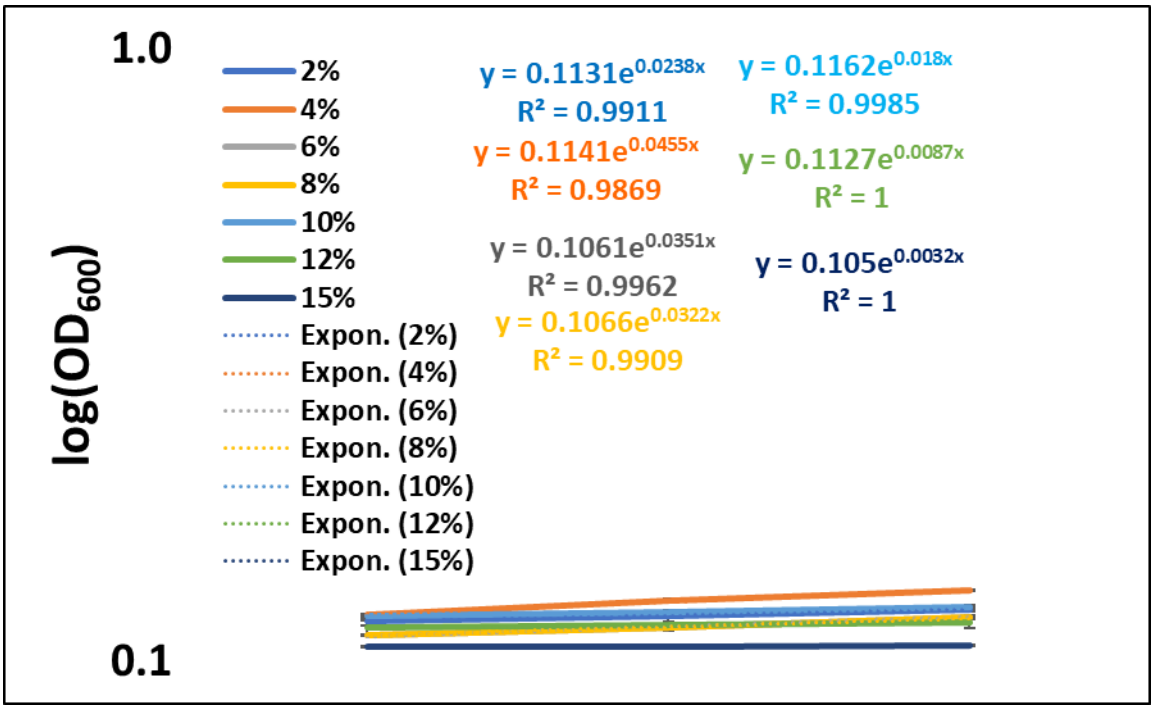

Figure S23: Exponential growth trendlines and R^2 values for xylose osmolarity microplate experiment with *P. putida* PaW85

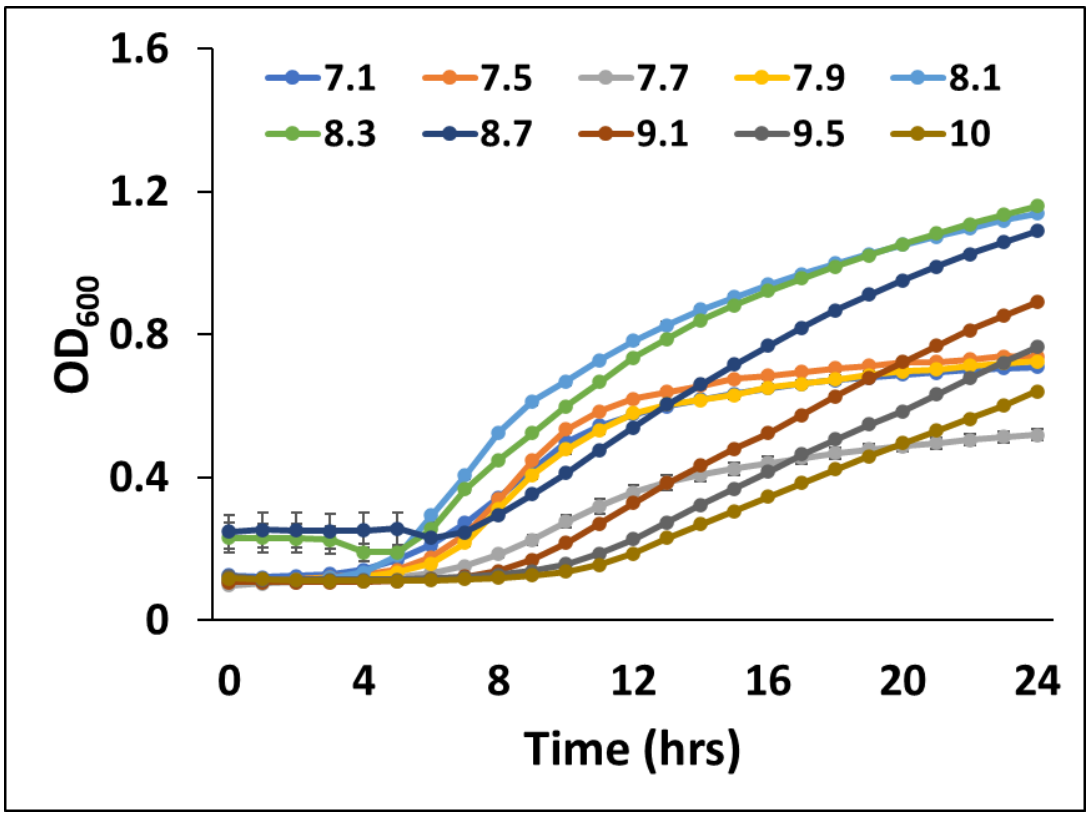

Figure S24. pH tolerance of *P. putida* PaW85. Growth curves at varying pH levels *of* in Wx/M9 minimal medium at 30 °C and 60 g·L^{-1} glucose. NaOH was used to adjust pH. Standard error was used for error bars.

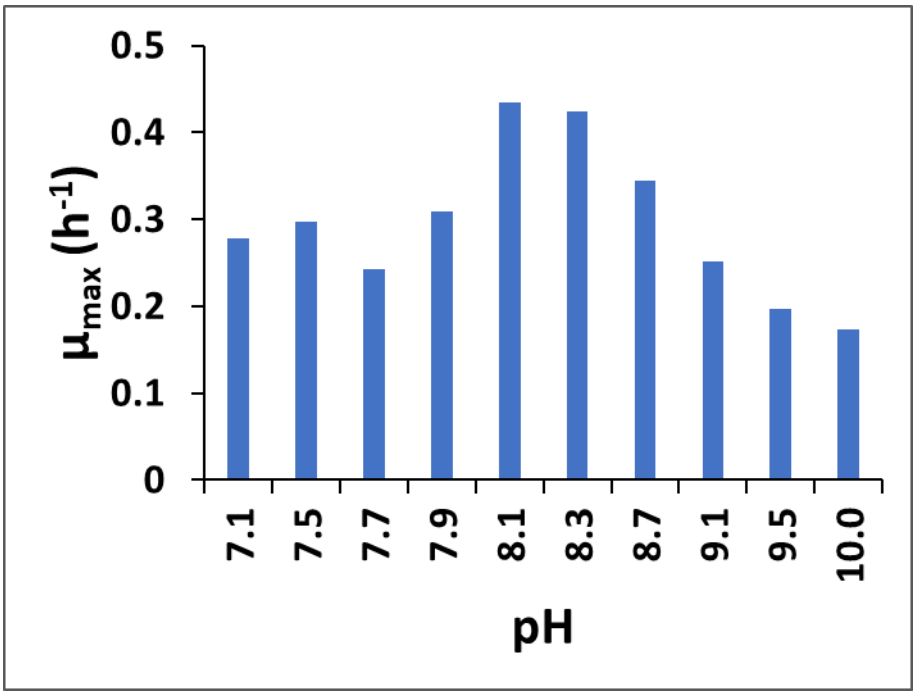

Figure S25. pH tolerance maximum specific growth rate of *P. putida* KT2440 in Wx/M9 minimal medium with varying pH levels at 30 °C and 6% glucose

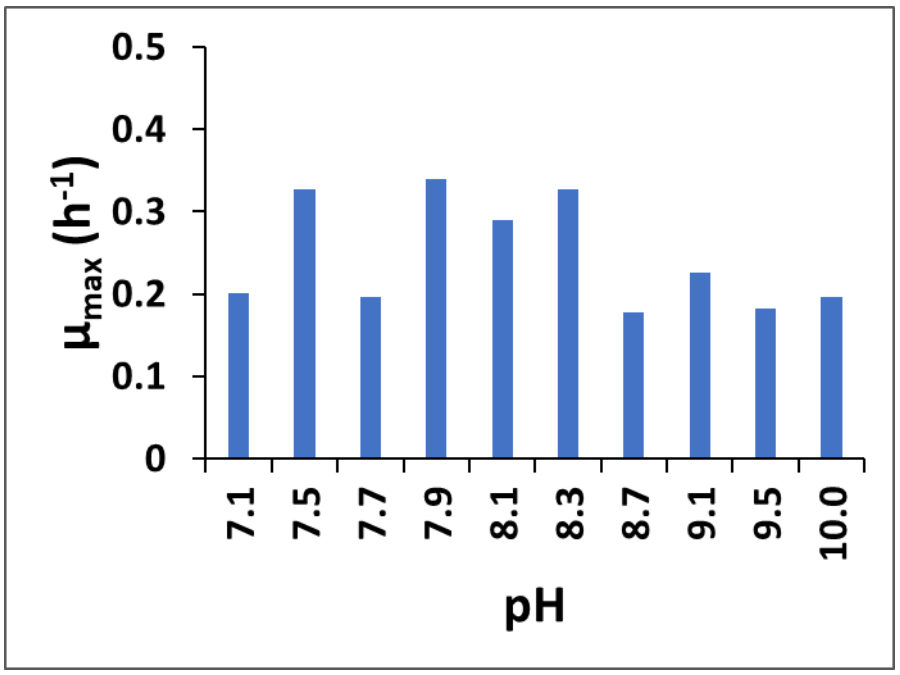

Figure S26. pH tolerance maximum specific growth rate of *P. putida* PaW85 in Wx/M9 minimal medium with varying pH levels at 30 °C and 6% glucose

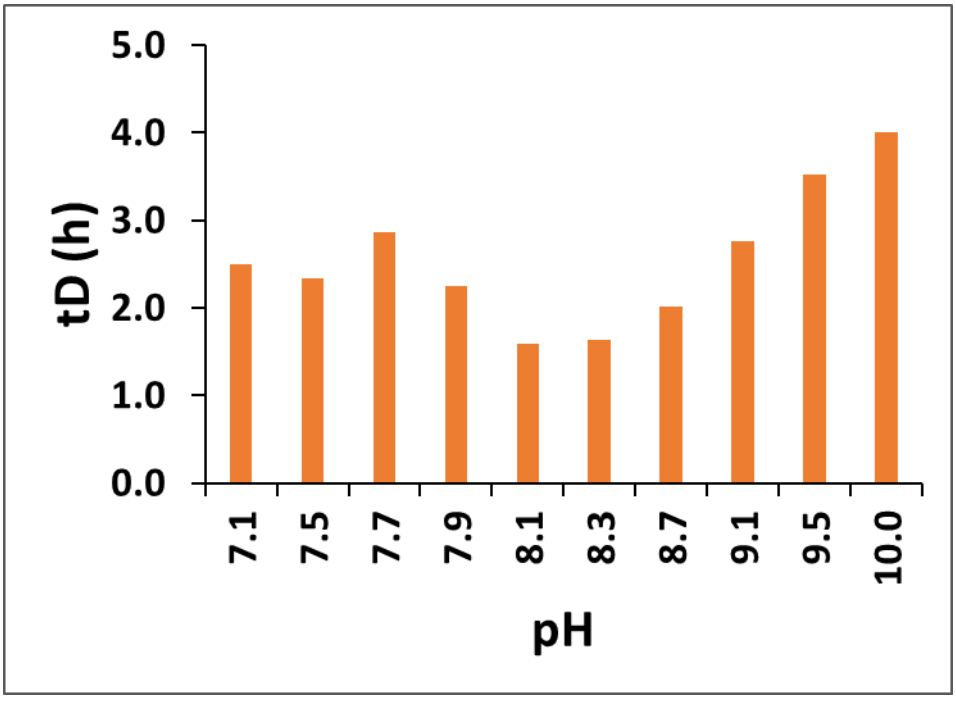

Figure S27. pH tolerance doubling time in hours of *P. putida* KT2440 in Wx/M9 minimal medium with various pH levels at 30 °C and 6% glucose

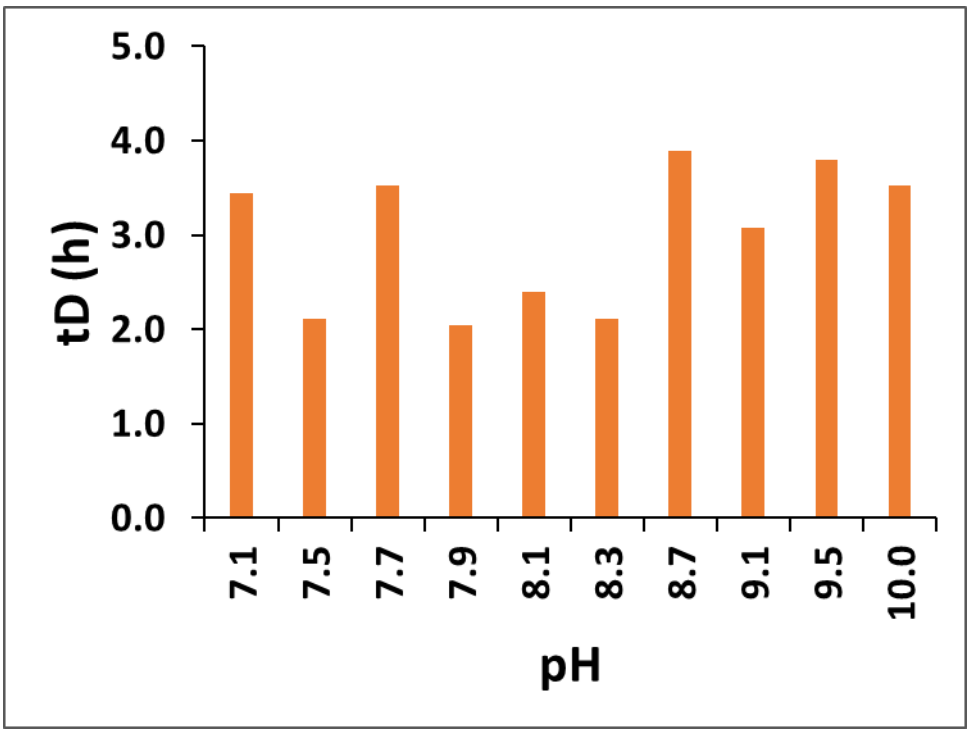

Figure S28. pH tolerance doubling time in hours of *P. putida* PaW85 in Wx/M9 minimal medium with various pH levels at 30 °C and 6% glucose

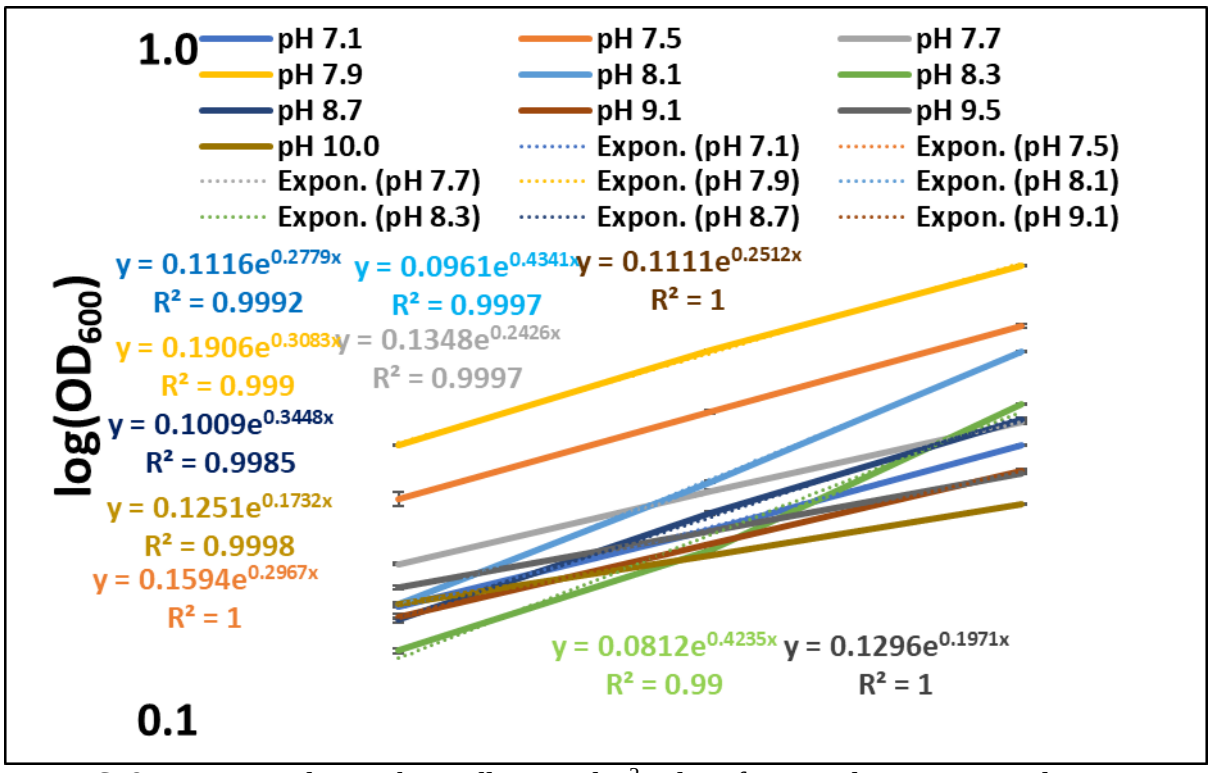

Figure S29. Exponential growth trendlines and R^2 values for pH tolerance microplate experiment with *P. putida* KT2440

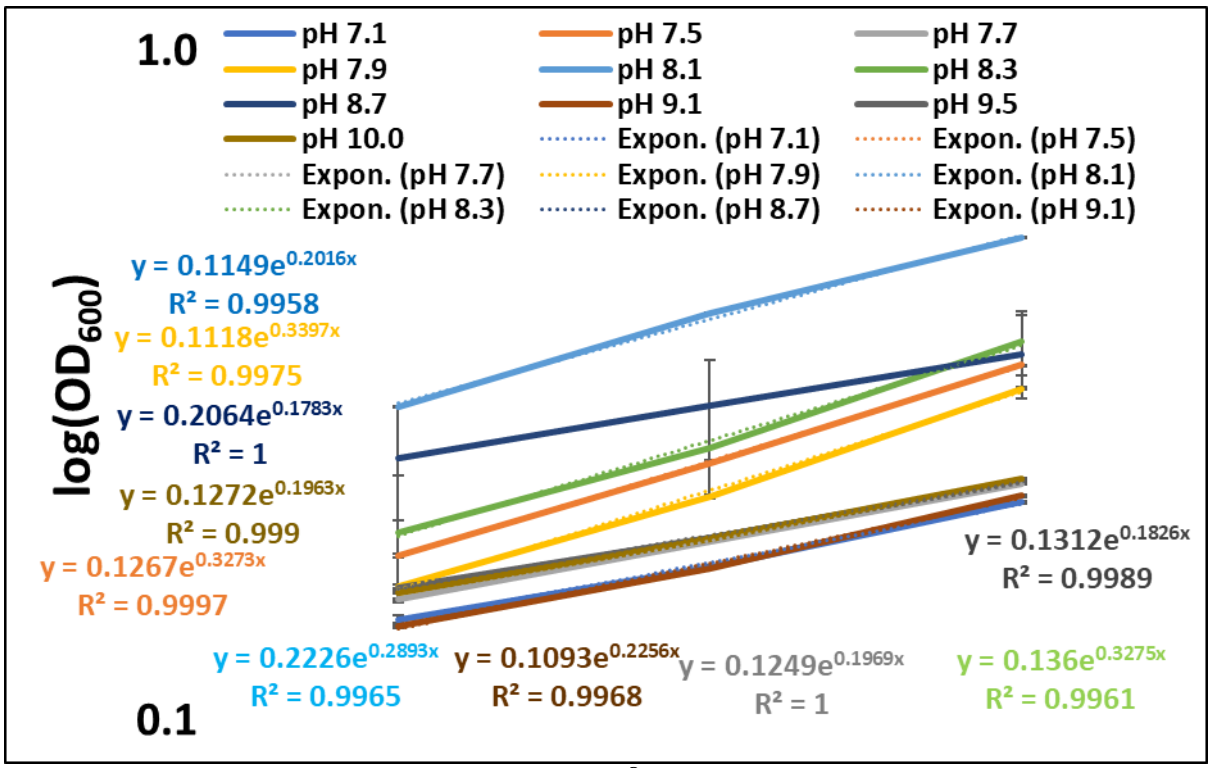

Figure S30. Exponential growth trendlines and R^2 values for pH tolerance microplate experiment with *P. putida* PaW85

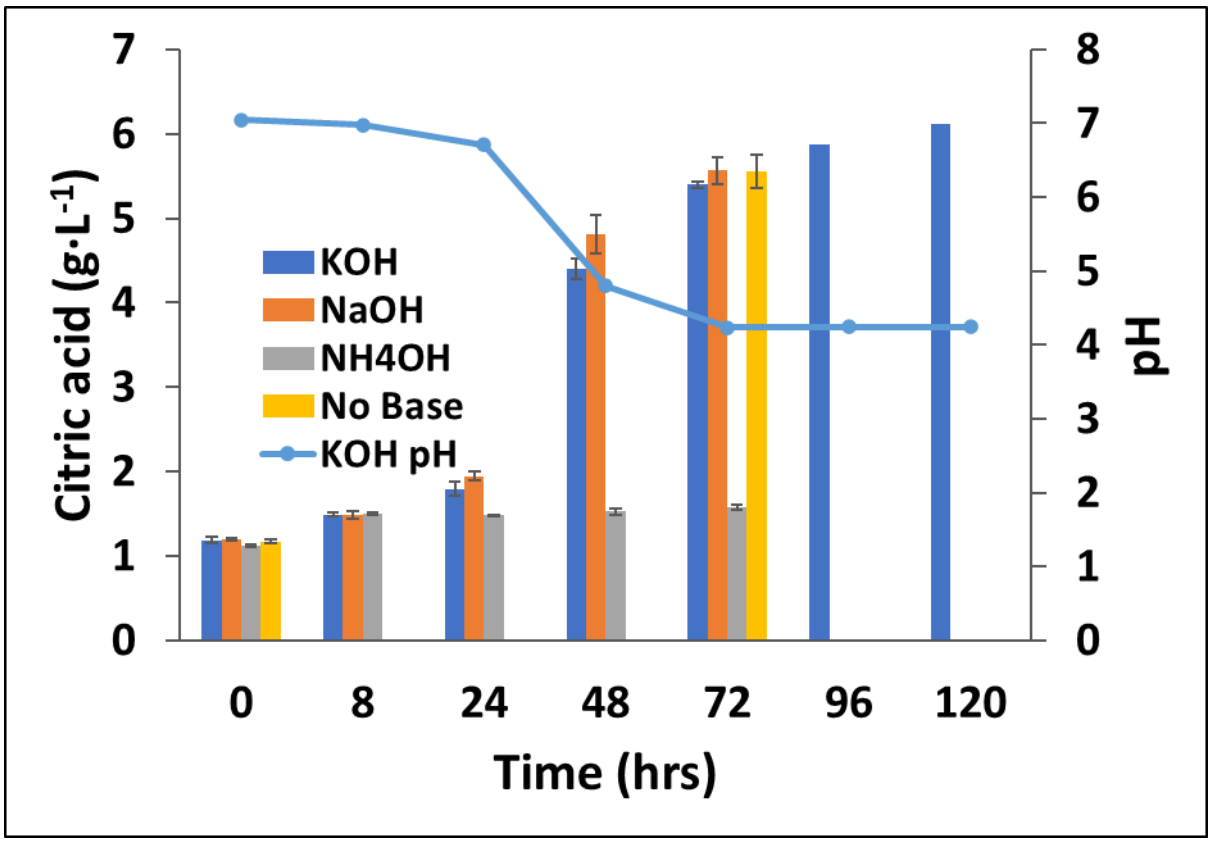

Figure S31. Citric acid concentration dynamics and pH level changes during 120-hour simulated fed-batch fermentation with P. putida KT2440 in alkalized and non-alkalized HL slurry media. Standard error was used for error bars

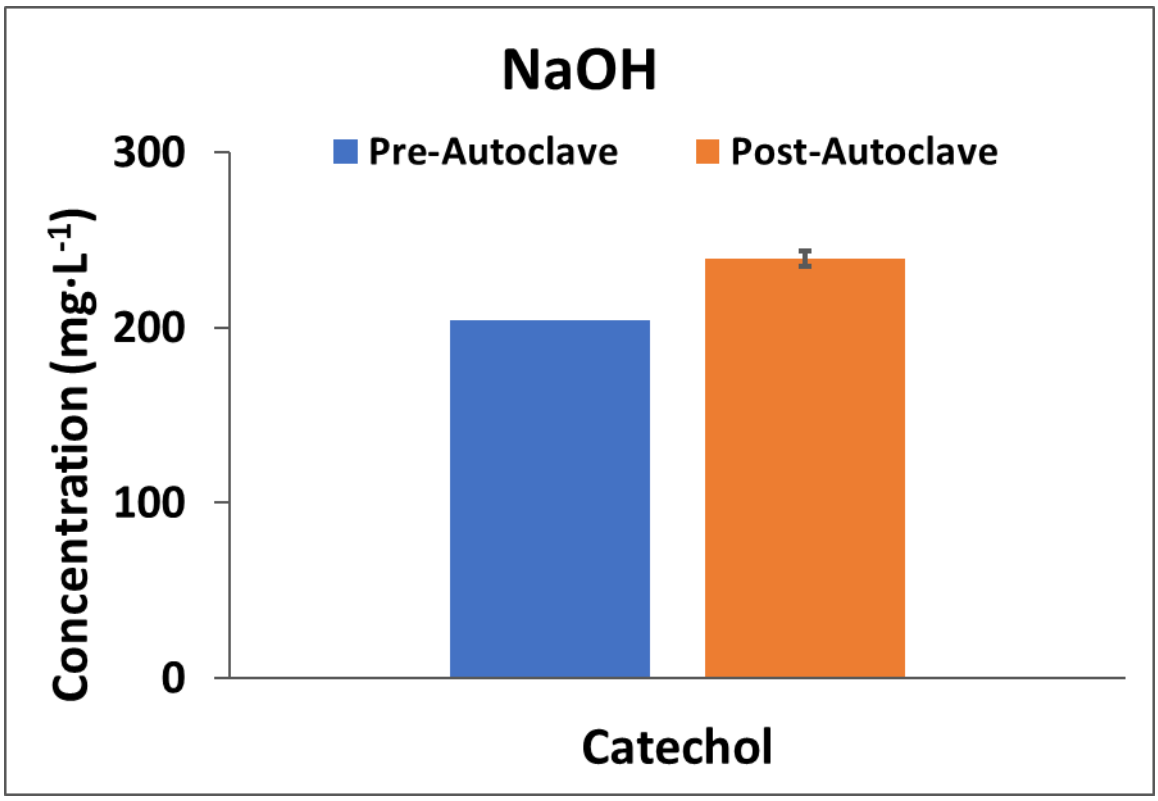

Figure S32. Change in catechol concentration in NaOH-alkalized HL slurry before and after SE.

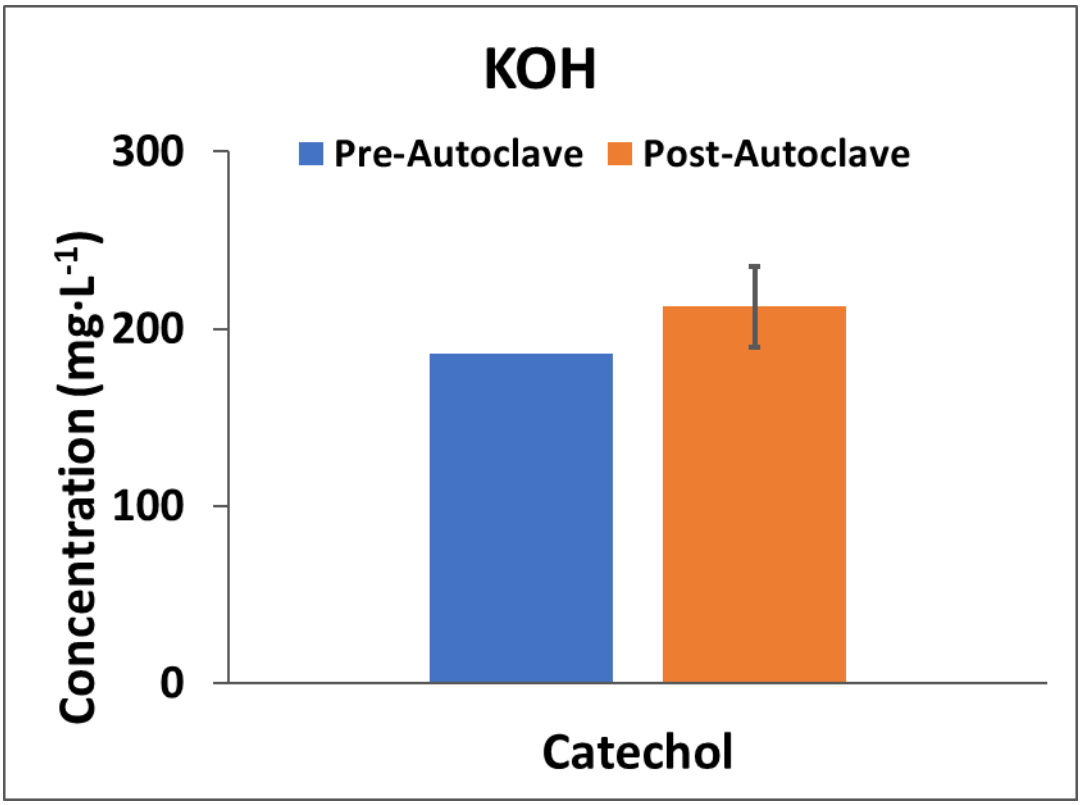

Figure S33. Change in catechol concentration in KOH-alkalized HL slurry before and after SE.

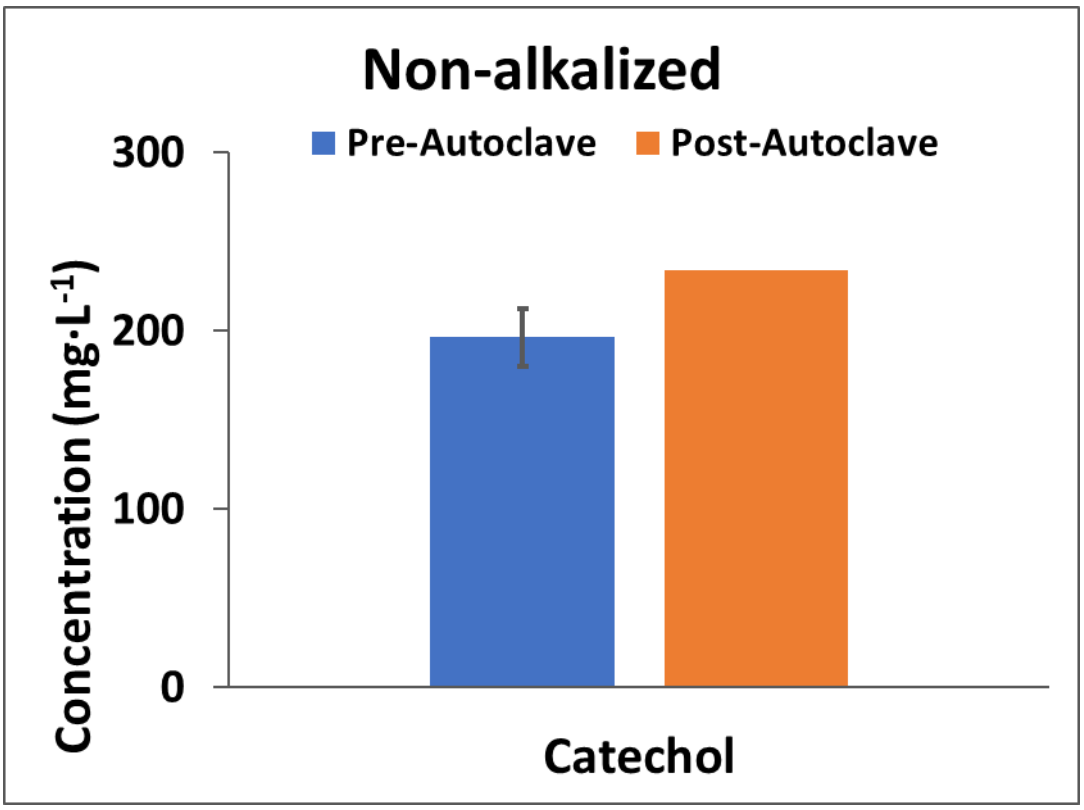

Figure S34. Change in catechol concentration in non-alkalized HL slurry before and after SE.

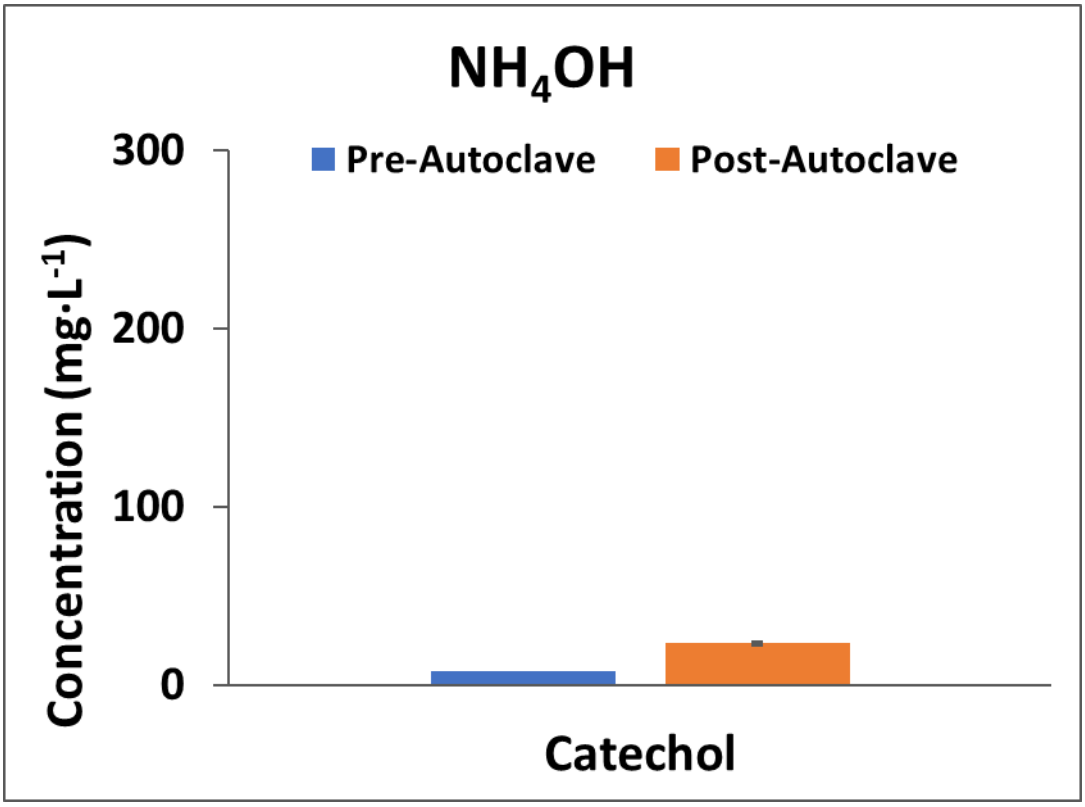

Figure S35. Change in catechol concentration in NH_4OH-alkalized HL slurry before and after SE.

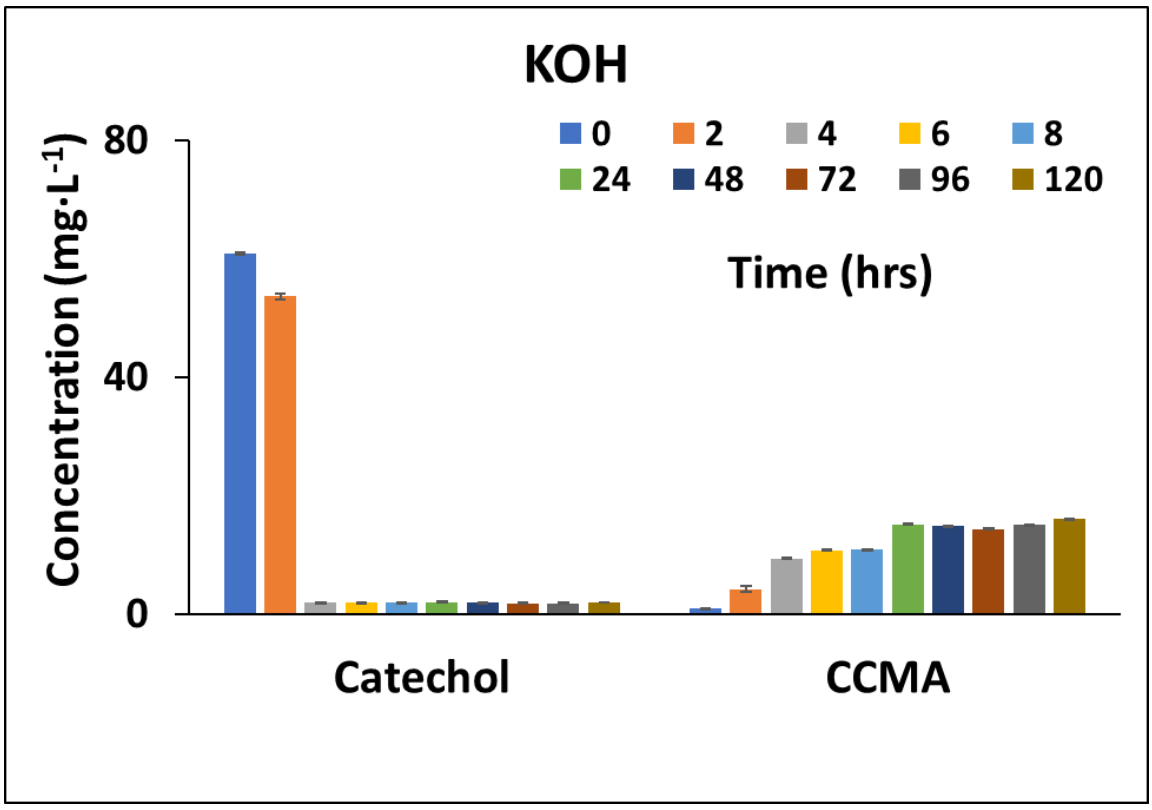

Figure S36. Changes in the concentrations of catechol and *cis,cis*-muconic acid during a 120-hour simulated fed-batch fermentation of an HL slurry made with Wx/M9 minimal medium and alkalized with KOH. Standard error was used for the error bars.

Table S37. Strains used in this work

Strains	**Species**	**Relevant Genotype**	**Source/Reference/Isolated by**
unknown strain	*Escherichia coli*	Harbors plasmid pGNW2	https://www.addgene.org/122086
PaW85	*Pseudomonas putida*	17 kb transposon Tn4652 in chromosome. Plasmid-free strain.	Bayley *et al*., 1977; gift from Maia Kivisaar
KT2440	*Pseudomonas alloputida*		Nelson *et al.,* 2002; DSMZ
KT2440	*Pseudomonas putida*	Plasmid-free derivative of *Pseudomonas putida* mt2	Gift from Maia Kivisaar
mt2	*Pseudomonas putida*	TOL plasmid	Williams and Murray, 1974; Eeva Heinaru (CELMS)
1R2A4	*Mitsuaria chitosanitabida*		Eeva Heinaru (CELMS)
1S7	*Pseudomonas putida*		Eeva Heinaru (CELMS)
T13	*Enterobacter* sp./*Lelliottia* sp.		Merike Jõessar (CELMS)
VAS4	*Pseudomonas* sp./*defluvii*		Merike Jõessar (CELMS)

PJK7	*Pseudomonas putida*		Merike Jõessar (CELMS)
T10	*Pseudomonas stutzeri/ xanthomarina*		Merike Jõessar (CELMS)
SM	*Serratia proteamaculans*		Merike Jõessar (CELMS)
A21	*Pseudomonas resinovorans*		Elerin Toomik (CELMS)
L19	*Rhodococcus erythropolis*		Elerin Toomik (CELMS)
A26	*Rhodococcus erythropolis*		Elerin Toomik (CELMS)
A15	*Rhodococcus erythropolis*		Elerin Toomik (CELMS)
A8	*Rhodococcus erythropolis*		Elerin Toomik (CELMS)
A11B	*Cellulomonas* sp.		Elerin Toomik (CELMS)
A4x	*Bacillus subtilis*		Elerin Toomik (CELMS)
A24	*Bacillus subtilis*		Elerin Toomik (CELMS)
L12ABA	*Bacillus simplex*		Elerin Toomik (CELMS)
A7	*Bacillus pumilus*		Elerin Toomik (CELMS)
RP2	*Rhodococcus* sp. */erythropolis*		Merike Jõessar (CELMS)
43SK1	*Kocuria rosea*		Eeva Heinaru, Sulev Kuuse, Julius Tarand (CELMS)
PC20	*Pseudomonas fluorescens*	AY538264 (16S rRNA gene), DQ178200 (carA gene), AY887963 (Plasmid pNAH20), KY503036 (Plasmid pPHE20), KX893538 (Plasmid pG20)	Heinaru *et al.*, 2000; Eeva Heinaru (CELMS)
6S4	*Acinetobacter johnsonii*		Eeva Heinaru & Sulev Kuuse (CELMS)
P101	*Pseudomonas thivervalensis*	MH061178 (plasmid pPHE101), MN560131 (16S rRNA gene)	Elken *et al.*, 2020; Eeva Heinaru (CELMS)
KM2R4	*Pseudomonas syringae*		Eeva Heinaru (CELMS)
VMR7	*Pseudomonas stuzeri*		Eeva Heinaru (CELMS)
Phe16	*Arthrobacter sulfonivorans*		Eeva Heinaru (CELMS)

CELMS - The strains were obtained from the Collection of Environmental and Laboratory Microbial Strains (CELMS; financed by the Estonian Ministry of Education and Research

(RLOMRCELMS), the public catalog of which is available on the Estonian Electronic Microbial dataBase (EEMB) web-site http://eemb.ut.ee

Table S38. Conversion of lignin derived compounds after 24-and 120 hours of bacterial cultivation compared to the contents in the uninoculated 24-hour and 120-hour controls.

	Tracked compounds											
Bacterial Strains	**5-HMF (24H)**	**5-HMF (120H)**	**PCA (24H)**	**PCA (120H)**	**SA (24H)**	**SA (120H)**	**Cat (24H)**	**Cat (120H)**	**CCMA (24H)**	**CCMA (120H)**	**VA (24H)**	**VA (120H)**
KT2440	---	---	--	++	+	---	----	----	+++	++++	+-	----
mt2	---	---	-	+	+	---	----	----	+++	++++	-	----
1R2A4	---	---	+++	+++	+-	+	----	----	++	++++	+-	----
1S7	---	---	--	-	---	----	----	----	++++	++++	----	----
T13	---	---	++++	++++	--	---	----	----	+	-	----	----
VAS4	---	---	-	+-	-	-	----	----	+++	+++	++	++
PJK7	---	---	-	+++	-	+-	----	----	+++	++++	++	++
PJK5	---	---	-	+	-	----	----	----	++	++	--	----
T10	---	---	+	--	-	-	----	----	+	+++	+	+
SM	--	---	+++	--	-	-	----	----	+	++++	+	----
A21	--	---	+	--	-	+	----	----	+++	+++	+-	++
L19	-	---	-	+	-	-	---	----	+-	+++	+-	++
A26	+-	---	+-	+	-	-	----	----	+-	+++	++	++
A15	+-	---	--	++	-	-	--	----	+-	+++	+	++
A8	-	---	-	-	-	-	----	----	+	+++	+	++
A11B	-	--	-	+	-	-	--	----	+-	-	+	-
A4X	-	+-	+-	+	--	-	+-	----	+-	+-	-	+
A24	-	-	+-	+	-	--	+-	----	-	+	-	--
L12ABA	+-	+-	+-	+-	-	-	--	----	+-	-	-	-
A7	+-	-	+-	+	-	-	-	--	+-	-	-	-
RP2	n/a	---	n/a	+	n/a	-	n/a	----	n/a	+++	n/a	+
435K1	n/a	--	n/a	+-	n/a	-	n/a	----	n/a	+	n/a	++
PC20	n/a	---	n/a	+-	n/a	-	n/a	----	n/a	+-	n/a	--
654	n/a	---	n/a	+-	n/a	-	n/a	----	n/a	++	n/a	-
P101	n/a	---	n/a	--	n/a	-	n/a	----	n/a	+++	n/a	+
KM2R1	n/a	---	n/a	--	n/a	--	n/a	----	n/a	+++	n/a	----
KM2R4	n/a	---	n/a	--	n/a	+	n/a	----	n/a	-	n/a	+
VMR7	n/a	---	n/a	--	n/a	+-	n/a	----	n/a	+++	n/a	+
Phe16	n/a	-	n/a	-	n/a	-	n/a	----	n/a	+-	n/a	-

Note The compounds are labelled as follows: 5-HMF: 5-hydroxymethylfurfural; PCA: protocatechuic acid; SA: syringic acid; Cat: catechol; CCMA: *cis,cis*-muconic acid; VA: vanillic acid. The symbols in the table indicate the percentage range of change in compound concentration. ----: >75% decrease; ---: 50-75% decrease; - -: 25-50% decrease; -: 5-25% decrease; + -: 5% decrease to 5% increase; +: 5-25% increase; ++: 25-50% increase; "+++": 50-75% increase; ++++: >75% increase.

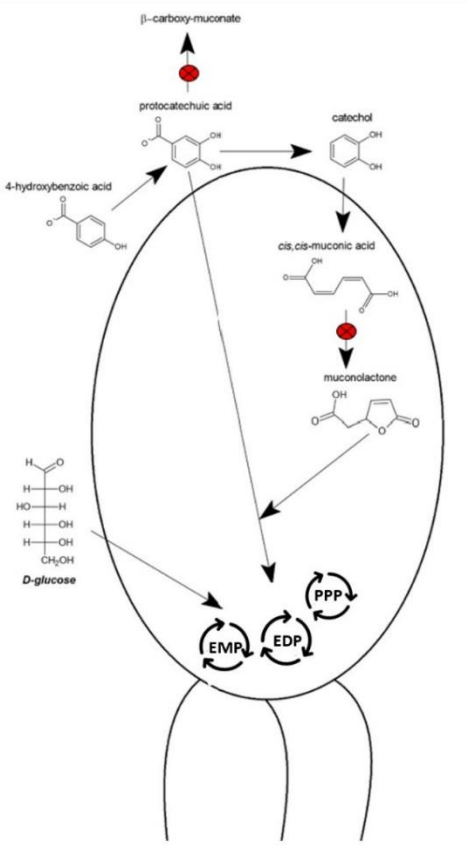

Figure 39. Metabolic pathway for the production of *cis,cis*-muconic acid from HL-derived monomers and two proposed targets for gene deletion. Entner-Duteroff Pathway (EMP), Embden-Meyerhof-Parnas Pathway (EMP), and Pentose Phosphate Pathway (PPP).

Table S40. DNA oligo annealing temperatures from Integrated DNA Technologies (IDT), New England Biolabs Tm Calculator (NEB), and Thermo Fisher Scientific Tm Calculator (TF)

Primer	**IDT**	**NEB**	**TF**
MucCycIso_HR1_FW	62.0 °C	65.0 °C	68.0 °C
MucCycIso_HR1_RV	60.7 °C	66.0 °C	68.6 °C
MucCycIso_HR2_FW	60.3 °C	67.0 °C	69.7 °C
MucCycIso_HR2_RV	60.2 °C	66.0 °C	69.0 °C
MCI_HR2a_RV	61.8 °C	65.0 °C	67.9 °C
MCI_HR2b_RV	62.0 °C	66.0 °C	68.5 °C
MCI_HR2c_RV	63.7 °C	65.0 °C	68.5 °C
pcaH_HR1_FW	61.7 °C	66.0 °C	69.1 °C
pcaH_HR1_RV	58.3 °C	63.0 °C	66.2 °C
pcaG_HR2_FW	60.8 °C	67.0 °C	67.7 °C
pcaG_HR2_RV	60.8 °C	66.0 °C	68.7 °C

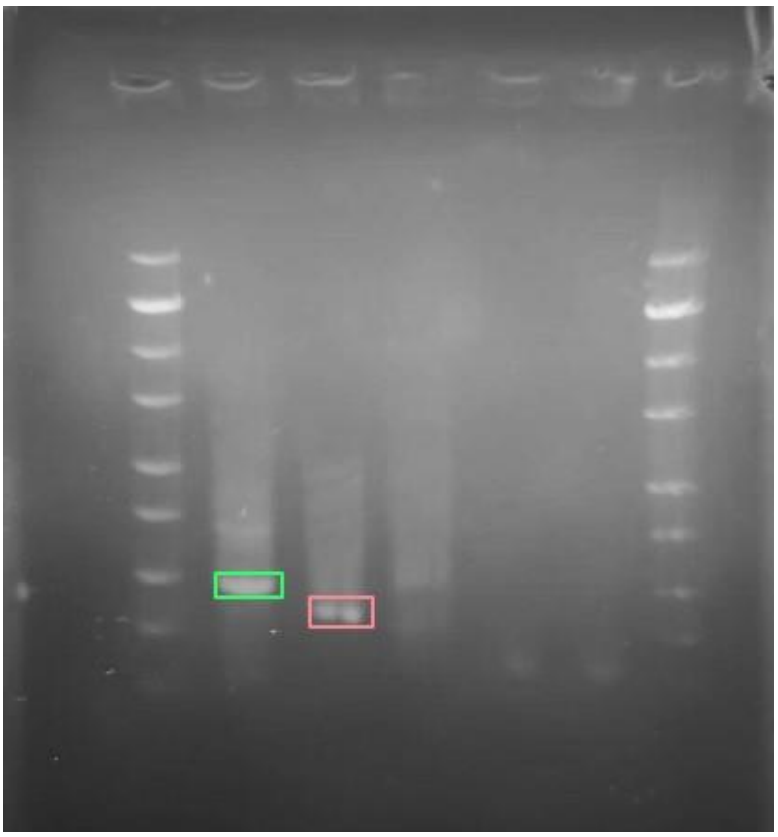

Figure S41. Snapshot of electrophoresis gel of MCI HR1, MCI HR2_Test, MCI HR2, MCI HR2a, and MCI HR2b. The annealing temperature was 64 °C for all fragments. Only MCI HR1 (green) and MCI HR2_Test (pink) were amplified.

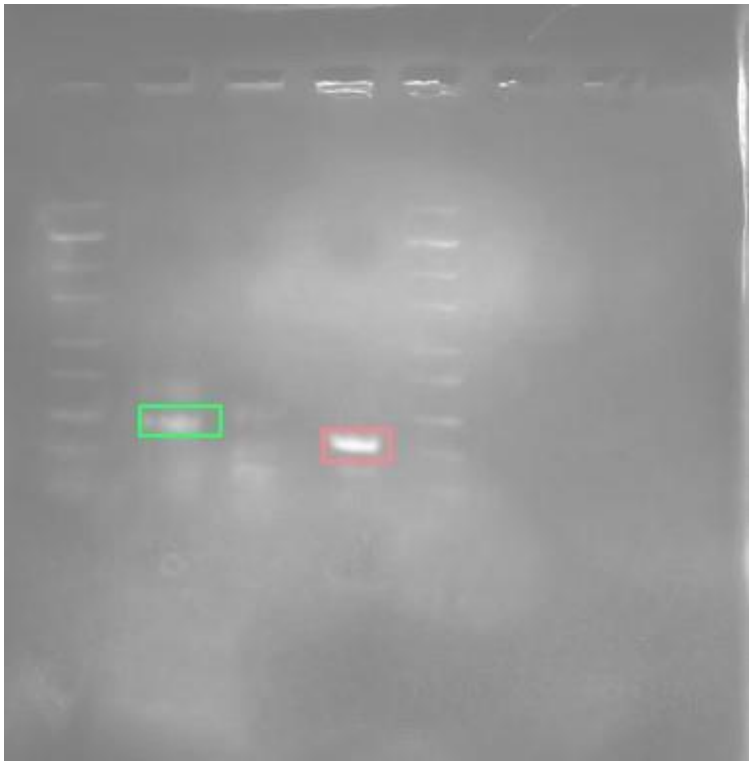

Figure S42. Snapshot of electrophoresis gel of MCI HR1, MCI HR2, MCI HR2_Test. The annealing temperature was 63 °C for all fragments. Only MCI HR1(green) and MCI HR2_Test (pink) were amplified.

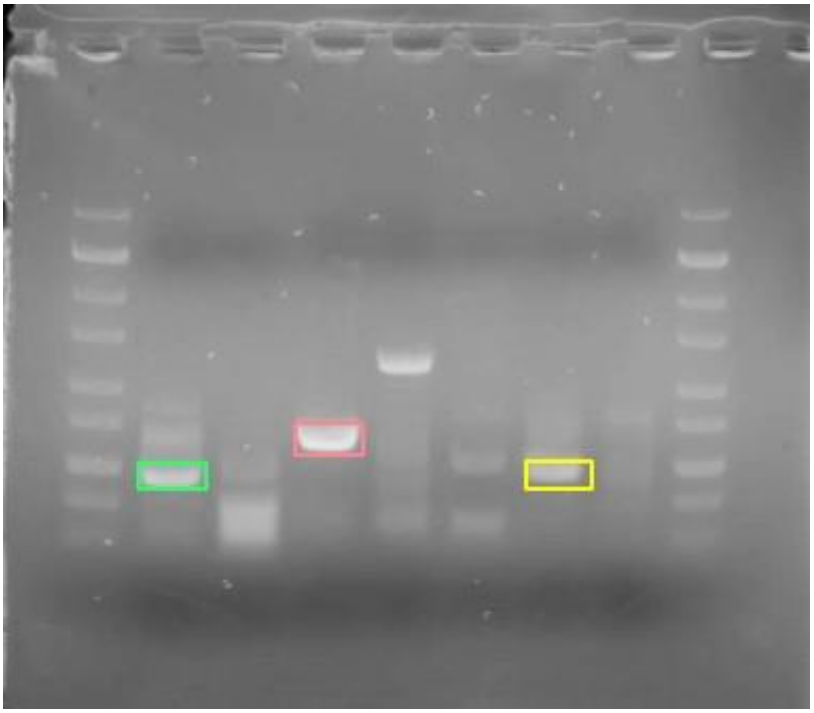

Figure S43. Snapshot of electrophoresis gel of MCI HR1, MCI HR2, MCI HR2a, MCI HR2b, MCI HR2c, pcaH HR1, and pcaG HR2. The annealing temperature was 68 °C for all fragments. Only MCI HR1 (green), MCI HR2a (pink), and pcaH HR1 (yellow) were amplified.

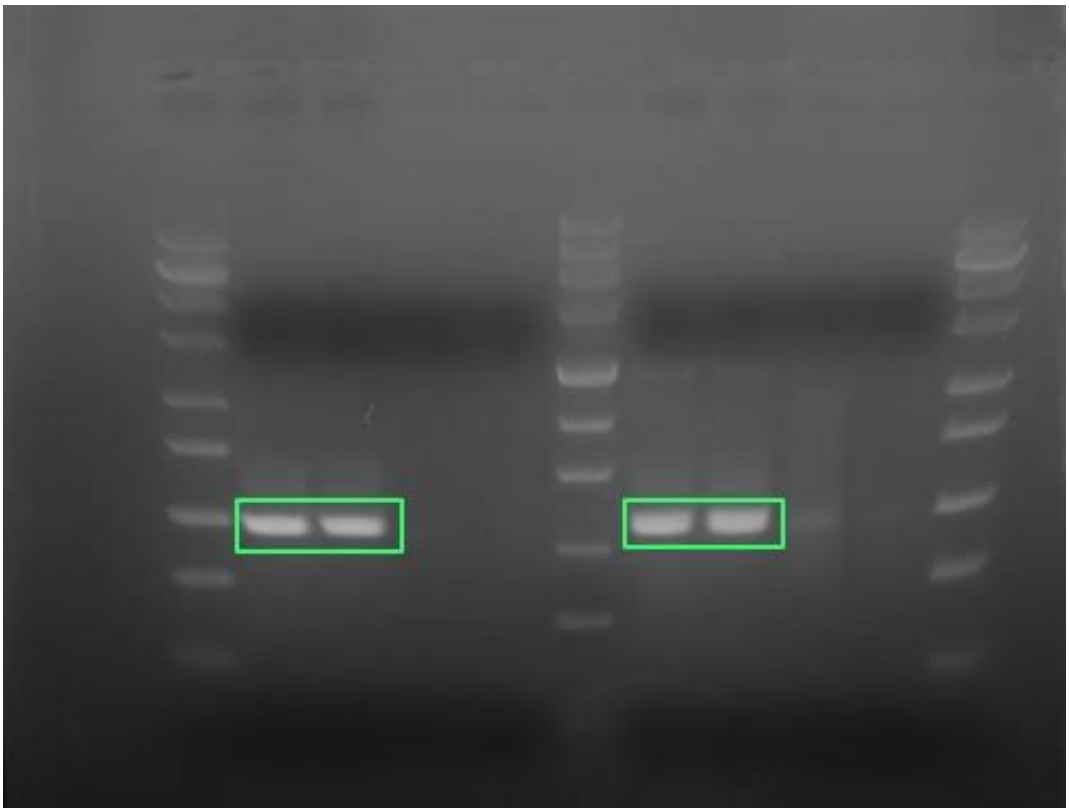

Figure S44. Snapshot of electrophoresis gel of MCI HR1 (65 °C), MCI HR1 (66 °C), pcaG HR2 (64 °C), pcaG HR2 (65 °C), MCI HR1 (65 °C + DMSO), MCI HR1 (66 °C + DMSO), pcaG HR2 (64 °C + DMSO), pcaG HR2 (65 °C + DMSO). All the MCI HR1 samples (green) were amplified but none of the pcaG HR2 samples.

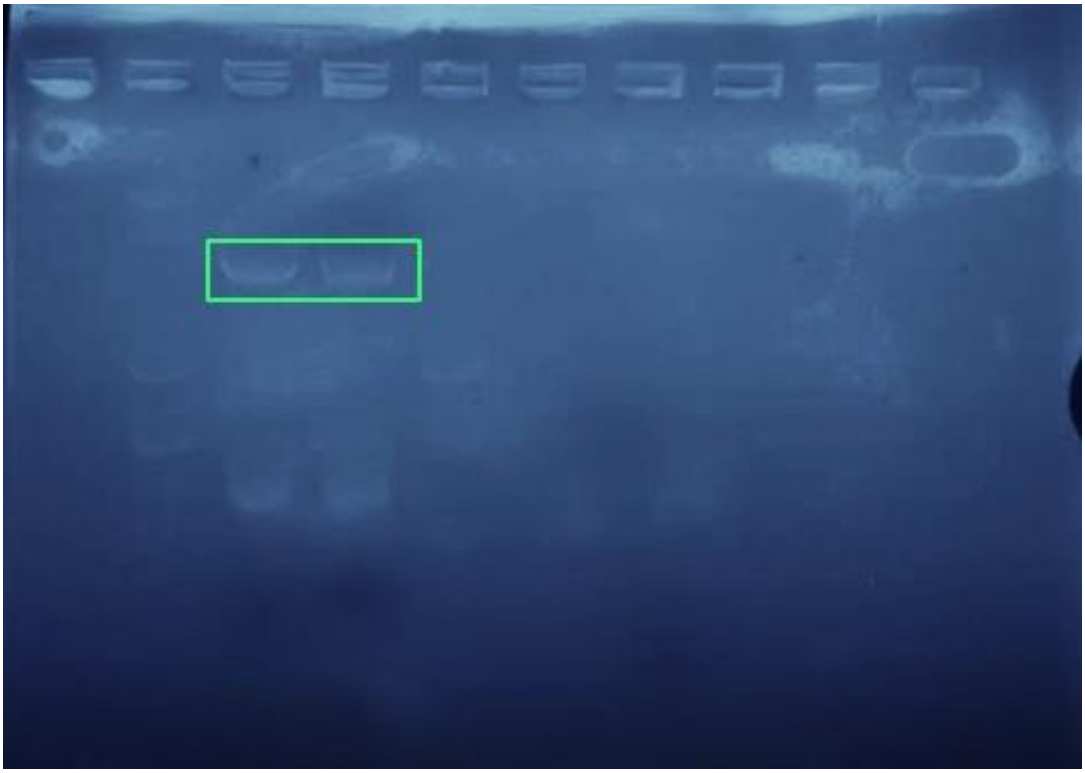

Figure S45. Snapshot of electrophoresis gel of linearized pGNW2 vector. The annealing temperature was 72 °C.

Table S46. Phosphate, nitrogen, fluoride, chloride, and sulfate concentration in water-and Wx/M9-fractionated HL

	Water-Fractionated CL ($mg \cdot L^{-1}$)	**Wx/M9-Fractionated CL ($mg \cdot L^{-1}$)**
PO_4	2480	3338
$NO_2 + NO_3$	0.94	1.05
Total N	1	249
Fluoride	13.28	0.94
Chloride	3.05	817.17
Sulfate	13.29	95.23

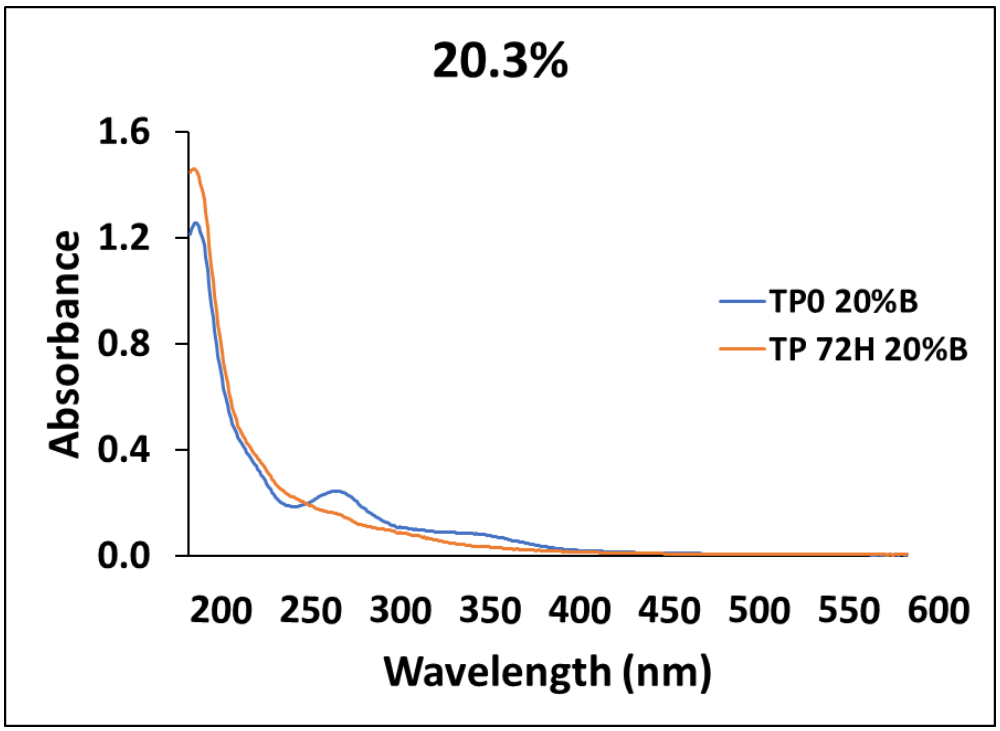

Figure S47. Absorbance spectra of filtered lignin hydrolysate solution (20.3% total solids) fermented with *P. putida* KT2440 at hour 0 and 72, and Wx/M9 media blank. Wavelength range is 200-600 nm. 100X dilution

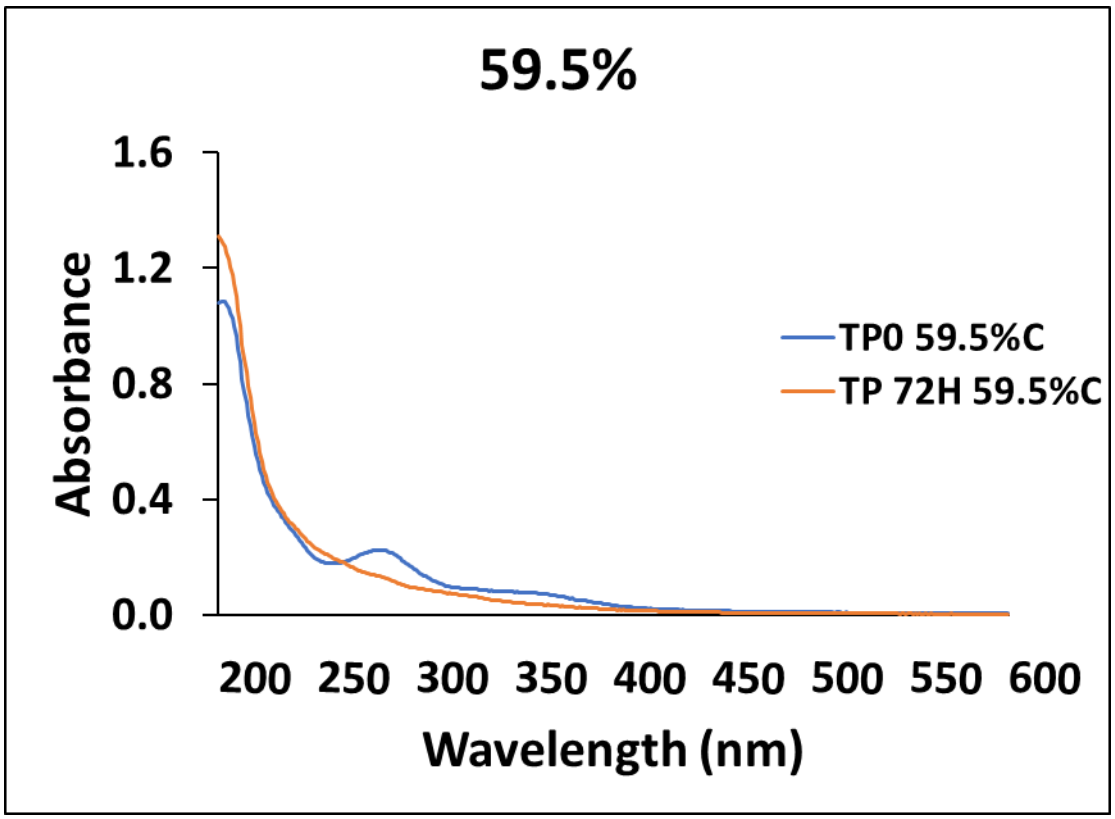

Figure S48. Absorbance spectra of filtered lignin hydrolysate solution (59.5% total solids) fermented with *P. putida* KT2440 at hour 0 and 72, and Wx/M9 media blank. Wavelength range is 200-600 nm. 50X dilution.

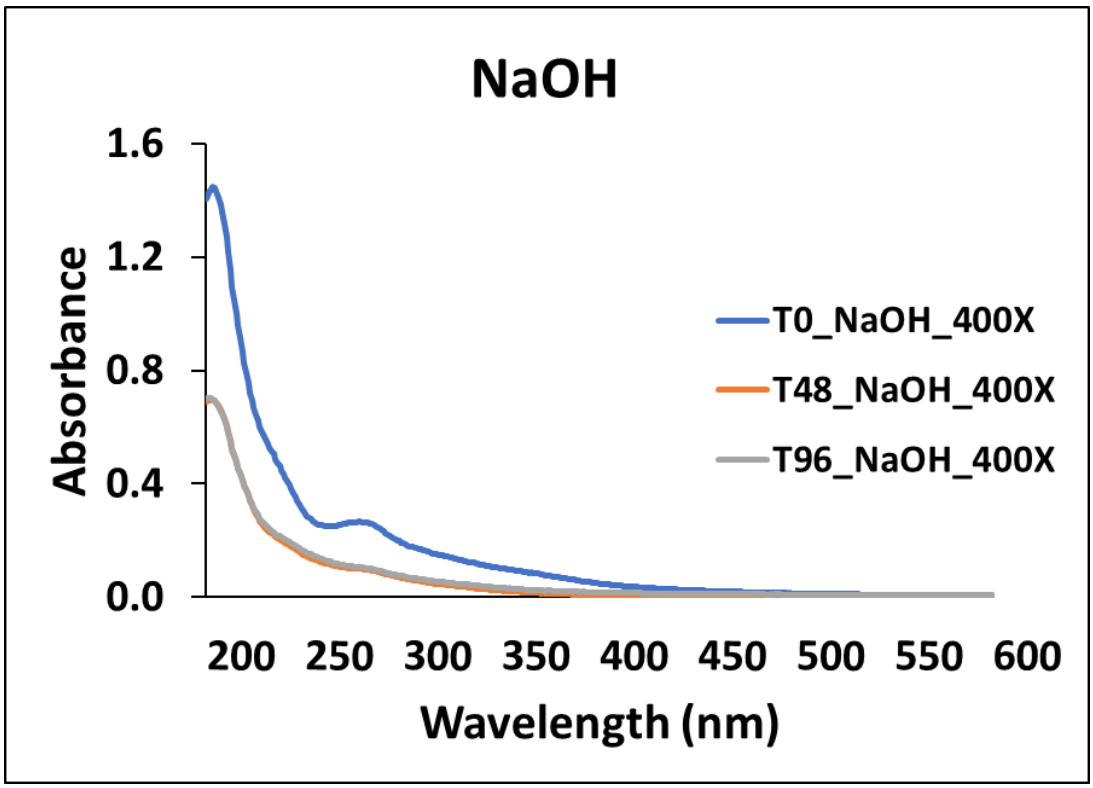

Figure S49. Absorbance spectra of filtered NaOH-alkalized HL slurry fermented with *P. putida* KT2440 at hours 0, 48, and 96. Wavelength range is 200-600 nm. 400X dilution

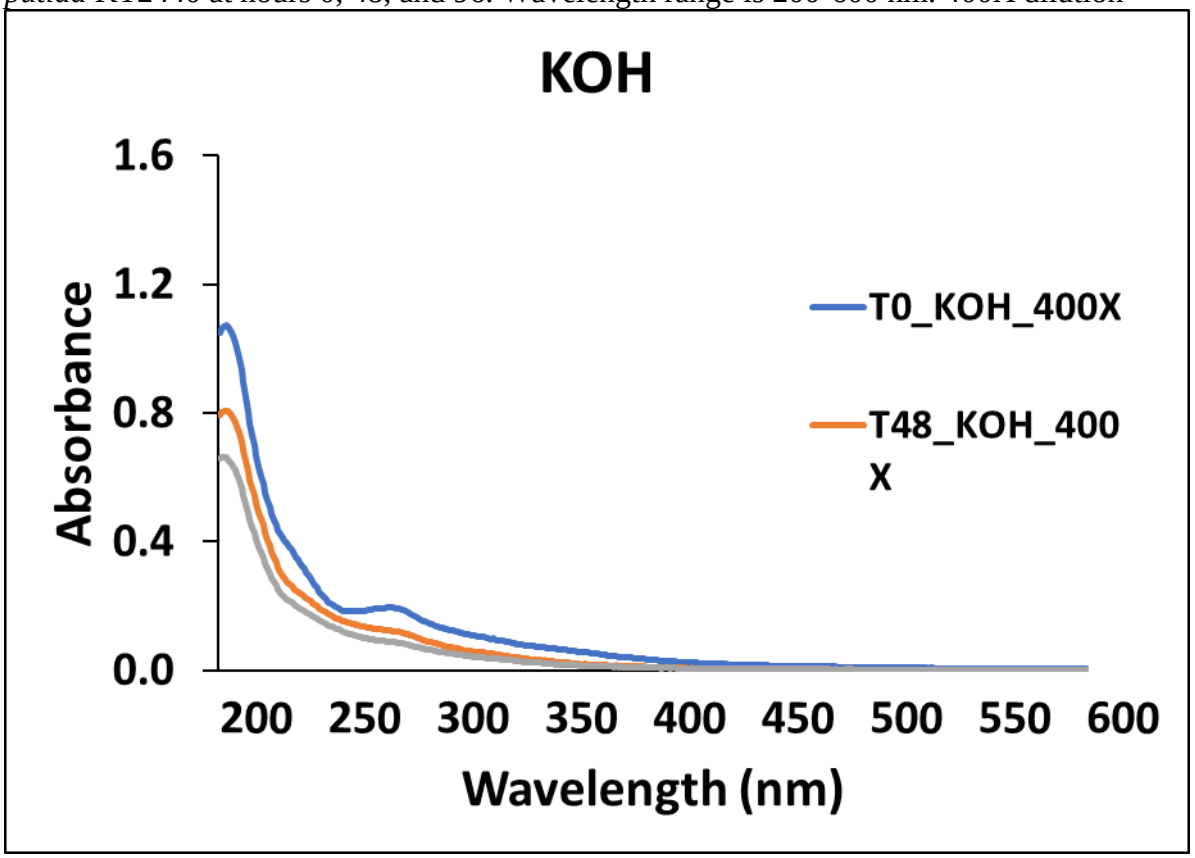

Figure S50. Absorbance spectra of filtered KOH-alkalized HL slurry fermented with *P. putida* KT2440 at hours 0, 48, and 96. Wavelength range is 200-600 nm. 400X dilution

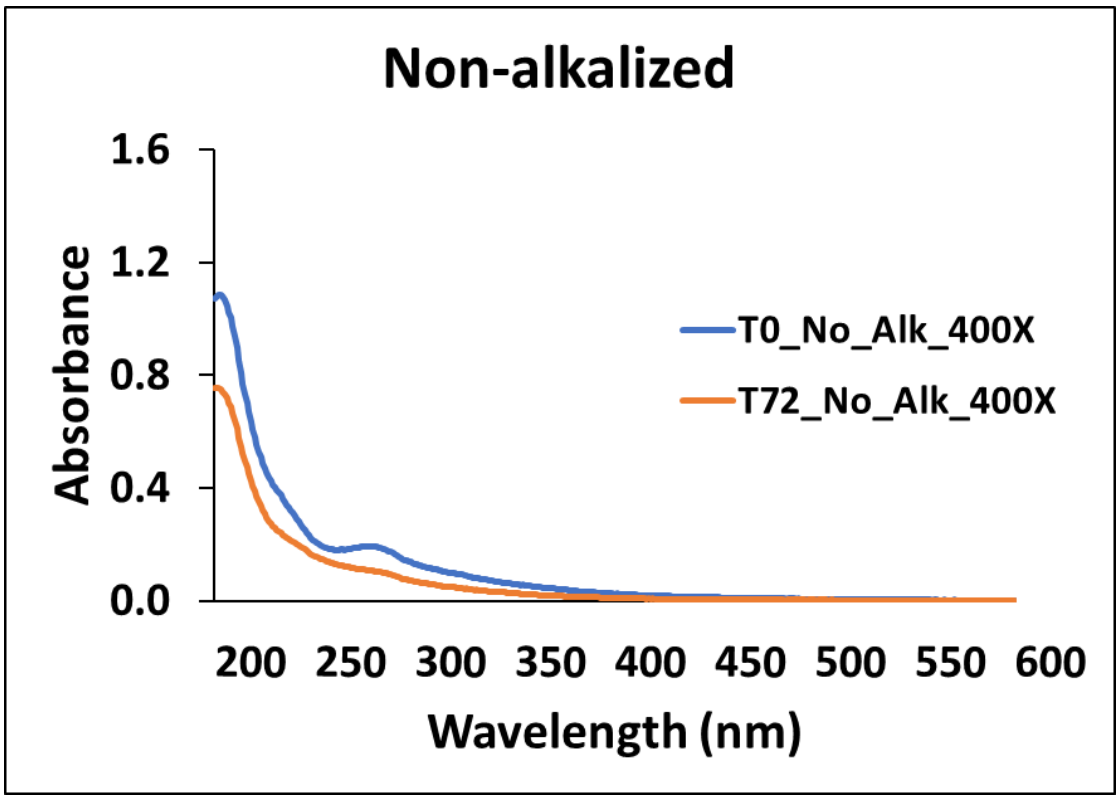

Figure 51. Absorbance spectra of filtered non-alkalized HL slurry fermented with *P. putida* KT2440 at hours 0 and 72. Wavelength range is 200-600 nm. 400X dilution

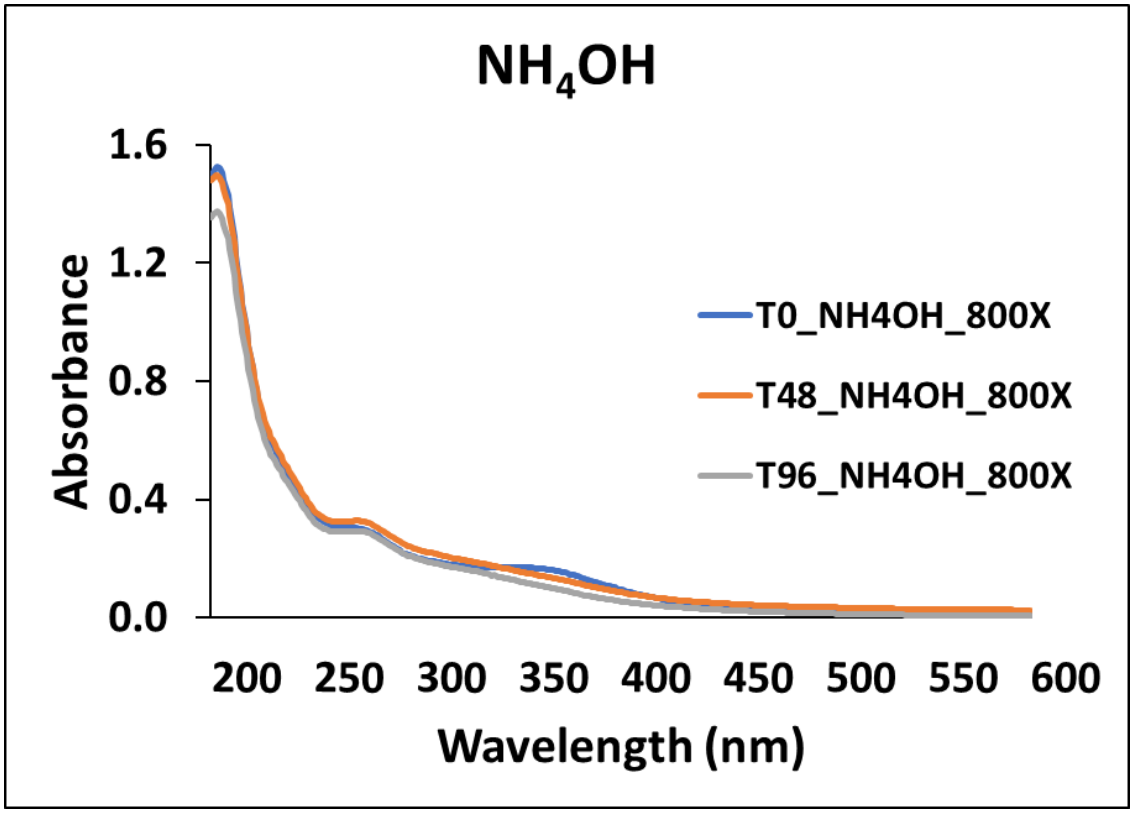

Figure 52. Absorbance spectra of filtered NH_4OH-alkalized HL slurry fermented with *P. putida* KT2440 at hours 0, 48, and 96. Wavelength range is 200-600 nm. 800X dilution

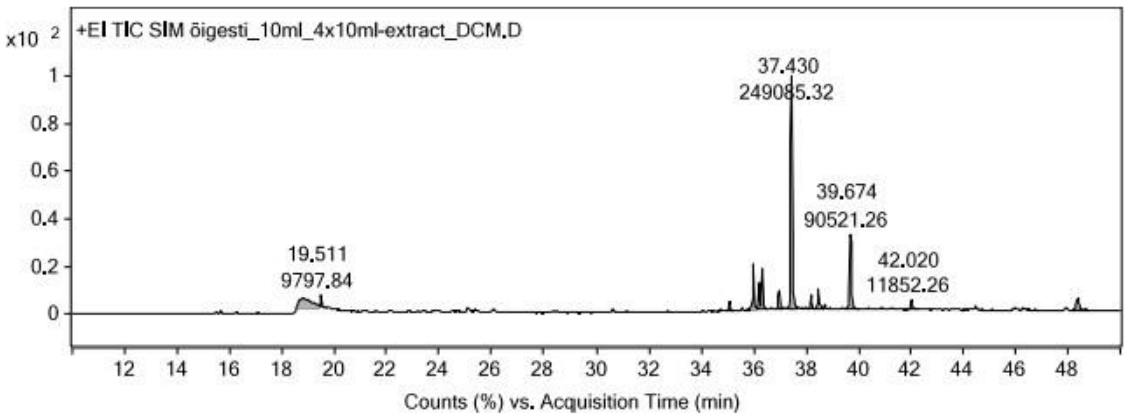

Figure S53. Chromatogram of the acquisition time of lignin-derived dimers at hour 0 of alkalized HL fractionation sample from simulated fed-batch fermentation with *P. putida* KT2440.

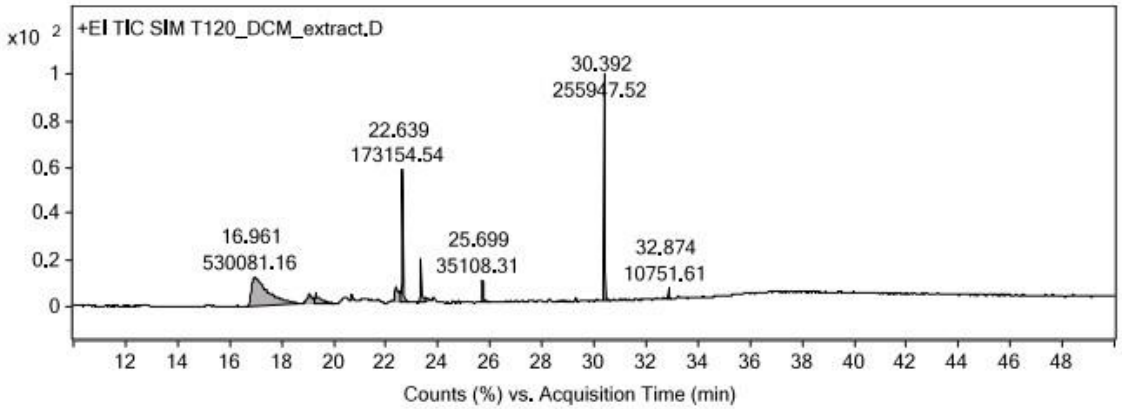

Figure S54. Chromatogram of the acquisition time of lignin-derived monomers at hour 120 of alkalized HL fractionation sample from simulated fed-batch fermentation with *P. putida* KT2440.

NON-EXCLUSIVE LICENCE TO REPRODUCE THESIS AND MAKE THESIS PUBLIC

I, Philip Arthur Morehead,

1. herewith grant the University of Tartu a free permit (non-exclusive licence) to

reproduce, for the purpose of preservation, including for adding to the DSpace digital archives until the expiry of the term of copyright,

Deploying *Pseudomonas putida* for the conversion of aromatic compounds from fractionated industrial hydrolysis lignin,

supervised by Scott Bottoms, Siim Salmar, and Mart Loog

2. I grant the University of Tartu a permit to make the work specified in *p.* 1 available to the public via the web environment of the University of Tartu, including via the DSpace digital archives, under the Creative Commons licence CC BY NC ND 3.0, which allows, by giving appropriate credit to the author, to reproduce, distribute the work and communicate it to the public, and prohibits the creation of derivative works and any commercial use of the work until the expiry of the term of copyright.

3. I am aware of the fact that the author retains the rights specified in *p.* 1 and 2.

4. I certify that granting the non-exclusive licence does not infringe other persons' intellectual property rights or rights arising from the personal data protection legislation.

Philip Arthur Morehead

25/05/2023